NOAA Technical Memorandum ERL NSSL-83

SPRING PROGRAM '76

SECTION I: METEOROLOGICAL SUMMARY

R. Alberty
J. Weaver

SECTION II: DOPPLER RADAR DATA QUALITY CONTROL SUMMARY

D. Sirmans
J. Dooley
B. Bumgarner

Property of
NWC Library
University of Oklahoma

National Severe Storms Laboratory
Norman, Oklahoma
December 1977

UNITED STATES
DEPARTMENT OF COMMERCE
Juanita M. Kreps, Secretary

NATIONAL OCEANIC AND
ATMOSPHERIC ADMINISTRATION
Richard A. Frank, Administrator

Environmental Research
Laboratories
Wilmot N. Hess, Director

Preface

In recent years, scientists interested in various aspects of the severe thunderstorm problem have increasingly migrated toward participation and support of the National Severe Storms Laboratory's annual observation effort. This cooperative spirit has allowed progressively more intense and broader attacks on the total complicated problem of more completely understanding thunderstorm processes and their evolution.

Spring Program '76 incorporated efforts or support from five University groups, twelve other federal agencies and the entire staff of NSSL. External participants and supporters, in alphabetical order, are given on the next page.

The total program was molded such that each element and individual was responsible for a key function and the total accomplishment was closely tied to each individual success. Response was outstanding and credit belongs to those who so unselfishly devoted their skills and energies, often at great personal sacrifice. The scientific enthusiasm and total dedication of participants is so intense it often amazes even the casual observer. For such dedication, I publicly express my sincere gratitude, both personally and as Meteorological Director of Spring Program '76.

Ron Alberty

Dr. Ron Alberty
Chief, Meteorological Research

PARTICIPANTS OF SPRING PROGRAM '76

Agriculture Research Service

Department of the Air Force

Department of the Army

Energy Research and Development Administration

Environmental Data Service

Federal Aviation Administration

Illinois State Water Survey

National Aeronautics and Space Administration

National Environmental Satellite Service

National Research Council

National Severe Storms Forecast Center

National Weather Service

Nuclear Regulatory Commission

University of Chicago

University of Oklahoma

University of Mississippi

University of Wyoming

SECTION I
TABLE OF CONTENTS

	PAGE
1. INTRODUCTION	1
2. OPERATIONAL DAYS, SPRING 1976	7
APPENDIX "A"	65
REFERENCES	130

SECTION II
TABLE OF CONTENTS

		PAGE
1.	INTRODUCTION	79
	1.1 Radar System Characteristics	79
2.	RADAR SYSTEM GENERAL PERFORMANCE PARAMETERS	88
	2.1 Antenna Orientation Checks	88
	2.2 Doppler Receiver Transfer Function	88
	2.3 Complex Video ADC Performance	91
3.	PARAMETERS PERTAINING TO INTENSITY MEASUREMENT	91
	3.1 Radar Peak Power Log	92
	3.2 Logarithmic Receiver Parameters	92
	3.3 Intensity Calibration Drift	92
4.	PARAMETERS PERTAINING TO VELOCITY MEASUREMENT	96
	4.1 Test and Calibration Parameters	96
	4.2 Weather Data Quality Control Spot Check Results	100
5.	DATA QUALITY ENGINEERING SUMMARY	100
6.	EXAMPLES OF QUALITY CONTROL PROGRAM OUTPUTS	103
	6.1 Intensity Calibration	103
	6.2 Noise Statistics	113
	6.3 Meteorological Data Quality	116
	6.4 Special Purpose Programs	126

SECTION I

PROGRAM SUMMARY

1. INTRODUCTION

The observational program at NSSL continues annually, with various degrees of surface and upper air measurements supporting storm sampling by both surveillance type and Doppler radars, an instrumented tower, various aircraft, and mobile teams of observers/photographers. We have recently mounted an effort to somewhat stabilize the background data from surface stations and tower to provide a larger data base with fixed sampling characteristics. We plan to essentially retain the surface network and tower configurations as shown in Figures 1.1 and 1.2 until valid reason for change is established. Tower data is now recorded in digital form and we plan to move to full digitization of surface data. The number of rawinsondes employed will unfortunately remain variable since available funds and other support fluctuates from year to year.

The WSR-57 surveillance radar, NSSL's two Doppler radars, the surface network and the tower typically collect data during about two months of Oklahoma's springtime thunderstorm maximum. Other data sources operate for various periods within this time window. There are usually roughly a dozen severe storm systems and one or two tornadic thunderstorms within the observing network during the period. Although NSSL interest currently culminates in tornadic thunderstorms, storms of lesser intensity are also studied by scientists both internal and external to the Laboratory.

Operational decisions, made after consultation with appropriate engineers and meteorologists, considered both equipment readiness and meteorological expectations of weather development. Of course, we are still imperfect in predicting precise time and location of severe thunderstorm development. But, with use of general outlook guidance from the National Severe Storms Forecast Center and the dedicated efforts of short range forecasters (Nowcasters) at NSSL, data collection decisions are facilitated.

General operating conditions have been described by Barnes (1974) and Wilk et al. (1976). Personnel assignments illustrated on Pages 4 and 5 suggest modifications that have evolved in recent years. Perhaps most noteworthy for 1976 were daily soundings from the nine rawinsonde stations at 0900 and 1430 CST, augmented with additional soundings on storm days, and the initial efforts at collecting coordinated data from three 10 cm Doppler radars. We anticipate significant research usage of these data in future years.

Brief descriptions of meteorological events and resulting observations are contained in the following pages of Section I along with illustrative radar and satellite photographs. Tower and rawinsonde data are available in digital tape form and surface data, except for a few selected time

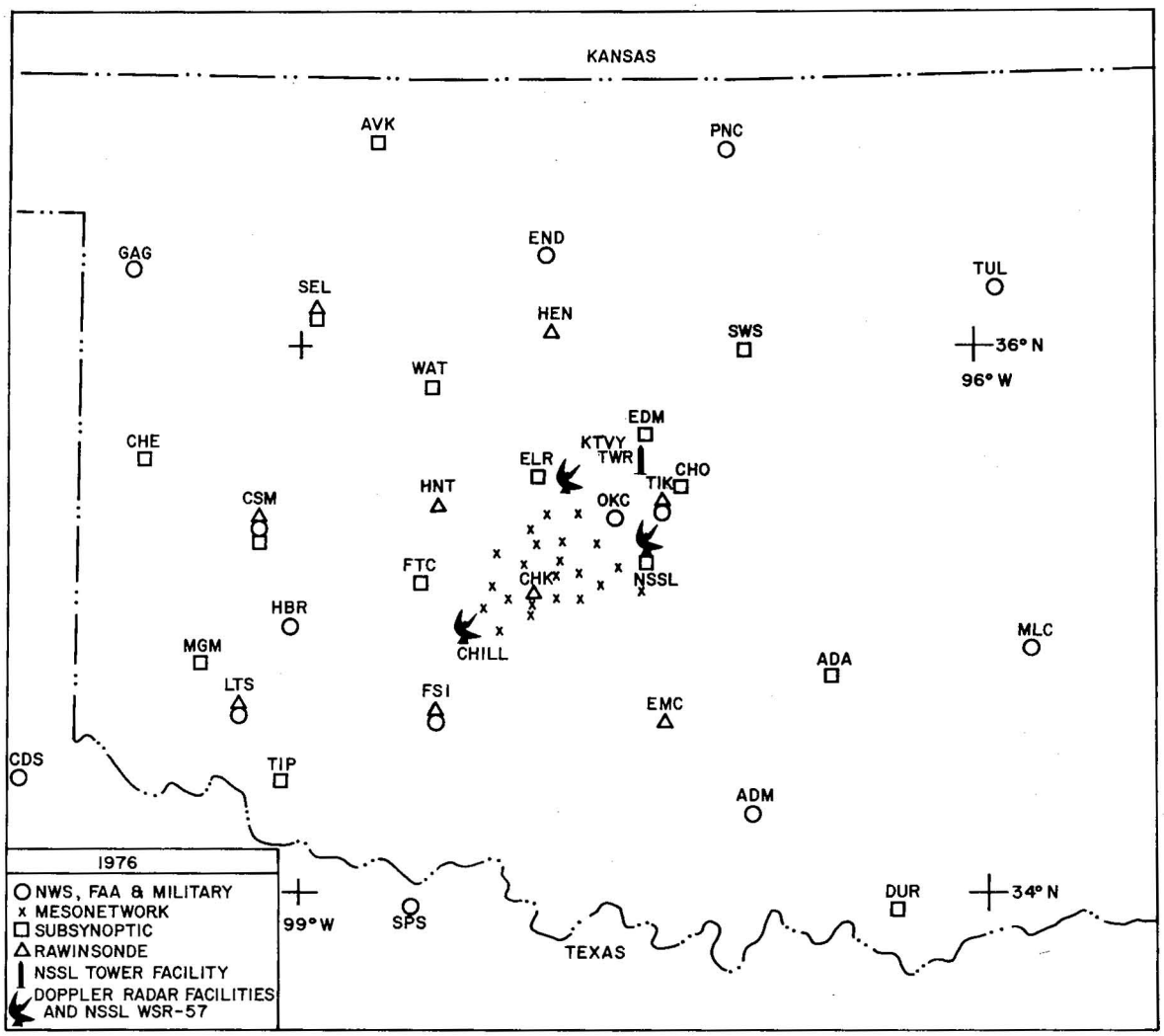

Figure 1.1. Deployment of sensors.

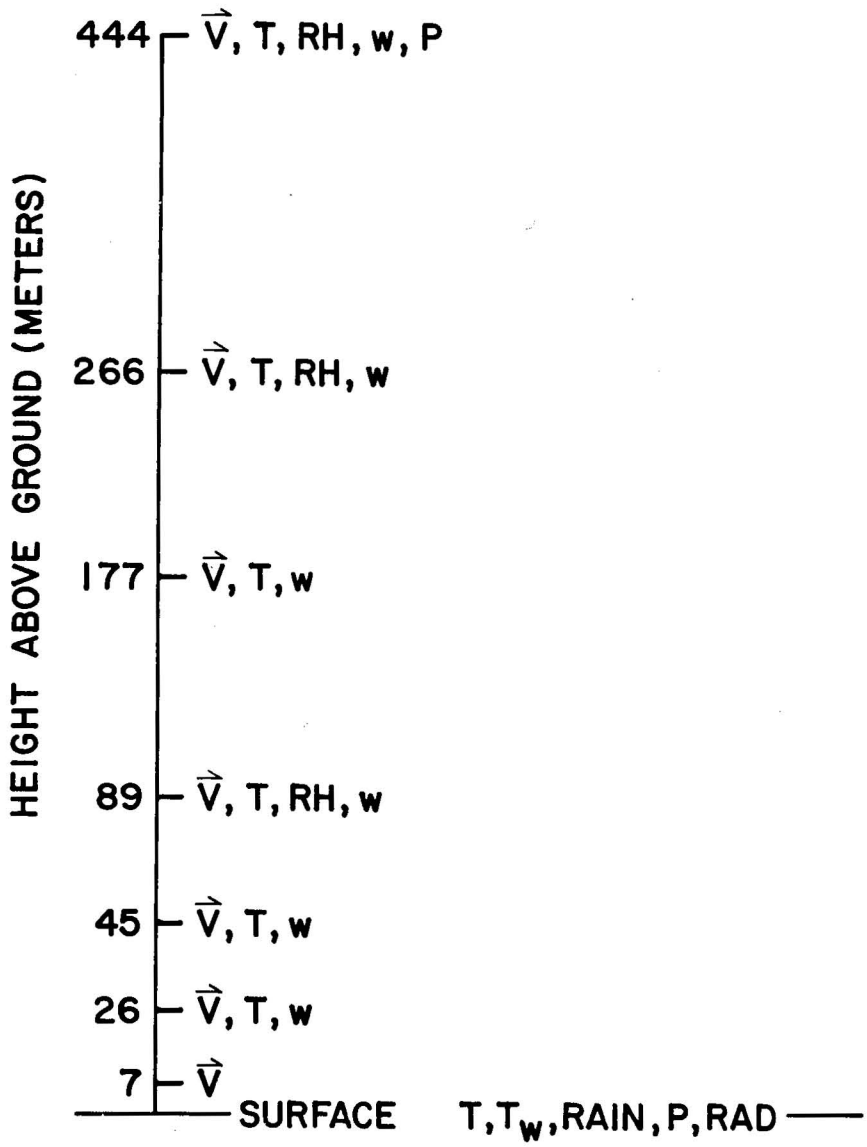

Figure 1.2. Schematic view of tower sensors. Numbers denote height of sensor systems in meters. V = horizontal wind speed and direction; T = dry-bulb temperature; T_w = wet-bulb temperature; RH = relative humidity; w = vertical velocity; P = pressure; Rad = solar radiation.

intervals which have been digitized, are available as copies of strip charts. Tower and surface systems were operated continuously during the entire observational period.

Section II details an intense effort to document quality control procedures for the two NSSL Doppler radars. This second section should prove to be a valuable resource document for those using our Doppler data.

Requests for data should be addressed to Mrs. Kathryn Gray, NSSL.

Spring Program '76 Personnel Assignments

Meteorological Director: Alberty; Alternate: Wilk

I. Forecast Team
Burgess
Burk
Davies-Jones, Doswell or Purcell
Alternates: Koch (OU) or Bensch (OU)

II. Weather Evaluation Team (Nowcasting)
Weaver
Killian
Zittel
Alternate: Safford

III. Storm Intercept Teams

#1	Davies-Jones or Doswell	#2	Watts	Alternates:	Berger
	Purcell		Leslie		Jobson
	Moore		Ziegler		Burk
	Photographer		Berger or Jobson		
#3	Audio Recording	#4	Argonne Labs Group		
	Roy Arnold (U. of Miss.)		Kornegay		
	Zipser				

IV. Storm Intercept Coordinator
Davies-Jones/Doswell (alternating)

V. Surveillance Meteorologist
Nelson; Alternate: McCarthy

VI. Norman Doppler Meteorologist (2 positions)
Brown/Brandes; Alternate: Burgess

VII. Cimarron Doppler Meteorologist
Burgess; Alternate: Safford

VIII. Multiple Doppler Coordinator
Ray; Alternate: Brown

IX. Aircraft Control Meteorologist
(FAA Controller/Gust Front Project/NASA Project)
Lee; Alternate: Wilk

X. Aircraft Control Meteorologist (OU-Wyoming)
McCarthy; Alternate: Marwitz

XI. Flight Meteorologist (OU)
Koch/Bensch/McCarthy

XII. Flight Meteorologist (Wyoming)
Marwitz/McCarthy/Bensch

XIII. Rawinsonde Coordination and Quality Control
Showell/Dooley/Helm

XIV. Doppler Data Quality Control
Sirmans/Dooley/Bumgarner

XV. WSR-57 Data Quality Control
Dooley/Gray/Weible

XVI. Tower Meteorologist
Goff/Johnson; Alternate: Zittel

XVII. Radar Scope Photography
Clark/Farris

XVIII. WSR-57 Operation
Jennings/Zittel

XIX. NOR Doppler Operation
Anderson/Heck/Sirmans

XX. CIM Doppler Operation
Shinn/Schmidt/Carter/Zahari

XXI. Surface Network Operation
Wardius/Lappie

XXII. Damage Survey Teams
(Volunteers will be selected to aid with this effort)

a) Overall Storm Structure and Damaged Areas
Leader: Wilk

b) Tornadic Damage Assessment
Leader: Davies-Jones

c) Volunteer Observer Network and Hail Survey
Leader: Nelson

XXIII. Ling Display
Hennington/Moore

2. OPERATIONAL DAYS, SPRING 1976

During the NSSL's Spring Program 1976, meso- and subsynoptic scale surface networks were operated daily. In addition, at least two special soundings were made routinely each day, whether storms occurred or not. However, in this report the term "operational day" refers primarily to thunderstorm days.

The following section summarizes the 1976 operational days. Table I lists weather events in the area of interest--starred dates are operational days. Summaries include a brief discussion of the synoptic situation; selected maps, photos and graphs are presented to give the reader an overview of storm data available for each day. Figure 1.3 may be consulted throughout this report for geographical references to radar photos. Approximate times of various data collections are also presented in graphical form. Especially noteworthy weather events occurred on May 26, 29 and 30 and these days are described in slightly greater detail. Precise listings of all data collected are given in Appendix I.

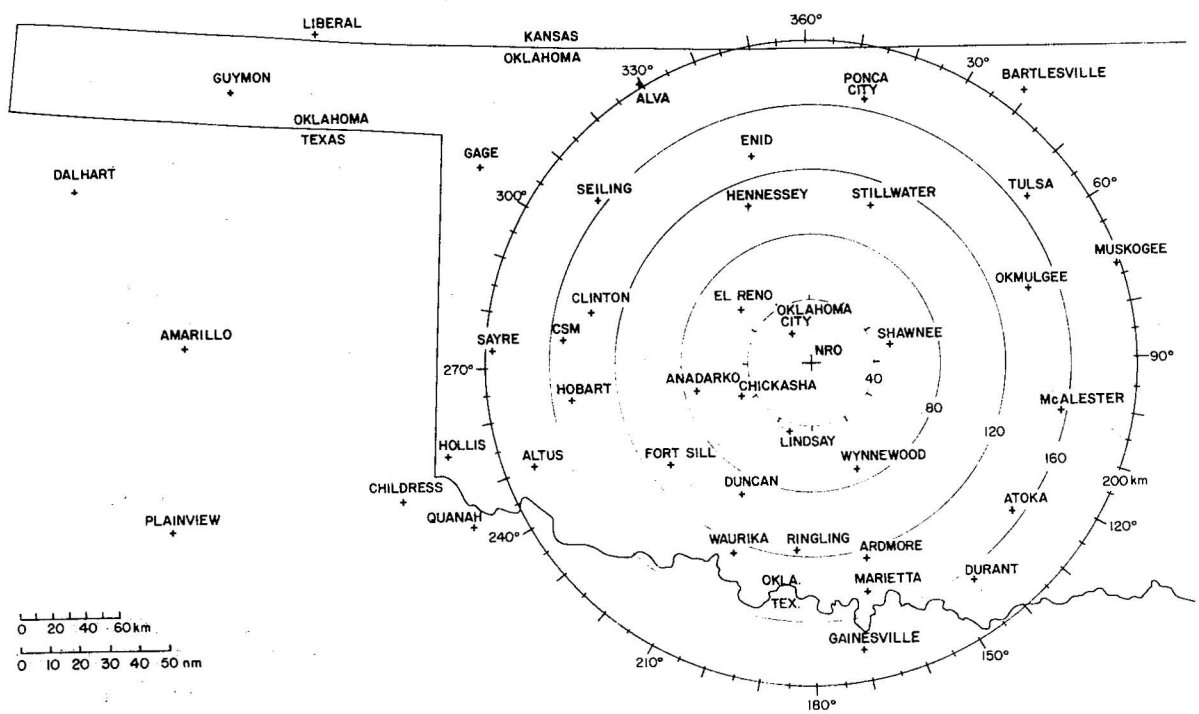

Figure 1.3. Map of Oklahoma with Norman centered AzRan grid superimposed. Range circle radii in 40 km increments.

INDEX OF DATA SETS

A. Severe thunderstorms--isolated

1. 19 Apr 76 - Isolated cells in a widespread area of convective activity.

2. 9 May 76 - Two individual storms in western Oklahoma.

3. 29 May 76 - Storm with a mesocyclone in mid-cloud levels producing a thunderstorm "heat burst" (i.e., surface heating via subsidence).

4. 30 May 76 - Splitting storm in southern Oklahoma which became tornadic.

B. Non-severe thunderstorms

1. 24 May 76 - Widely scattered, early afternoon thundershowers.

2. 12 Jun 76 - High based thundershowers in northwestern Oklahoma.

3. 14 Jun 76 - Small, isolated storm elongating dramatically in strong vertical wind shear.

4. 17 Jun 76 - High based thundershowers in northwestern Oklahoma.

C. Squall lines

1. 15 Apr 76 - Dissipating north-south oriented line.

2. 12 May 76 - Strong east-west oriented line moving southward.

3. 22 May 76 - Squall line initiated along a dry line.

4. 13 Jun 76 - A relatively short, north-south oriented line with extremely deep convection and strong reflectivity cores which produced only small hail.

D. Thunderstorm aggregates

1. 5 May 76 - Large storm complex with strong, embedded cores.

2. 25 May 76 - Widespread activity in western Oklahoma.

3. 26 May 76 - Widespread activity about an occluded low pressure system of great vertical depth. Synoptic-scale circulation evident on radar data. Regions of isolated activity quickly filling in.

4. 30 May 76 - Storm complex in southwestern Oklahoma.

Table I: Thunderstorm activity, Spring, 1976. Regions A-F are arbitrary divisions selected by the forecast team. Numbers represent intensity of activity: 0 - No thunderstorms, 1 - Non-severe thunderstorms, 2 - Severe storms and 3 - severe storms with tornadoes. Starred dates are data collection days.

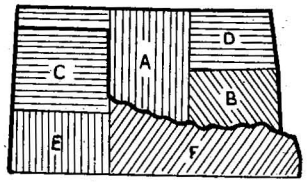

Date	A	B	C	D	E	F	Date	A	B	C	D	E	F	Date	A	B	C	D	E	F	Date	A	B	C	D	E	F
4-15*	1	0	3	1	3	3	5-1	0	0	0	0	0	1	5-17	0	0	0	0	1	0	6-2	1	0	1	0	1	1
4-16	1	0	1	0	0	1	5-2	0	0	0	0	0	0	5-18	0	0	0	0	0	0	6-3	0	0	0	0	0	0
4-17	3	1	1	1	1	1	5-3	0	0	0	0	0	0	5-19	0	0	0	0	0	1	6-4	0	0	1	0	1	1
4-18	0	0	0	0	0	1	5-4	0	0	1	0	1	1	5-20	0	0	1	0	1	1	6-5	1	1	2	0	1	1
4-19*	3	3	3	1	1	3	5-5*	2	1	3	1	1	3	5-21*	1	0	2	0	2	1	6-6	1	1	1	1	1	1
4-20	0	0	0	0	0	0	5-6	0	0	0	0	0	2	5-22*	2	1	1	1	2	2	6-7	1	0	1	0	1	1
4-21	0	0	0	0	0	0	5-7	0	0	0	0	0	1	5-23	0	1	2	1	1	3	6-8	0	0	1	0	1	0
4-22	1	0	2	0	2	0	5-8	0	0	1	0	0	0	5-24*	1	1	1	1	2	1	6-9	0	0	1	0	0	0
4-23*	0	1	0	1	1	2	5-9*	2	1	1	1	1	1	5-25*	1	1	2	1	1	3	6-10	0	0	1	0	1	0
4-24	0	2	0	0	0	2	5-10	0	1	0	1	0	2	5-26*	2	3	1	1	1	3	6-11	1	0	2	0	1	1
4-25	0	0	0	0	0	0	5-11	1	1	1	1	1	1	5-27	0	0	0	0	0	0	6-12*	0	1	0	0	1	1
4-26	1	1	2	1	2	1	5-12*	2	2	1	1	1	3	5-28	0	0	1	0	1	0	6-13*	2	0	1	1	1	1
4-27	1	1	3	1	2	0	5-13	1	1	1	1	1	1	5-29*	3	1	2	0	1	0	6-14*	2	0	0	2	0	0
4-28	1	1	0	1	2	1	5-14	0	1	0	1	0	1	5-30*	3	1	2	3	1	2	6-15	0	1	0	0	0	2
4-29	0	0	0	0	1	1	5-15	0	1	0	1	0	1	5-31	2	0	1	2	0	2	6-16	0	0	0	0	0	0
4-30	1	1	1	1	1	1	5-16	0	0	0	0	0	0	6-1	0	1	0	0	0	1	6-17*	2	1	2	1	1	2

April 15, 1976

The dominant synoptic feature was a broad, upper-air trough centered over the extreme western United States. A moderately strong shortwave (height falls 50-80 m) had moved around the southern tip of the trough and was traveling rapidly northeastward toward western Oklahoma. All severe weather parameters seemed favorable for the occurrence of violent storms. The air mass over the study area was unstable, with lifted indices between -5 and -9. Generally, there was strong vertical wind shear, low-level convergence and upper diffluence with drier air aloft. The only problem was cool low-level air from the passage of early morning storms. The forecast called for activity to develop in southwest Texas and spread northeastward into the Texas Panhandle and western Oklahoma.

Thunderstorms began by early morning in eastern New Mexico and western Texas and by noon had spread north and east into the Texas Panhandle. Intercept crews were dispatched toward Sayre, Oklahoma.

1430 Central Standard Time (CST) sounding data from FSI revealed a strong capping inversion near 750 mb which had not been present on the morning soundings. Additionally, satellite photos indicated that upper flow had become oriented parallel to the existing squall line (Fig. 1.4). Thus, the nowcast update at 1630 CST foresaw diminishing chances of severe storm formation in western Oklahoma and suggested that the squall line, moving toward Oklahoma from the Texas Panhandle, would soon dissipate due to the inversion and lack of storm ventilating flow.

At 1900 CST, a squall line with several strong, embedded cores (50 dbz or stronger) entered Oklahoma, then lost intensity dramatically (Figs. 1.5 and 1.6). Radar data were collected as a trial run of coordinated operations. No unusual slides or movies were obtained.

DATE 4-15-76

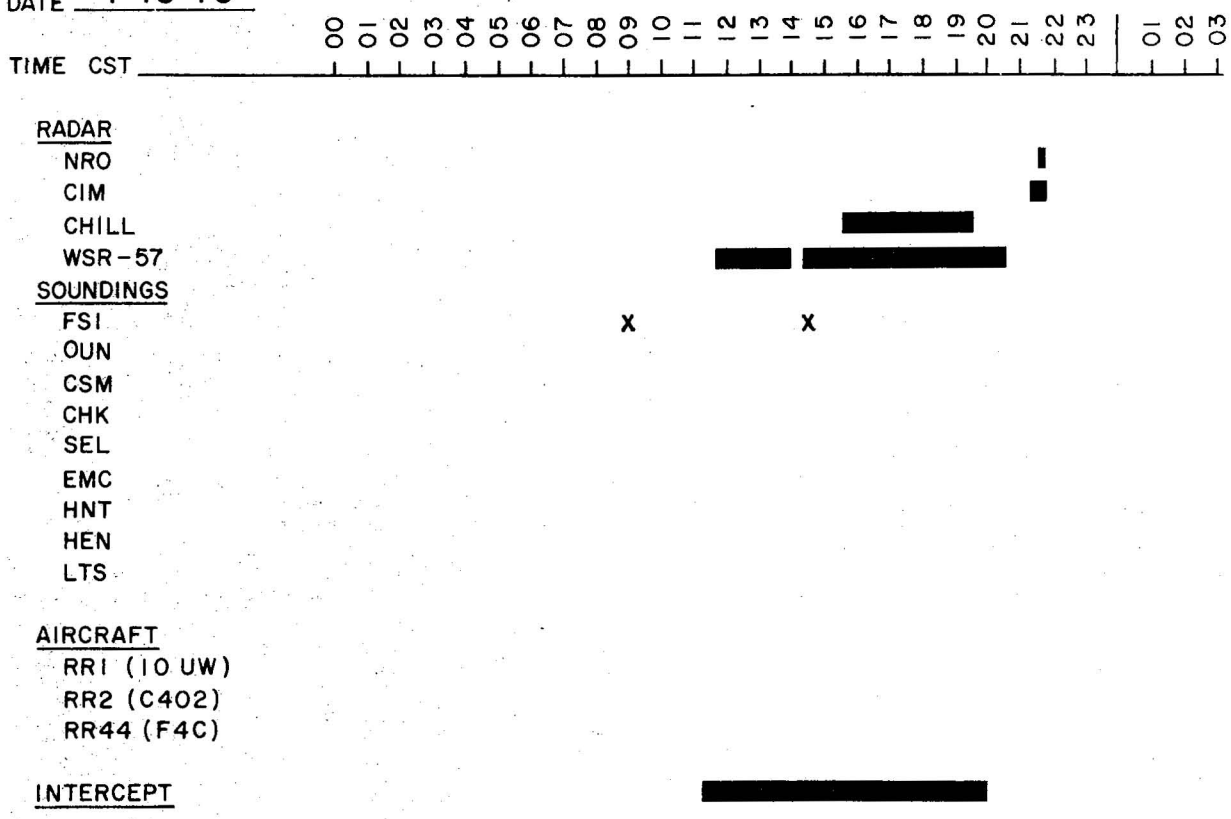
TIME CST
00 01 02 03 04 05 06 07 08 09 10 11 12 13 14 15 16 17 18 19 20 21 22 23 01 02 03
RADAR
NRO
CIM
CHILL
WSR-57
SOUNDINGS
FSI
OUN
CSM
CHK
SEL
EMC
HNT
HEN
LTS
AIRCRAFT
RR1 (10 UW)
RR2 (C402)
RR44 (F4C)
INTERCEPT

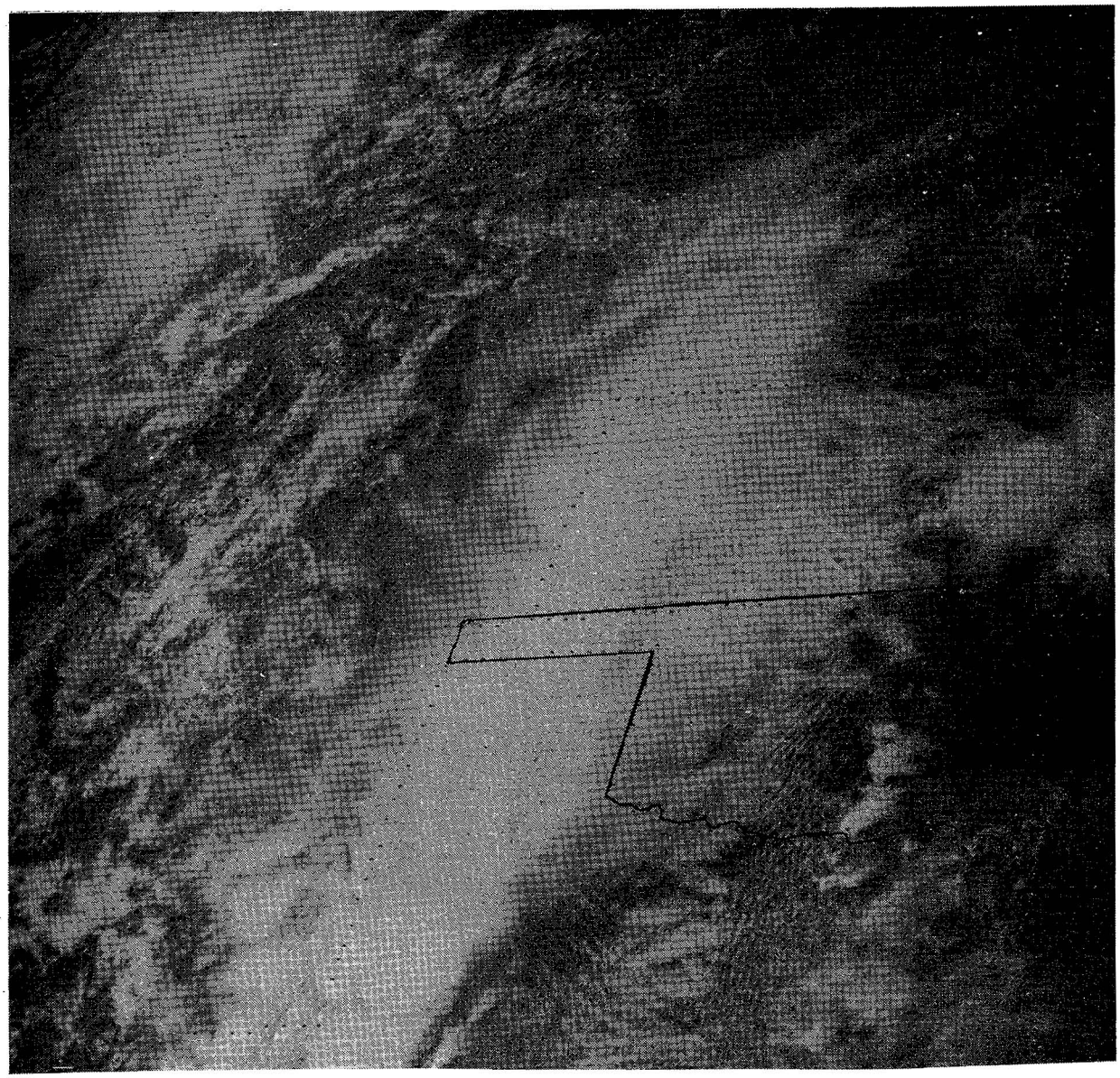

Figure 1.4. Satellite photo 1500 CST: 15 April 1976. Note the N-S oriented squall line in western portions of Kansas and Texas with anvil material apparently blowing toward the north.

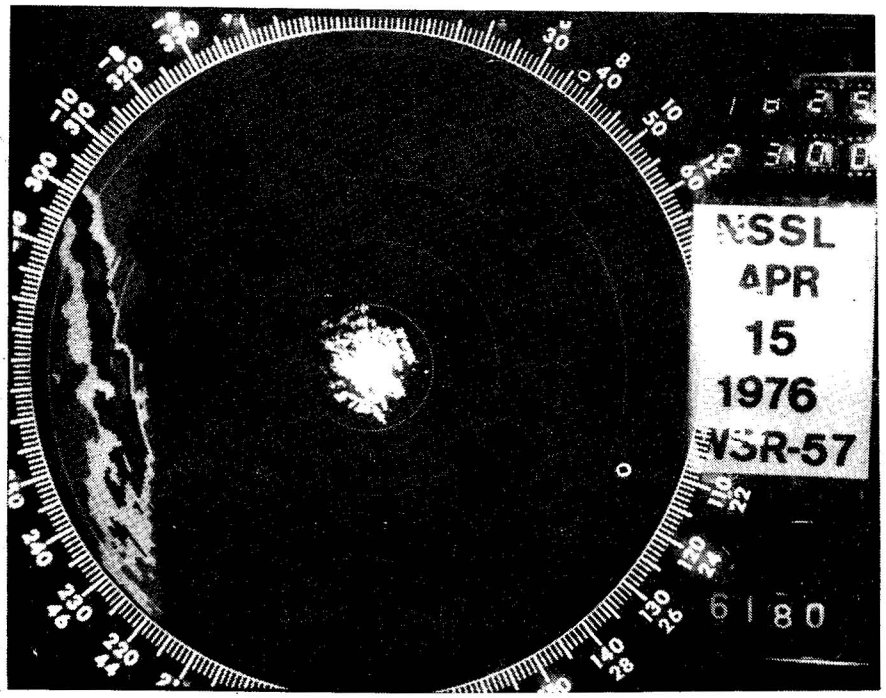

Figure 1.5. WSR-57 radar photo 1825 CST: 15 April 1976. Range interval 40 km, 0° tilt. Squall line entering Oklahoma.

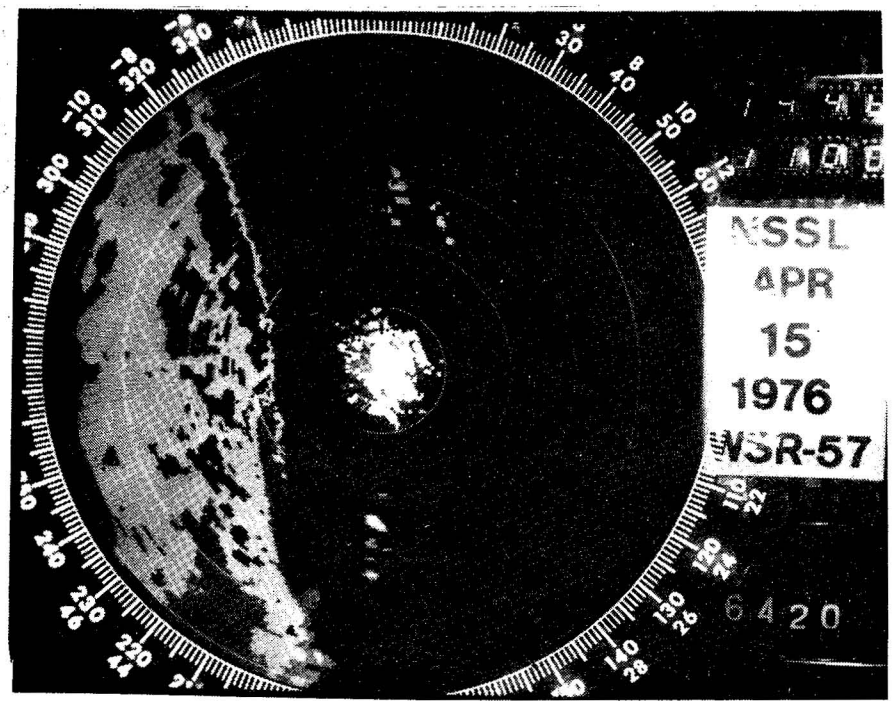

Figure 1.6. WSR-57 radar photo 1946 CST: 15 April 1976. Range interval 40 km, 0° tilt. Squall line diminishes in intensity.

April 19, 1976

The morning surface analysis (0900 CST) showed a deepening low pressure system on the Texas Panhandle - New Mexico border with a dryline extending southward toward Wink, Texas. A warm front stretched eastward across southern Oklahoma.

At 500 mb, a shortwave trough was situated over New Mexico and was expected to move across both Oklahoma and Texas during the day. 700 mb analysis indicated that drying would occur at mid-levels and at 850 mb a tongue of moist air extended through central Texas into Oklahoma. A moderately unstable air mass (lifted indices, -4) was expected to become more unstable as the day progressed.

The morning forecast was for activity to develop along the dryline as it moved eastward through western Texas. Severe storms were expected by mid-afternoon in the Texas Panhandle and west-central Texas and by late afternoon in western Oklahoma.

Activity began at about 1400 CST in central Texas, along the 850 mb moisture ridge, and shortly thereafter, had spread northward into south-central Oklahoma. CB development was also reported by mobile observing units in the Texas Panhandle by about 1500 CST (Fig. 1.7).

A tornado producing mesocyclone, which formed in Montague County, Texas and moved into Love County, Oklahoma, (175°/150 km) was monitored utilizing the Doppler multimoment display from 1750 to 1840 CST (see WSR-57 photo, Fig. 1.8). No digital data were collected for this period. Digital dual-Doppler data were gathered on an isolated storm, to the southwest of Norman, at approximately 2130 CST (Fig. 1.9) and on severe storms in northern Oklahoma City two hours later (Fig. 1.10). Intercept crews obtained 35 mm slides of two funnels and a small, short lived tornado in the central Texas Panhandle.

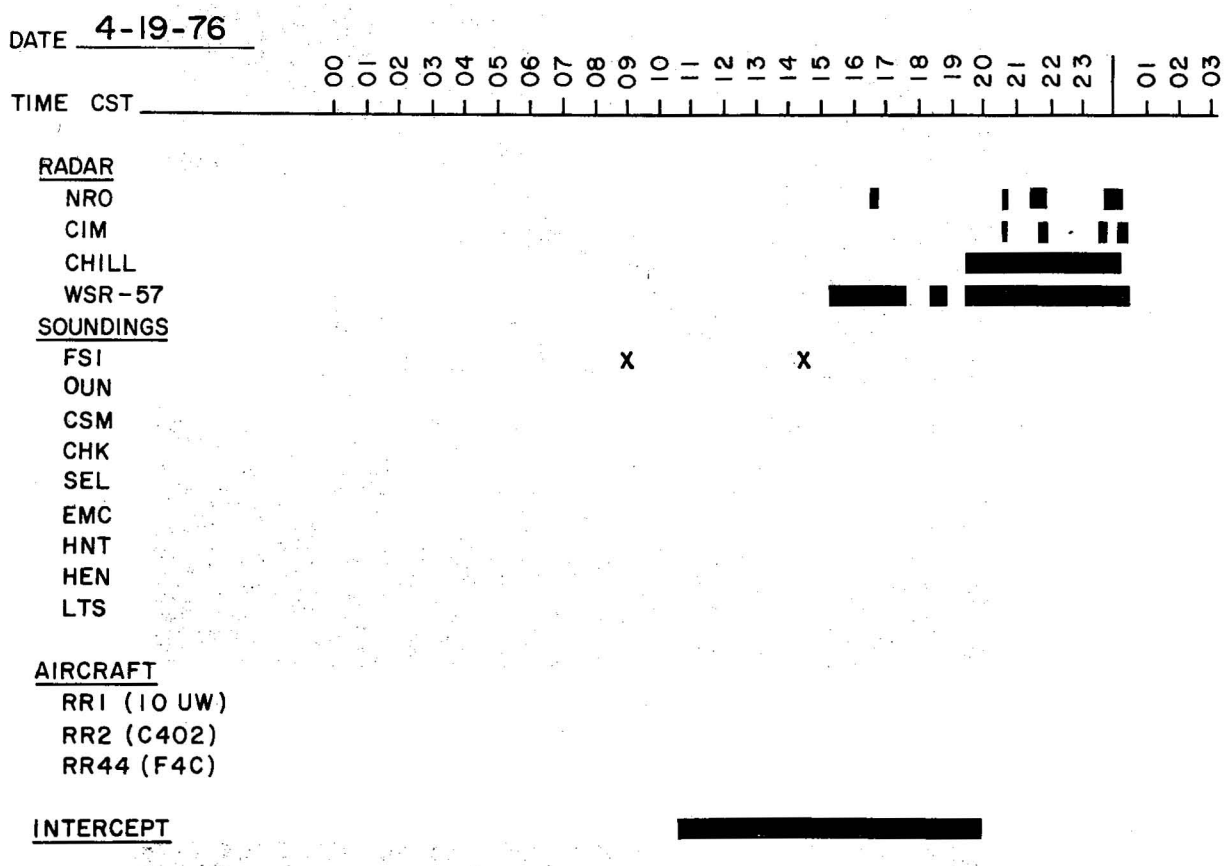

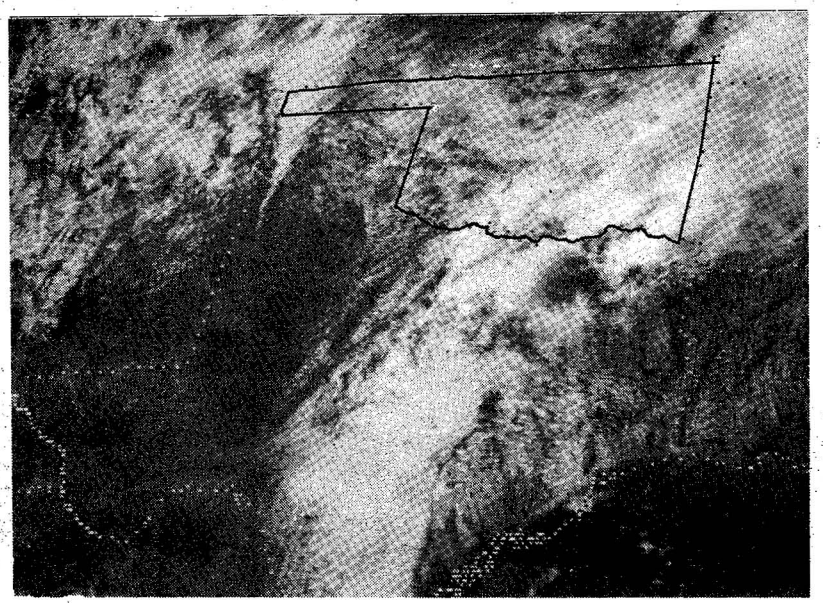

Figure 1.7. Satellite photo 1330 CST: 15 April 1976. Thunderstorm activity in the Texas Panhandle, northern Texas and south-central Oklahoma.

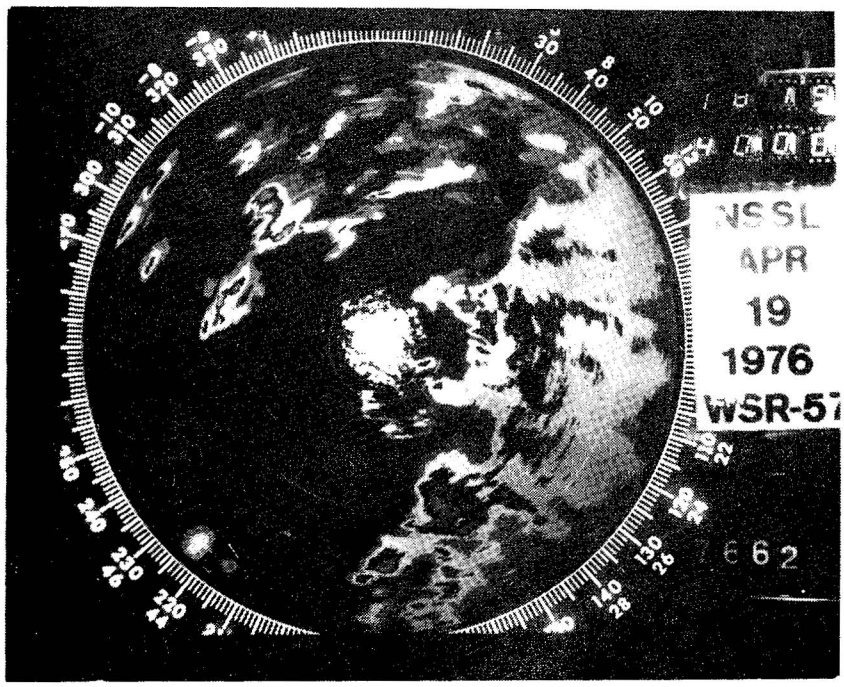

Figure 1.8. WSR-57 radar photo 1815 CST: 19 April 1976. Range interval 40 km, 0° tilt. Tornadic storm entering southern Oklahoma (180° at 155 km).

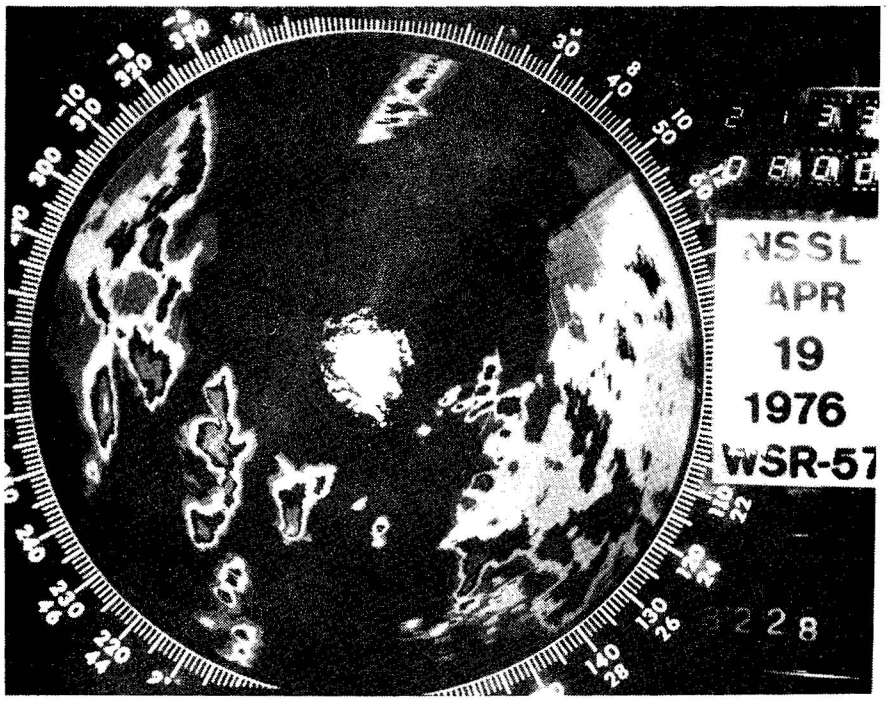

Figure 1.9. WSR-57 radar photo 2133 CST: 19 April 1976. Range interval 40 km 0° tilt. Strong storms to the southwest.

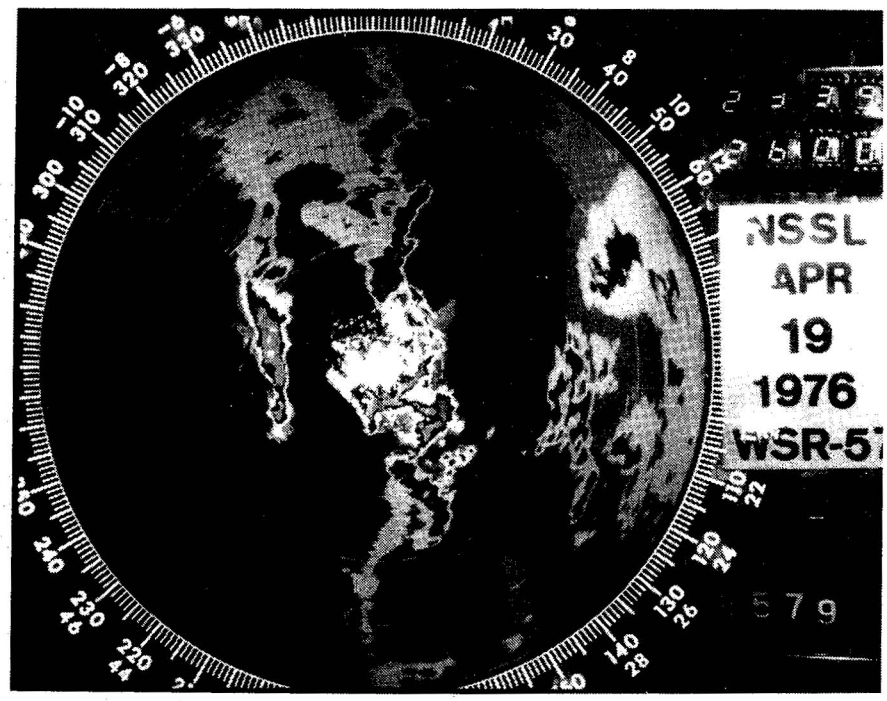

Figure 1.10. WSR-57 radar photo 2339 CST: 19 April 1976. Range interval 40 km, 0° tilt. Squall line crosses central Oklahoma.

April 23, 1976

A long wave trough over the western United States continued to dominate Oklahoma weather. A shortwave impulse, approaching from eastern New Mexico, was expected to trigger thunderstorms as it phased with a surface dry front during the afternoon.

At 0900 CST, primary surface features were a low pressure system in north-central Kansas, a cold front extending from the low through southwestern Kansas and southern Colorado and a dryline that intersected the front near Garden City, Kansas and from there stretched into southeastern New Mexico. In central and southern Kansas, moisture just ahead of the dryline was relatively shallow and, thus, the main thrust of the dry push was expected to occur there.

The most severe weather was predicted for Kansas during the afternoon with further development along the dry front in western Oklahoma by evening. Forecasters felt that any storms spawned in the Texas Panhandle would lose their upper level support before becoming severe.

Chase units left for Wichita, Kansas at 1100 CST. By noon the surface low had slipped southward to Salina, Kansas and had begun to fill, while at the same time pressures were falling in southwest Oklahoma. By 1300 CST, the Chase Coordinator and Nowcaster had made the decision to send intercept crews to southwestern Oklahoma. The potential for severe activity seemed to be increasing in that region and the desirability of obtaining high quality tornado films in the area of triple Doppler coverage offset any misgivings concerning the change in the forecast.

The only severe weather during the day occurred in Kansas and northern Texas. Neither Doppler data nor films were acquired. Thereby, a major decision regarding chase coordination and nowcasting was reached--namely, that the general area outlined by the morning forecast for potential severe weather would be considered the day's "operational area". Nowcast analyses of surface data, showing unexpected local changes, were not to be considered sufficient reason to alter the morning outlook, UNLESS such changes persisted for two or more hours and/or midday soundings, satellite photos or radar data supported the change. This procedure proved extremely valuable to operations as the season progressed.

DATE 4-23-76

TIME CST	00	01	02	03	04	05	06	07	08	09	10	11	12	13	14	15	16	17	18	19	20	21	22	23	01	02	03
RADAR																											
NRO																											
CIM																											
CHILL																											
WSR-57																		■	■	■							
SOUNDINGS																											
FSI										X						X											
OUN																											
CSM																											
CHK																											
SEL																											
EMC																											
HNT																											
HEN																											
LTS																											
AIRCRAFT																											
RR1 (10 UW)																											
RR2 (C402)																											
RR44 (F4C)																											
INTERCEPT												■	■	■	■	■	■										

May 5, 1976

The morning 500 mb analysis showed a closed low over southern New Mexico with an associated axis of strong height falls (80 m) in southeastern New Mexico and extreme southwestern Texas. Indications were that this system would move toward the northeast during the day. Throughout Texas and Oklahoma, considerable low cloudiness was inhibiting heating, but a clearing zone was moving rapidly into western Texas with the upper wave (Fig. 1.11). Because of this low cloudiness, morning soundings were not encouraging; however, mid-level cooling and drying was expected by mid-afternoon. The principal surface features at 0900 CST (Fig. 1.12) were: (1) a cold front running from Omaha, Nebraska to Raton, New Mexico; (2) a region of low pressure near Tucumcari, New Mexico; (3) a trough line stretching from the low to near San Angelo, Texas, and (4) a second trough west of a line DDC-GAG-MWL (see map).

The morning forecast, issued at 1030 CST, was for severe activity in both the Texas Panhandle and western Oklahoma--timing to coincide with the passage of the upper disturbance.

Storms began developing at approximately 1400 CST in the Texas Panhandle. Intercept crews, directed to a storm which formed near Childress, Texas, obtained movies and 35 mm slides of the storm as it passed Quanah, Texas (see satellite and radar photographs, Figs. 1.13 and 1.14). They also photographed a short lived funnel at 1830 CST. This same storm complex maintained its strength (echo core intensity ≃ 50 dBZ) for several hours. Second trip Doppler data were acquired by NRO from 1820 to 1912 CST as it moved into southwestern Oklahoma (Fig. 1.15); triple Doppler data were gathered at intervals between 2030 and 2140 CST. NRO and CIM continued to collect until 2230 CST.

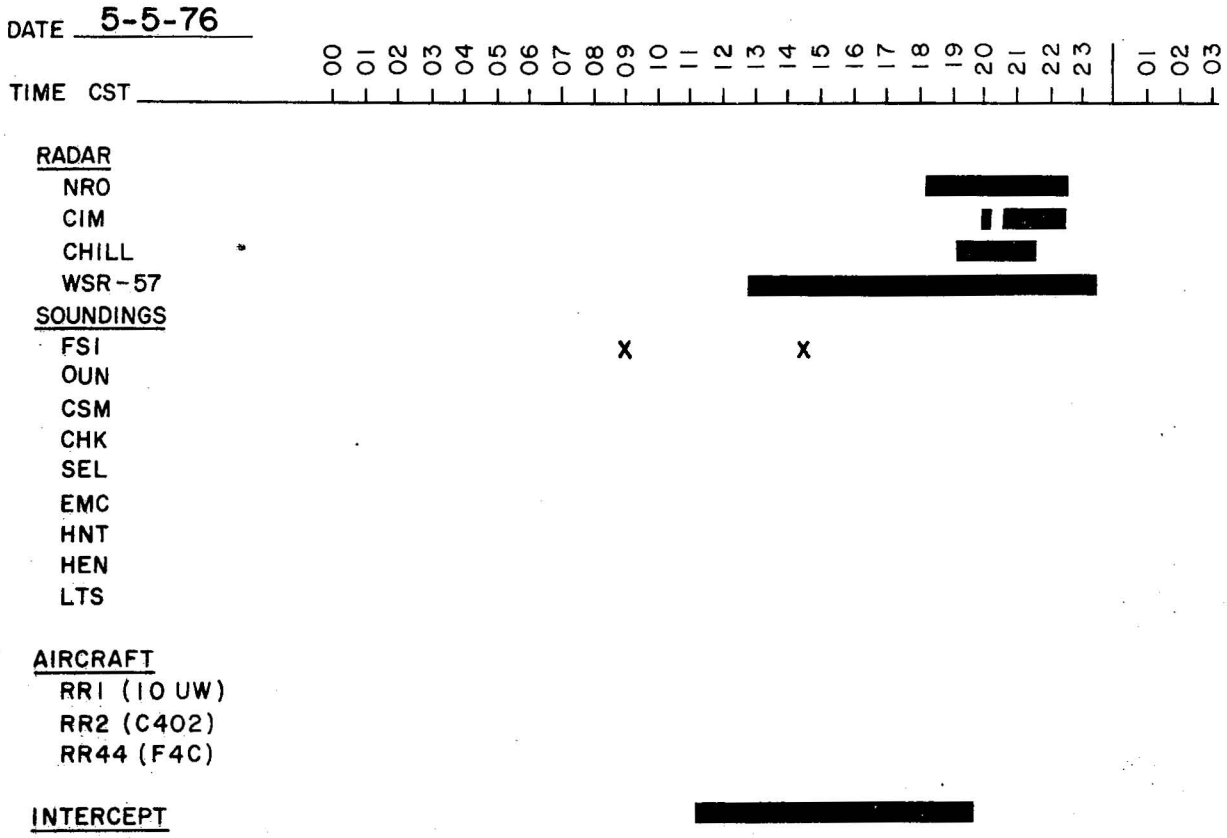

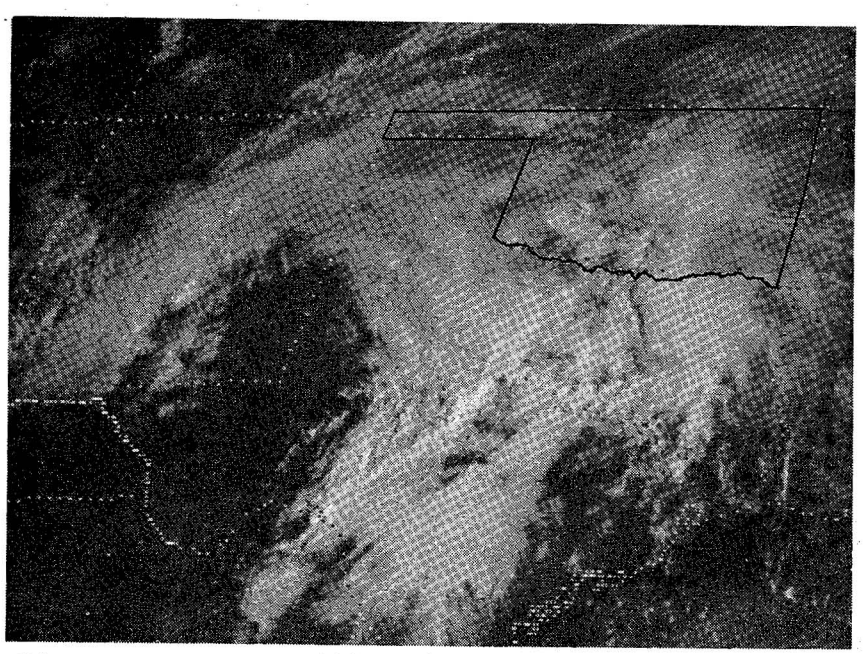

Figure 1.11. Satellite photo 0830 CST: 5 May 1976. Strong disturbances entering western Texas.

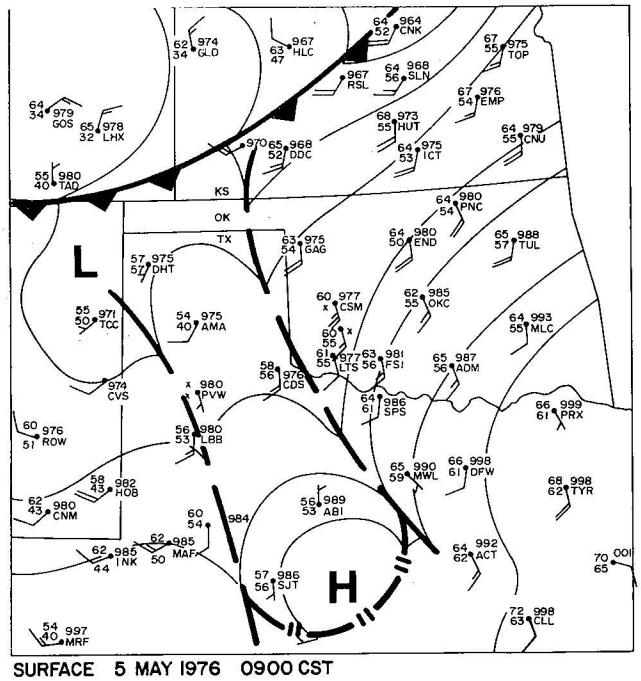

Figure 1.12. Surface analysis 0900 CST: 5 May 1976. Altimeter isobars; analyzed increments in .05".

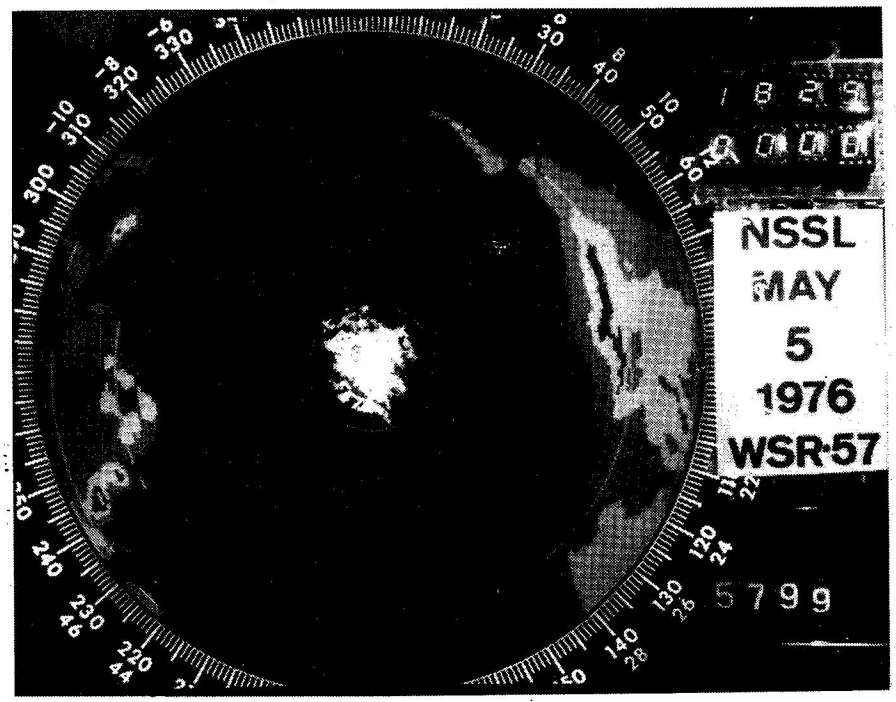

Figure 1.13. WSR-57 radar photo 1829 CST: 5 May 1976. Range intervall 100 km, 0° tilt. Storm near Quanah, Texas.

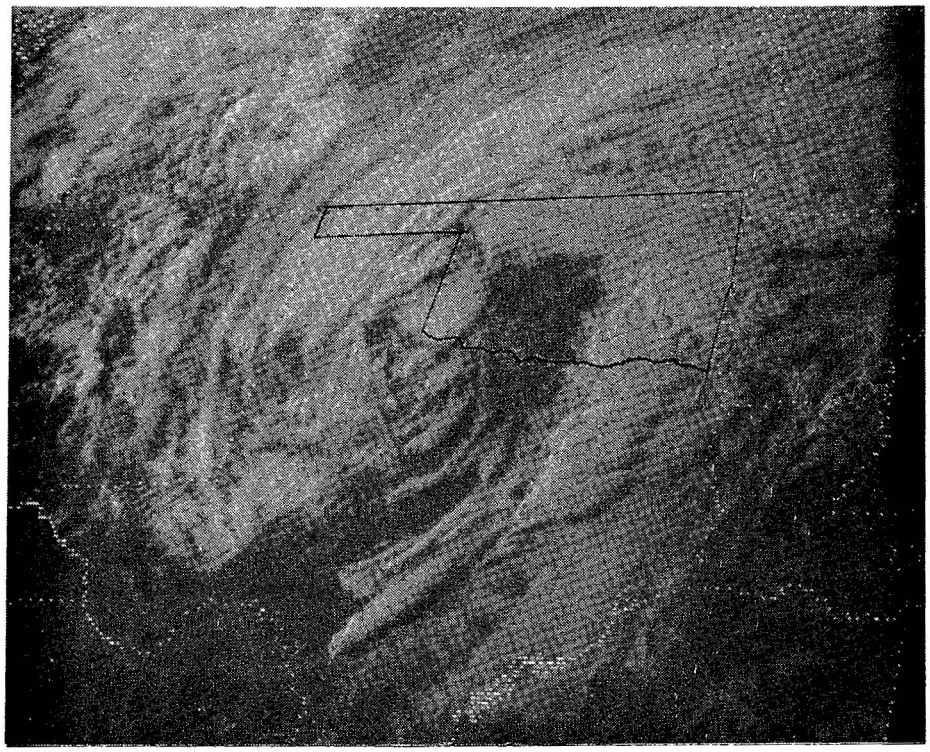

Figure 1.14. Satellite photo 1829 CST: 5 May 1976. CB entering southwestern Oklahoma. A small funnel cloud, associated with this storm, was spotted by NSSL storm intercept personnel a short time later.

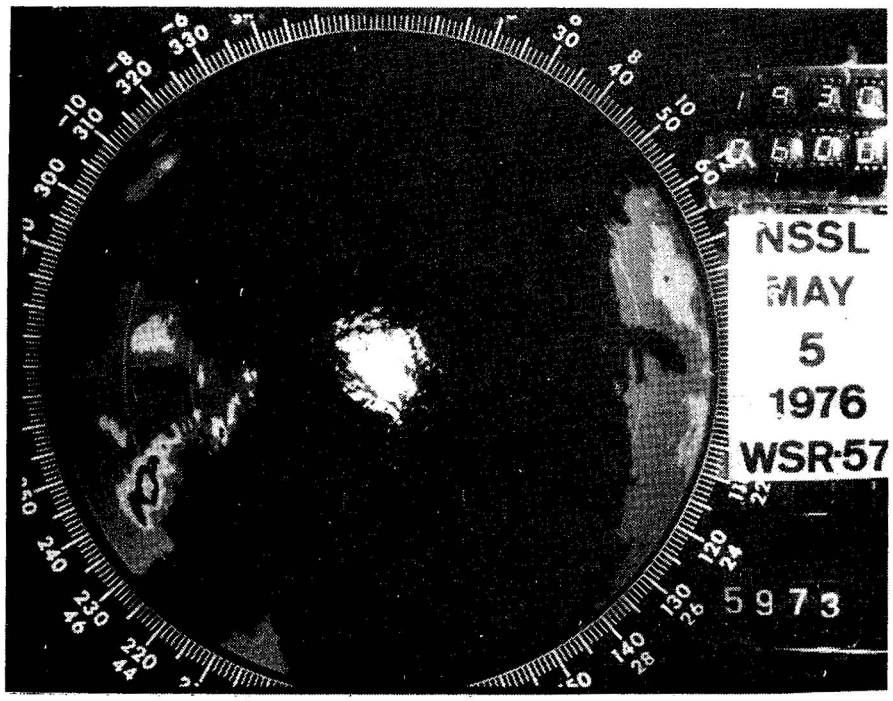

Figure 1.15. WSR-57 radar photo 1930 CST: 5 May 1976. Range interval 40 km 0° tilt. Storm near Altus, Oklahoma.

May 9, 1976

A rapidly moving closed low at 500 mb, situated over southeastern Colorado at 0600 CST, was forecast to move eastward across southern Kansas during the day. An associated surface low was located in southeastern Colorado. The most promising sign for severe weather was a broad region of strong winds aloft in Oklahoma. However, low level moisture was limited and, therefore, the air mass was only slightly unstable (LI; 0 to -2). Numerical prognoses moved the upper support across the study area early--before sufficient moisture could arrive to destabilize the atmosphere.

The morning outlook called for showers and thundershowers (non-severe) in western Oklahoma and the Texas Panhandle. May 9 was a holiday (Mother's Day) with personnel released for the day, however, the situation was somewhat tricky and some staff continued to monitor the developing pattern.

Analysis at 1400 CST revealed that moisture had returned throughout most of western Oklahoma and that the surface trough had not moved as rapidly as expected. The nowcast update showed increasing chances for severe activity in western Oklahoma.

By 1500 CST, strong convective growth had appeared on satellite photographs in western Oklahoma (see e.g., Fig. 1.16). Chase crews left Norman at about 1600 CST. They obtained samples of 1/2" hail (taken from 6" deep drifts near Cordell, Oklahoma), but saw no funnels or tornadoes. CHILL Doppler data were gathered from 1700 CST to 0200 CST (May 10, 1976). NRO began collecting data on a cell to the northwest of Norman at 2130 CST and CIM was operating by 2230 CST. Doppler data gathered after midnight were collected in support of a gust front study at the KTVY instrumented tower.

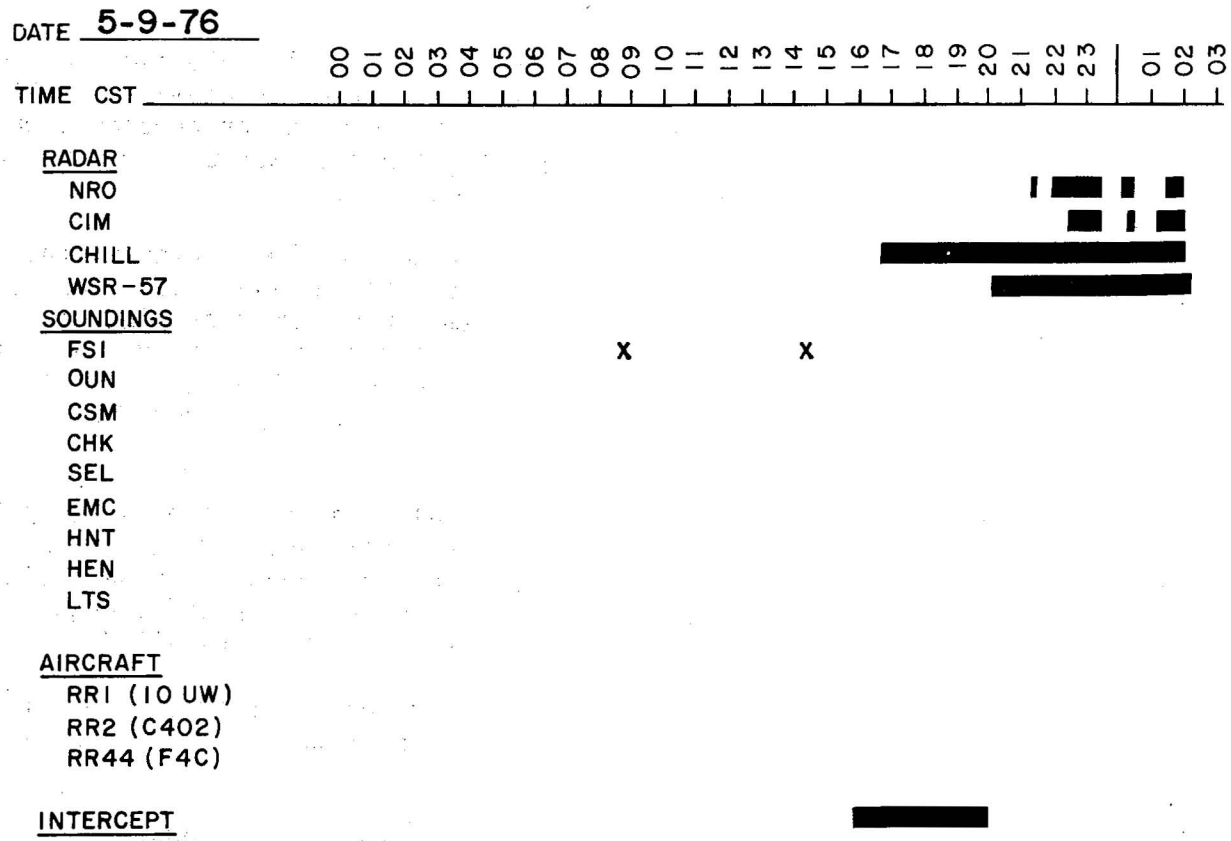

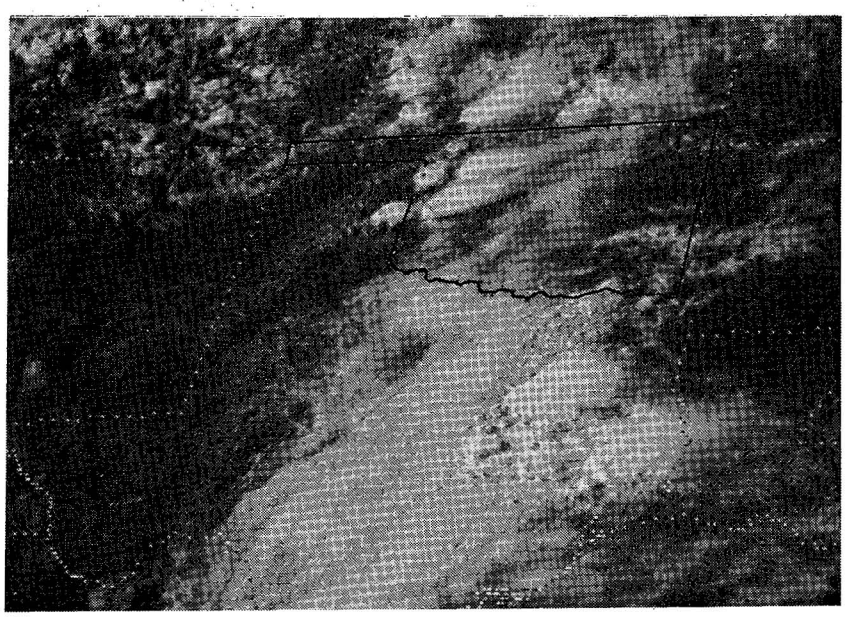

Figure 1.16. Satellite photo 1630 CST: 9 May 1976. Thunderstorms in western Oklahoma.

May 12, 1976

The 36 hour outlook, issued on the morning of May 11, 1976 had been for severe storms to form in the Texas Panhandle and western Oklahoma by early afternoon on May 12. This forecast was based on NMC Computer prognoses which predicted that a surface low, with strong upper support, would be moving into the northern Texas Panhandle by the following morning.

Actual morning position of the surface low was further southeast than suggested--the 0900 CST position was in extreme western Oklahoma. Upper air support was very strong. Because of the system's rapid movement into the state, thunderstorms had already begun in northwestern Oklahoma by the time personnel began arriving at the lab (0700 CST) (Figs. 1.17 and 1.18). The morning forecast, issued at 0930 CST, was for a potentially severe squall line to move across the state during the day.

Intercept teams reached the developing squall line (location - 205°/70 km) shortly after noon (Fig. 1.19) and reported large hail and strong surface winds, but no funnels or tornadoes. The speed of the advancing squall line was such that isolated activity, forming to its south, was rapidly engulfed. Vehicles were unable to stay ahead of the activity, so were recalled early.

Aircraft attempted to collect data during the early afternoon, but the planes were unable to penetrate the squall line and returned to Norman within a few minutes.

Dual-Doppler data were obtained on a strong storm near Anadarko, Oklahoma at 1250 CST and single-Doppler surveillance data are available for the period 1400-1600 CST (Fig. 1.20 and 1.21) on various portions of the squall line. Triple Doppler RHI scans were made from 1300-1330 CST in support of an experiment to study the structure of deep convection. Four special soundings were released at each on nine RAOB sites.

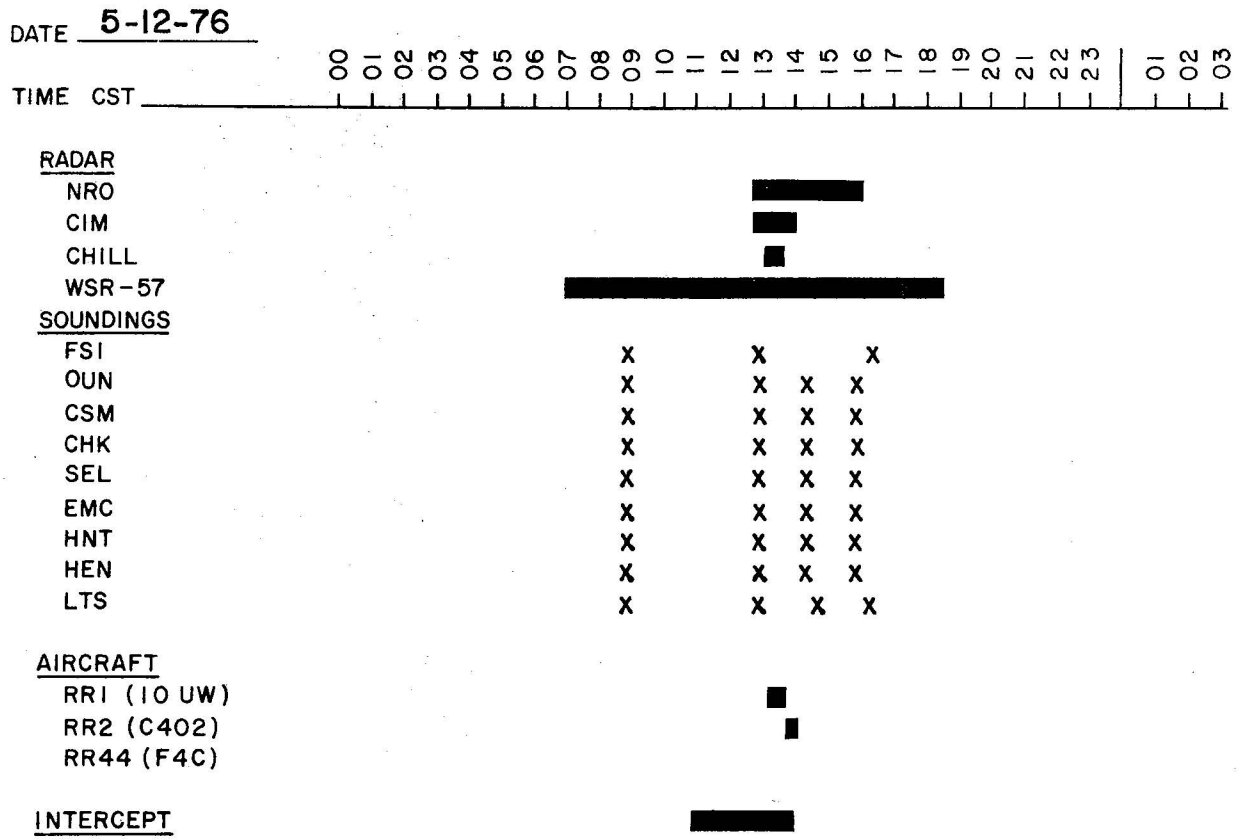
DATE 5-12-76
TIME CST
00 01 02 03 04 05 06 07 08 09 10 11 12 13 14 15 16 17 18 19 20 21 22 23 01 02 03
RADAR
NRO
CIM
CHILL
WSR-57
SOUNDINGS
FSI
OUN
CSM
CHK
SEL
EMC
HNT
HEN
LTS
AIRCRAFT
RR1 (10 UW)
RR2 (C402)
RR44 (F4C)
INTERCEPT

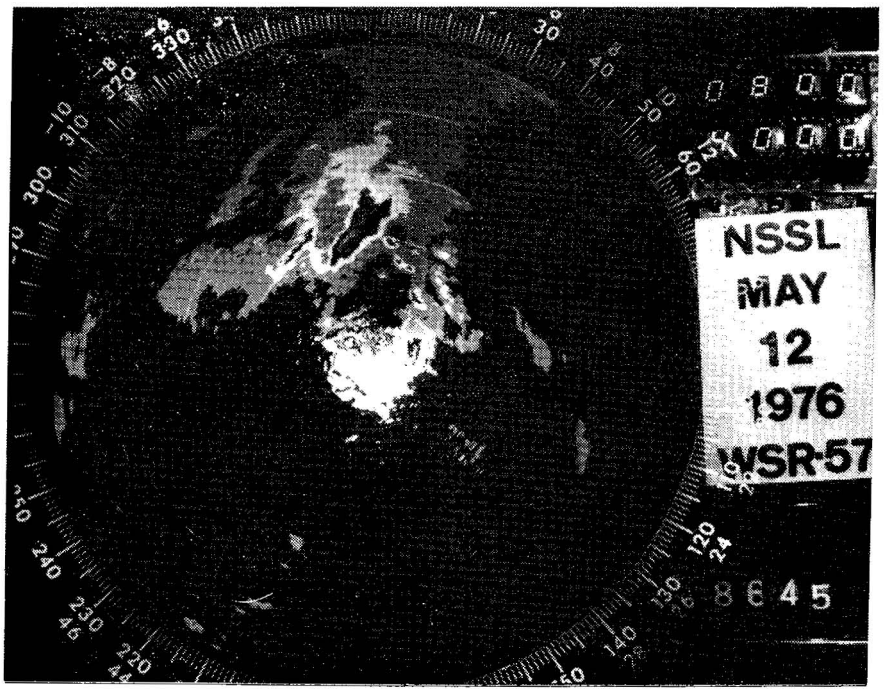

Figure 1.17. WSR-57 radar photo 0800 CST: 12 May 1976. Range interval 40 km, 0° tilt. Early morning activity to the north.

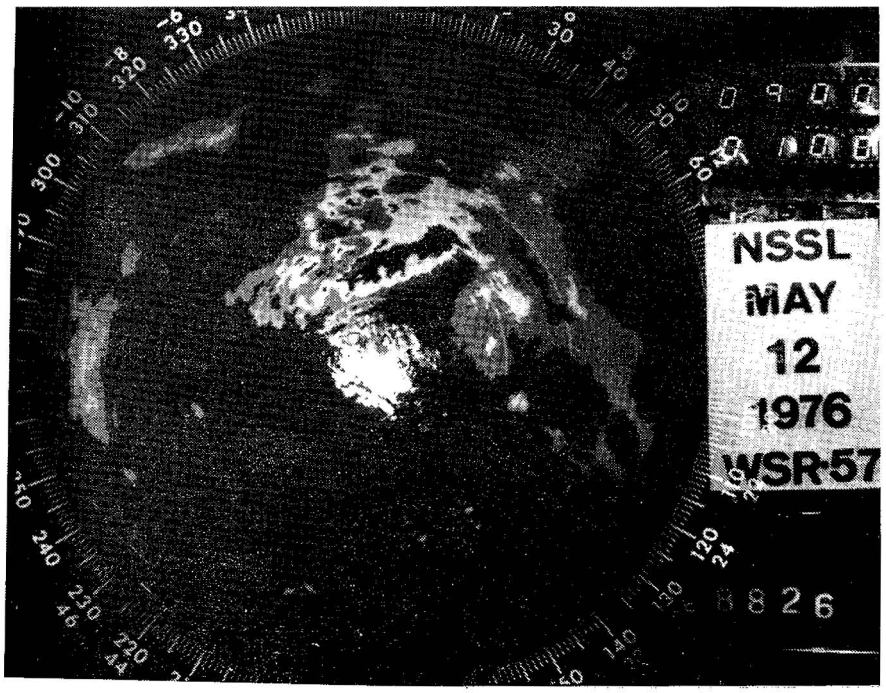

Figure 1.18. WSR-57 radar photo 0900 CST: 12 May 1976. Range interval 40 km, 0° tilt. Building squall line approaches from the north.

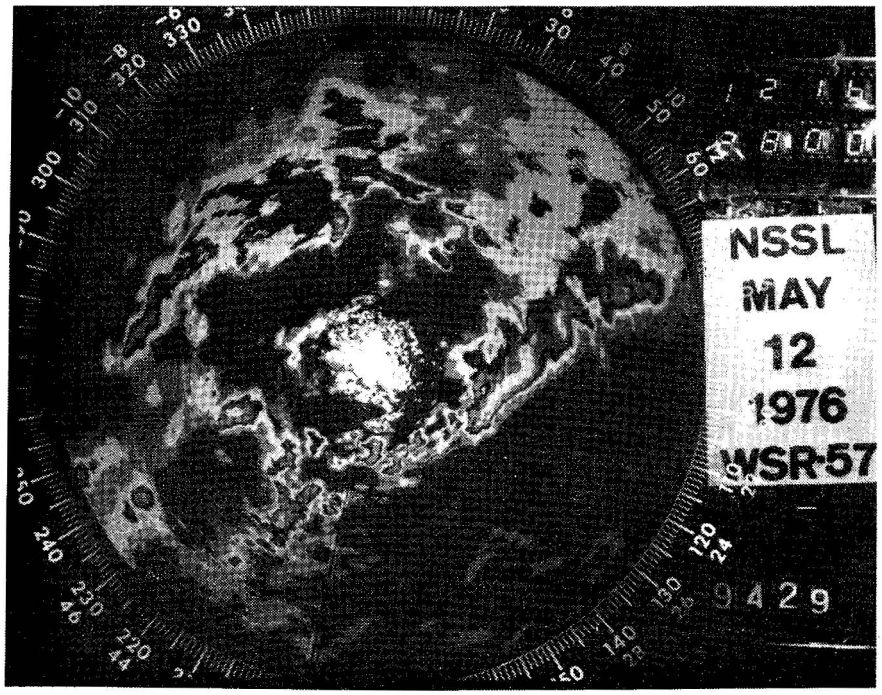

Figure 1.19. WSR-57 radar photo 1216 CST: 12 May 1976. Range interval 40 km, 0° tilt. Squall line to the south. Overrunning storms north.

Figure 1.20. WSR-57 radar photo 1359 CST: 12 May 1976. Range interval 40 km, 0° tilt. Squall line "filling in".

Figure 1.21. WSR-57 radar photo 1445 CST: 12 May 1976. Range interval 40 km, 0° tilt. Nearly solid squall line.

May 21, 1976

Morning synoptic features included a moderately unstable air mass over most of western Oklahoma (LI -2 to -4) with greater instability in western Texas (LI -6). The upper wind structure which had been weak for several days, was changing; a splitting jet stream left western Texas beneath moderately intense, diverging winds. A region of strong cyclonic wind shear was evident at 500 mb and 850 mb analysis revealed a low level moisture ridge in western Texas. At the surface, a trough line extended southward from a low in northeastern New Mexico, through west Texas. It was expected that dry air at mid-levels over New Mexico would develop a surface dry front along the trough line. Severe thunderstorms were forecast to form on the dryline in Texas and move into western Oklahoma by late afternoon.

The earliest activity was identified on satellite at approximately 1200 CST near Plainview, Texas (Figs. 1.22 and 1.23). Intercept crews photographed a funnel near Lockney, Texas (1714 CST), a funnel near Cap Rock, Texas (1822 CST) and extreme wind damage near Slaton, Texas (1932 CST). Two inch diameter hail was observed on the ground near Post, Texas at 1920 CST. Storms lost intensity dramatically before reaching the Oklahoma border. No Doppler data were collected.

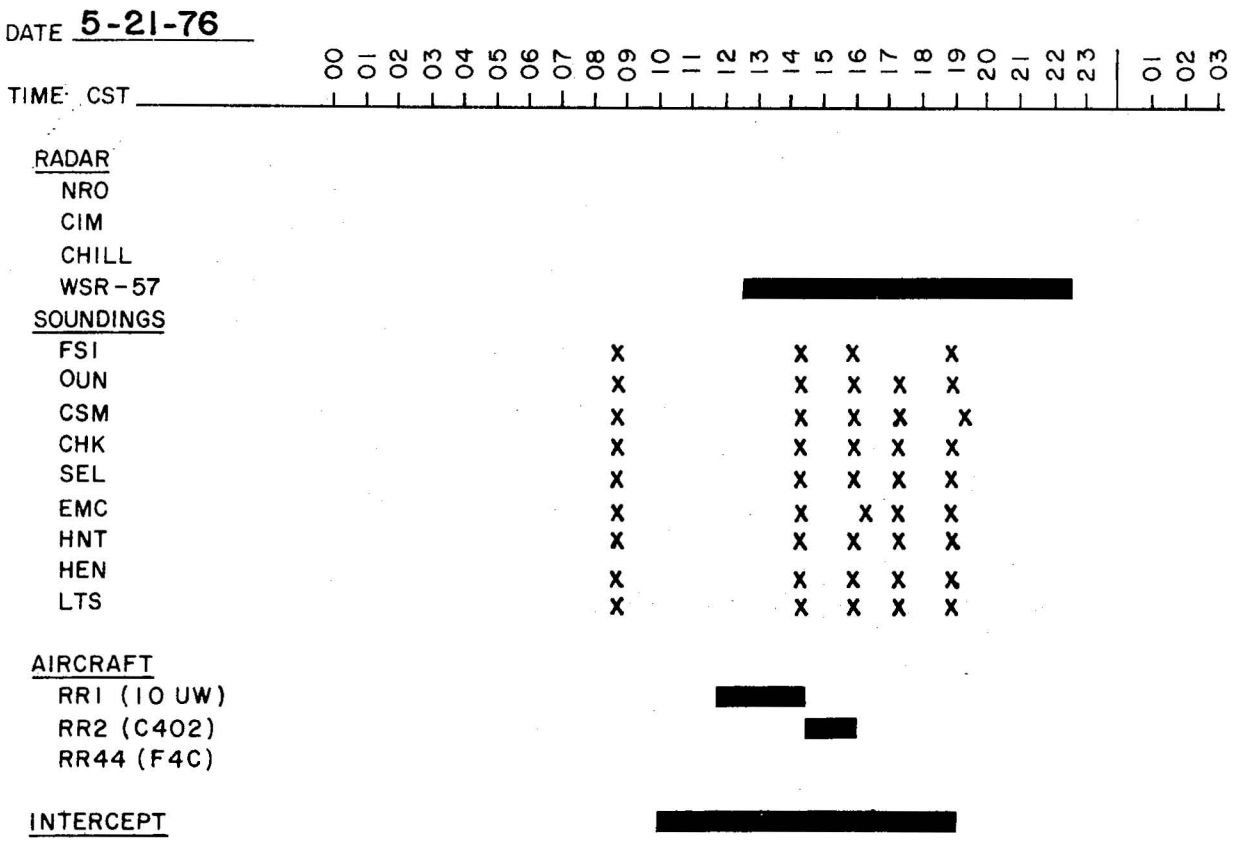

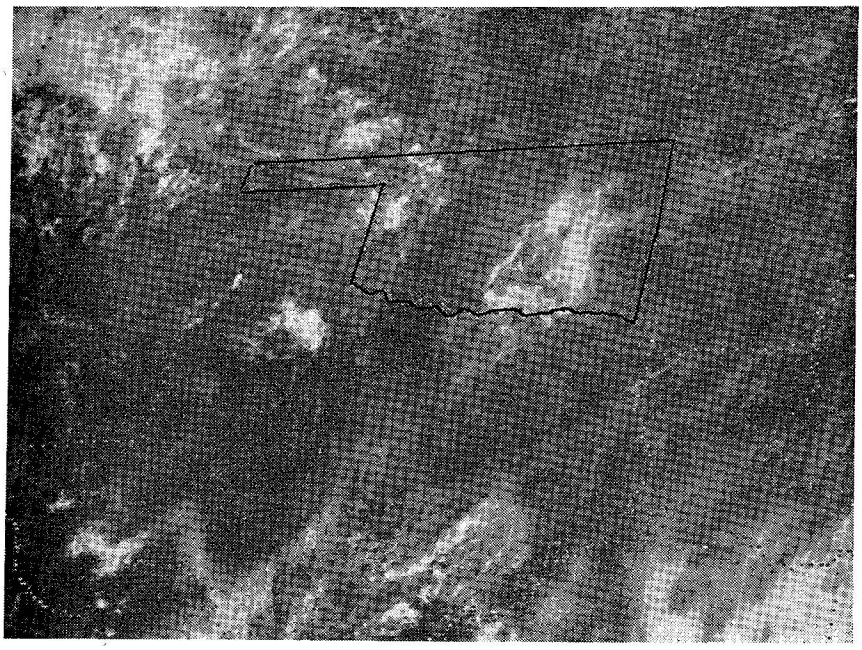

Figure 1.22. Satellite photo 1200 CST: 21 May 1976. Growing towers near Plainview, Texas.

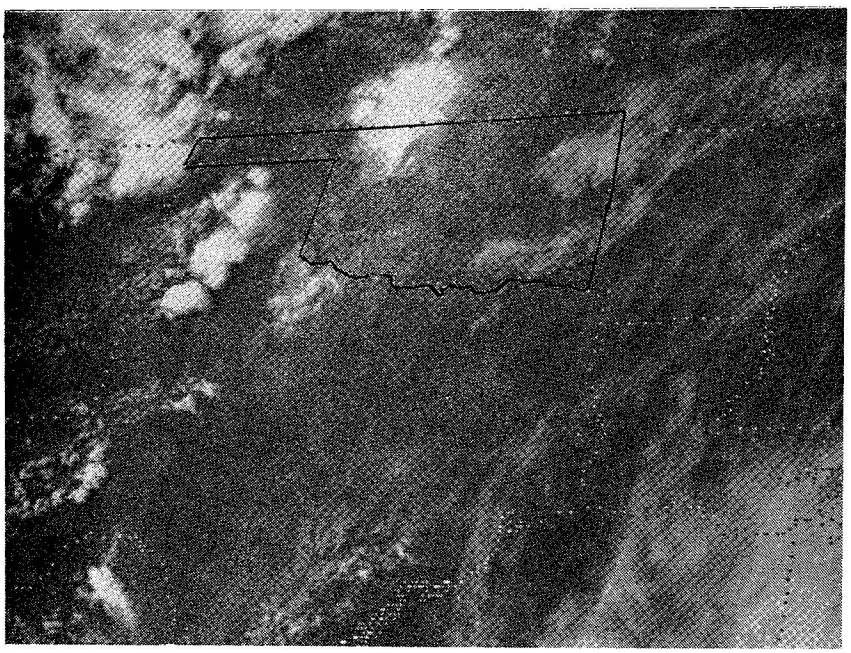

Figure 1.23. Satellite photo 1530 CST: 21 May 1976. Strong convective activity in the central Texas Panhandle.

May 22, 1976

At 0600 CST, a moderately strong upper air trough was approaching Oklahoma from the west with the axis of maximum positive vorticity advection (PVA) over western New Mexico. A splitting jet stream again left western Texas beneath relatively strong, diverging winds. The 700 mb "no change" line was in the eastern Texas Panhandle and the center of the 850 mb moisture ridge extended along an arc from Stephenville, Texas to the central Texas Panhandle. Over western Oklahoma, the air mass was conditionally unstable (LI -4). There was low level convergence along a surface cold front in the western portion of Oklahoma and surface lows were found near Dodge City, Kansas and Childress, Texas. Severe thunderstorms were expected to form on the cold air boundary in southwestern Oklahoma during the afternoon.

By 1500 CST, surface analysis revealed that the cold air behind the front had heated and mixed to the point that the boundary was no longer identifiable and that a dryline in the central Texas Panhandle had become the dominant surface feature. Further verification was supplied by satellite photos (Fig. 1.24) which showed rapidly growing convective towers in the Texas Panhandle. Nowcast update called for this activity to intensify and move into Oklahoma by 2000 CST. Intercept crews--originally directed to Altus, Oklahoma were instructed to continue west into Texas, where they collected 1 inch to 2 inch diameter hail samples (near Turkey, Texas) at 1700 CST. They reported no tornadic activity.

At 1830 CST, a squall line began forming in western Oklahoma ahead of the older activity (Figs. 1.25 and 1.26). A very complete data set was obtained on this line. Several hours worth (see bar graph) of triple Doppler and aircraft data were gathered. A portion of the squall line crossed the NSSL surface mesonetwork (beginning about 2030 CST) and gust front data were obtained as the storms approached the KTVY instrumented tower. In addition, 81 soundings were obtained prior to and during squall line passage.

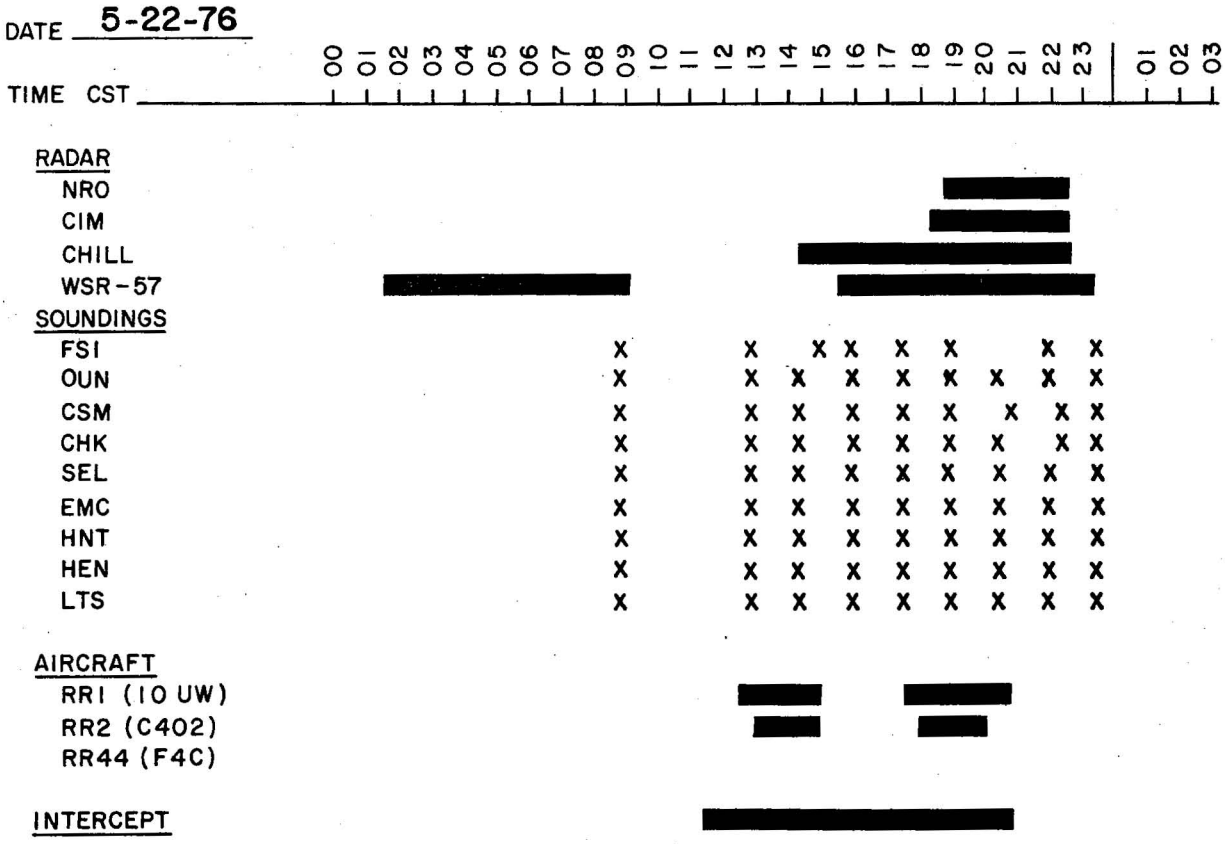

Figure 1.24. Satellite photo 1430 CST: 22 May 1976. Convective activity in western Texas.

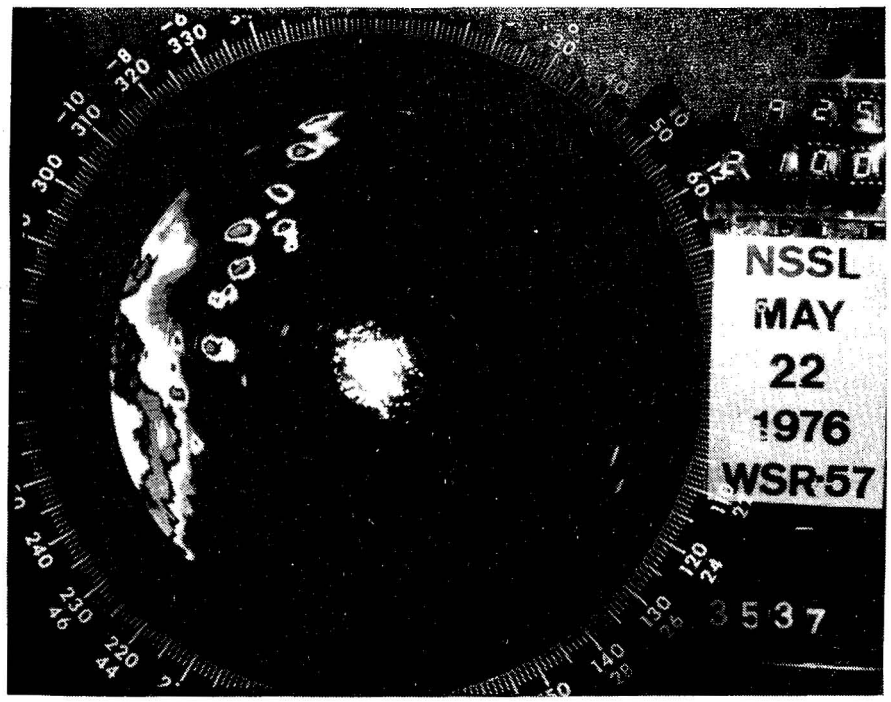

Figure 1.25. WSR-57 radar photo 1925 CST: 22 May 1976. Range interval 40 km 0° tilt. Squall line entering western Oklahoma.

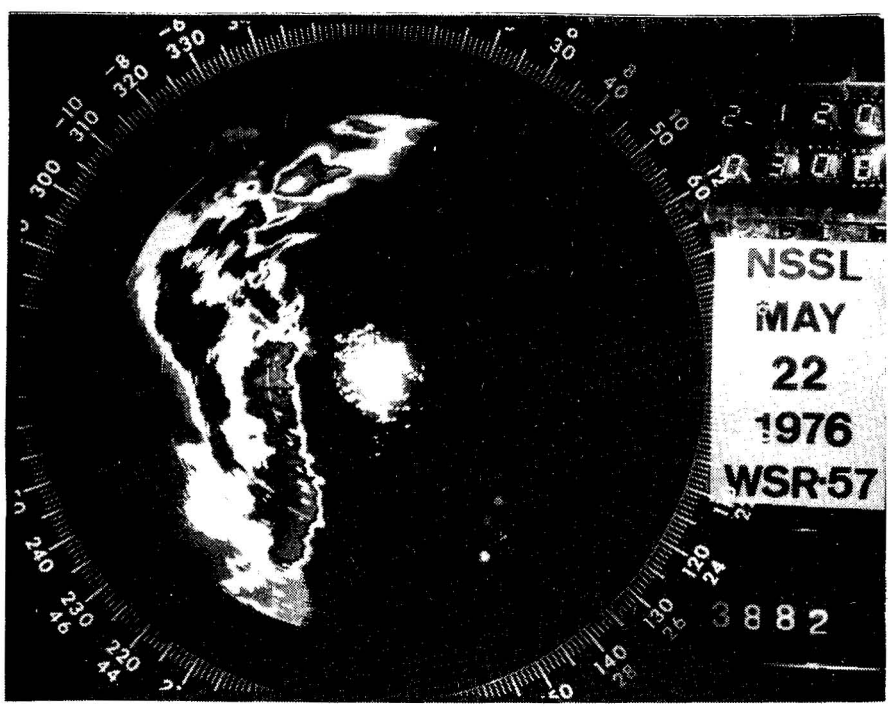

Figure 1.26. WSR-57 radar photo 2120 CST: 22 May 1976. Range interval 40 km, 0° tilt. Squall line approaching Norman.

May 24, 1976

Morning surface analysis showed slightly cooler and drier air approaching from the northwest and numerical progs indicated that mild ridging would occur throughout the day. Because there was a mildly unstable air mass over Oklahoma (LI -2), and strong winds aloft, a chance for high based, non-severe thunderstorms was carried in the morning forecast.

Storms formed to the east of Norman at 1230 CST. They did not become severe and by late afternoon had dissipated. Aircraft and dual-Doppler data were collected on these storms during a short portion of the afternoon (see graph).

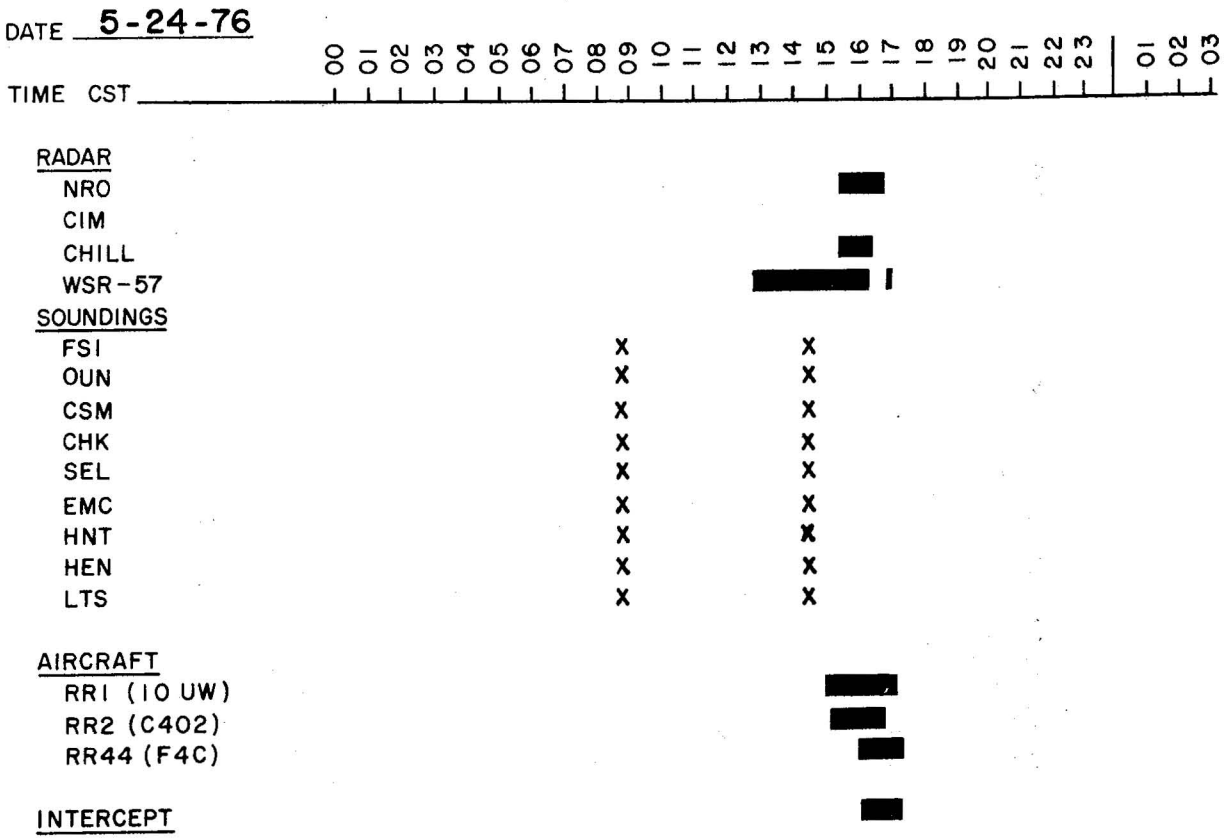

May 25, 1976

A surface low was located about 60 miles north of Midland, Texas with a warm front extending eastward along the Red River. A dryline extended from eastern New Mexico to the surface low in Texas--then due southward from there. A strong shortwave to the west was expected to move into Texas during the day and to be affecting western Oklahoma by early evening. Lifted indices ranged from (-2) in central Oklahoma, to (-7) in the Texas Panhandle, to as high as (-10) in southwestern Texas. Winds above 30,000 ft exceeded 100 knots.

A dry push was expected to develop in southwest Texas in response to the approaching shortwave. The morning forecast called for severe storms (potentially tornadic) to build during the afternoon in western Texas and move into Oklahoma after dark. Strong hailstorms were considered possible along the warm front in southern Oklahoma.

At 1200 CST, it was noted that a large supercell, which had formed near Trinidad, Colorado some 24 hours earlier, was continuing to propagate across northern Texas. Low-level, cool outflow from this storm was essentially destroying the warm fronts' potential for triggering severe activity in Oklahoma and, thus, the prospect of hailstorm formation in southern Oklahoma was removed from the updated forecast. The wide extent of activity is evident in Fig. 1.27.

Storms formed near Abilene, Texas at about 1300 CST. Intercept crews photographed a large funnel cloud 5 miles southwest of Rising Star, Texas at 1746 CST. Activity next appeared in the Texas Panhandle, then crossed into western Oklahoma at approximately 1630 CST. No tornadic activity occurred in the state. CHILL Doppler data were collected beginning at 2140 CST and all three Dopplers operated between 2315 CST and 0130 CST (May 26); however, due to a lightning strike, CIM Doppler was out of operation for twelve minutes, from 0007 to 0019 CST (May 26). A strong squall line gust front passed the KTVY instrumented tower at 0014 CST (May 26). A well defined "thin line" was observed on radar in association with this gust front (Fig. 1.28).

May 26, 1976

At 0600 CST, a 500 mb closed low was situated over the Texas Panhandle with a moderately strong, embedded shortwave. Morning soundings showed that the air mass over the study area was extremely unstable and that the vertical wind structure was conducive to severe storm formation (Fig. 1.29). Central Texas and western Oklahoma had the prime moisture influx at 850 mb.

Surface analysis at 0800 CST revealed a cold front along the western Oklahoma border and a thunderstorm cold air boundary (associated with early morning activity) extending from Ponca City, Oklahoma to Oklahoma City to Chillicothe, Texas, where it intersected a region of low pressure on the cold front. A warm front extended from the low, across southeastern Oklahoma.

The surface low was forecast to move eastward during the day. Severe activity was expected to form by early afternoon at the warm front-surface low intersection--possibly in the prime Doppler area.

By 1020 CST, newly formed convection near Duncan, Oklahoma (Fig. 1.30), was appearing on radar. At 1150 CST, NRO Doppler reported an extremely well defined circulation signature in the Elmore City, Oklahoma vicinity (Fig. 1.31) and, shortly thereafter, "chase" reported photographing a funnel cloud at the location. Storm intercept units provided 35 mm slides of funnels near Pike City, Oklahoma (182°/95km) (1220 CST), Nebo, Oklahoma (155°/110km) (1323 CST), Gainesville, Texas (170°/180km) (1415 CST), and Denton, Texas (175°/230 km) (1450 CST). Time lapse films were obtained of rotating regions of lowered cloud base (wall clouds) near Gainesville, Texas (170°/180 km) (1415 CST) and Denton, Texas (175°/230 km) (1450 CST). A short-lived tornado was photographed near Marietta, Oklahoma (168°/145 km) (1512 CST) and movies were taken of a small tornado near Aubrey, Texas (168°/220 km) (1320 CST) and a larger tornado in Dallas, Texas (1630 CST). Figure 1.32 illustrates activity near the time of the Dallas tornado.

Multiple Doppler data were collected during a large portion of the afternoon (see bar graph--also Figures 1.30 through 1.35) and aircraft data were obtained near a strong gust front in the early morning and in the vicinity of strong storms (south of Norman) during the afternoon. A rather unusual data set was collected by NRO Doppler. At approximately 1400 CST, a strong circulation (diameter 15 km) was detected in a storm near Lindsay, Oklahoma. During the next one and one half hours the cell lost intensity, finally becoming a large area of light rain; however, the circulation remained--increasing in diameter as the shower area increased--until it filled an area too large to be effectively mapped by the radar. 1400 CST surface analysis shows that this cell originally developed near the center of a low pressure region (Fig. 1.36) about which circulation was strong. Although the exact point at which the scale transition was made and the mechanism thereof, is not clear; enough data exist to make a case study possible.

DATE 5-26-76

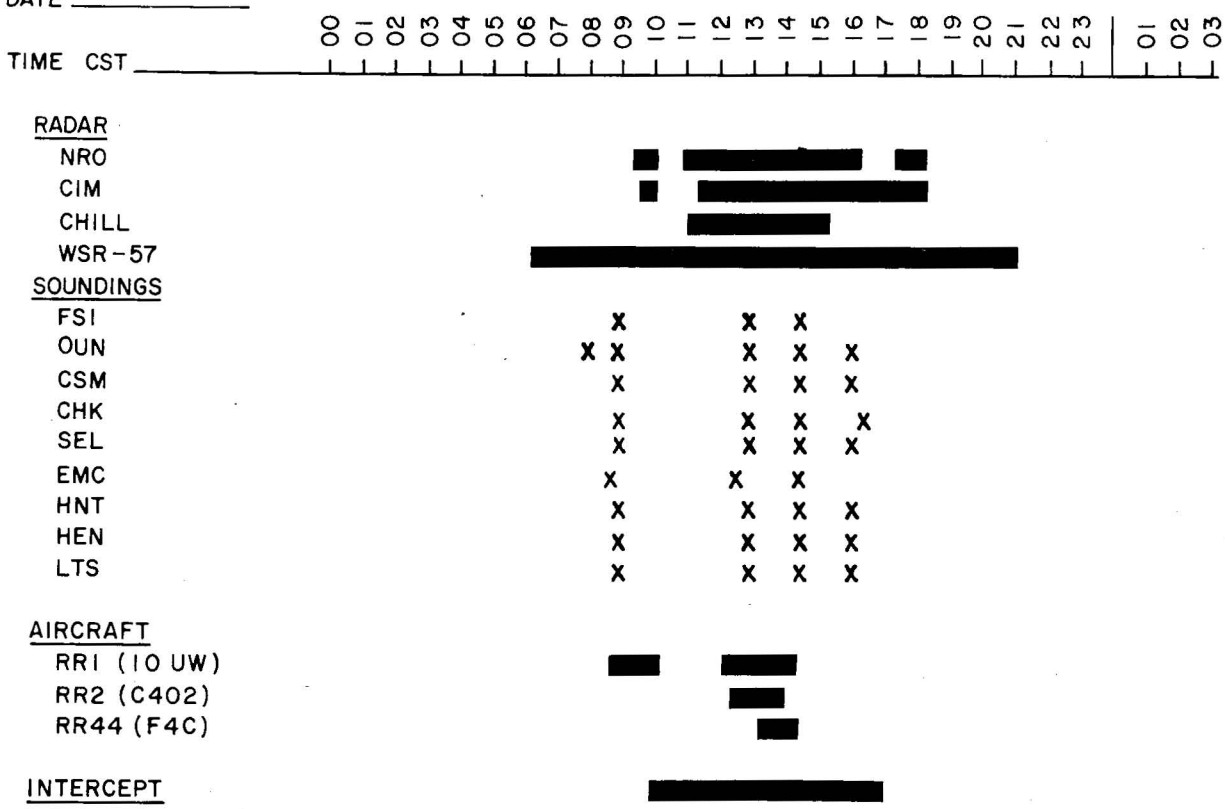
TIME CST
00 01 02 03 04 05 06 07 08 09 10 11 12 13 14 15 16 17 18 19 20 21 22 23 01 02 03
RADAR
NRO
CIM
CHILL
WSR-57
SOUNDINGS
FSI
OUN
CSM
CHK
SEL
EMC
HNT
HEN
LTS
AIRCRAFT
RR1 (10 UW)
RR2 (C402)
RR44 (F4C)
INTERCEPT

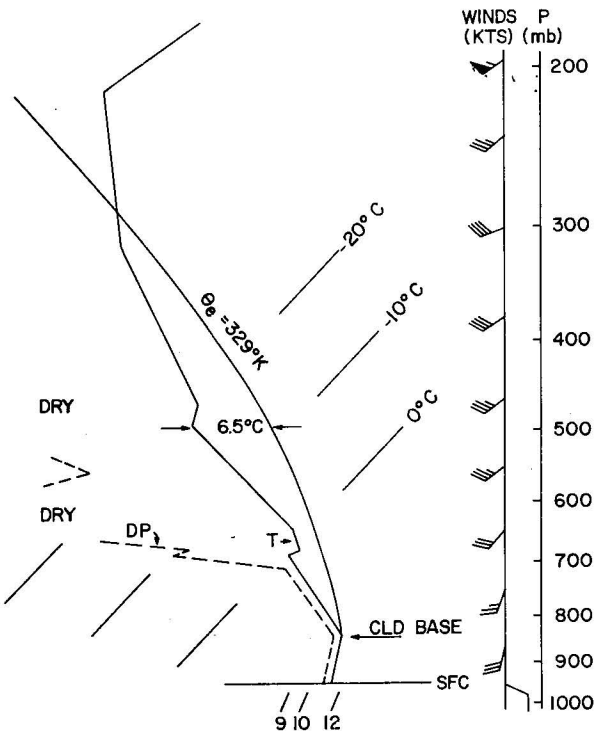

Figure 1.29. Oklahoma City sounding 0600 CST: 26 May 1976, plotted on Skew T-Log P diagram. Temperature (T) and dewpoint (DP) traces so indicated. Lifted parcel moist lapse rate corresponds to $\theta_e = 329° K$ based on afternoon mixed boundary layer.

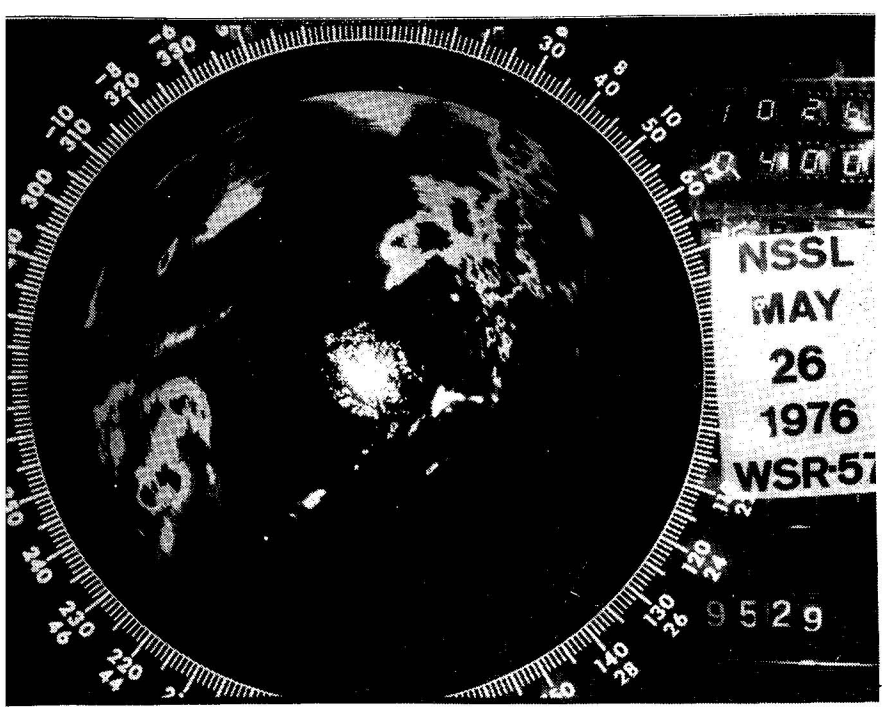

Figure 1.30. WSR-57 radar photo 1026 CST: 26 May 1976. Range interval 40 km, 0° tilt. New convective activity south. Activity to the north dissipating while that to the southwest remains constant in strength.

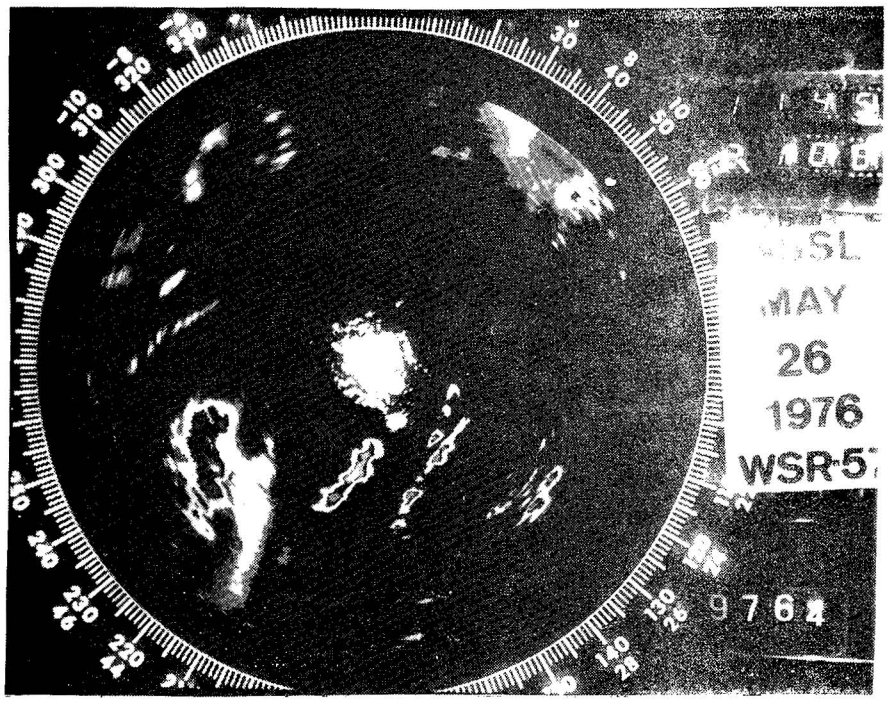

Figure 1.31. WSR-57 radar photo 1145 CST: 26 May 1976. Range interval 40 km, 0° tilt. Compare with Figure 1.30.

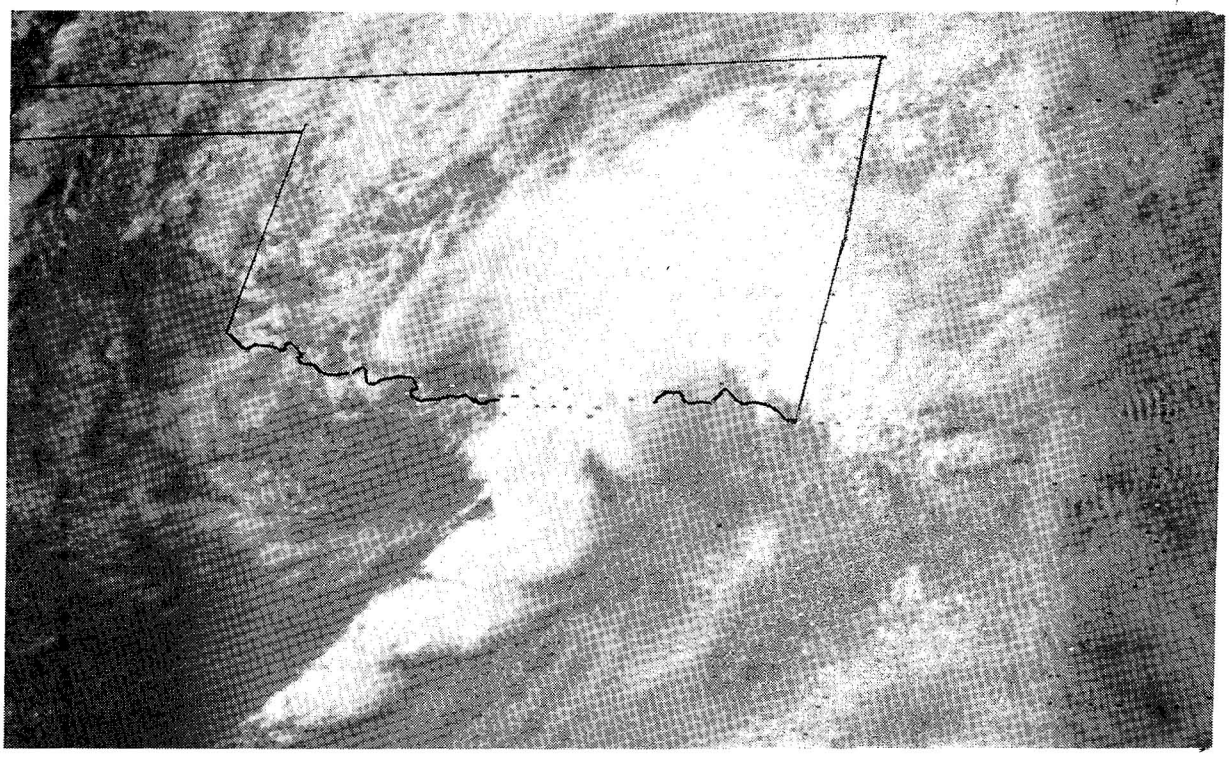

Figure 1.32. Satellite photo 1600 CST: 26 May 1976. CB's along cold front in north-central Texas near the time of the Dallas tornado.

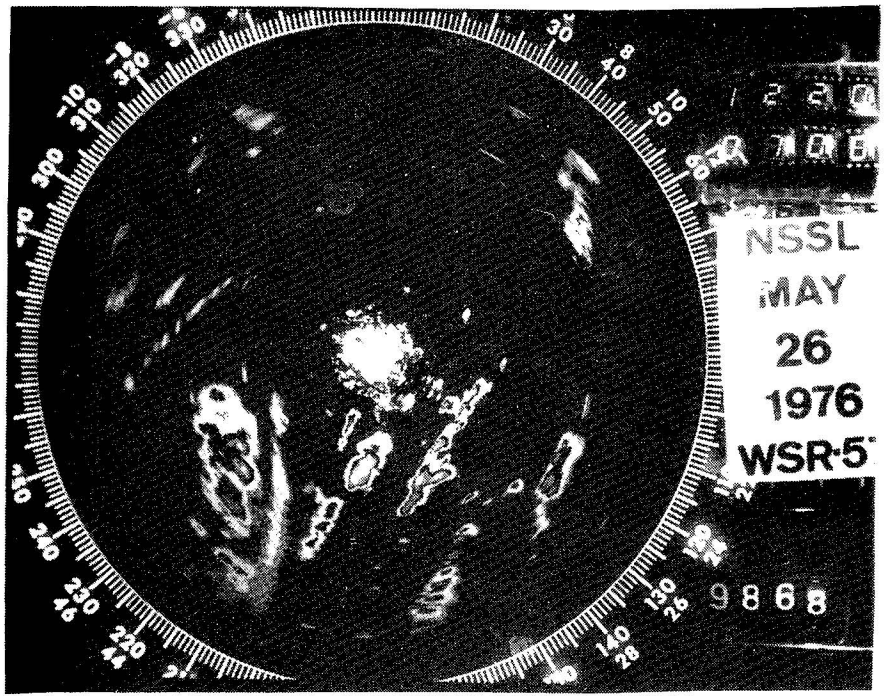

Figure 1.33. WSR-57 radar photo 1220 CST: 26 May 1976. Range interval 40 km, 0° tilt. Compare Figure 1.30, 1.31.

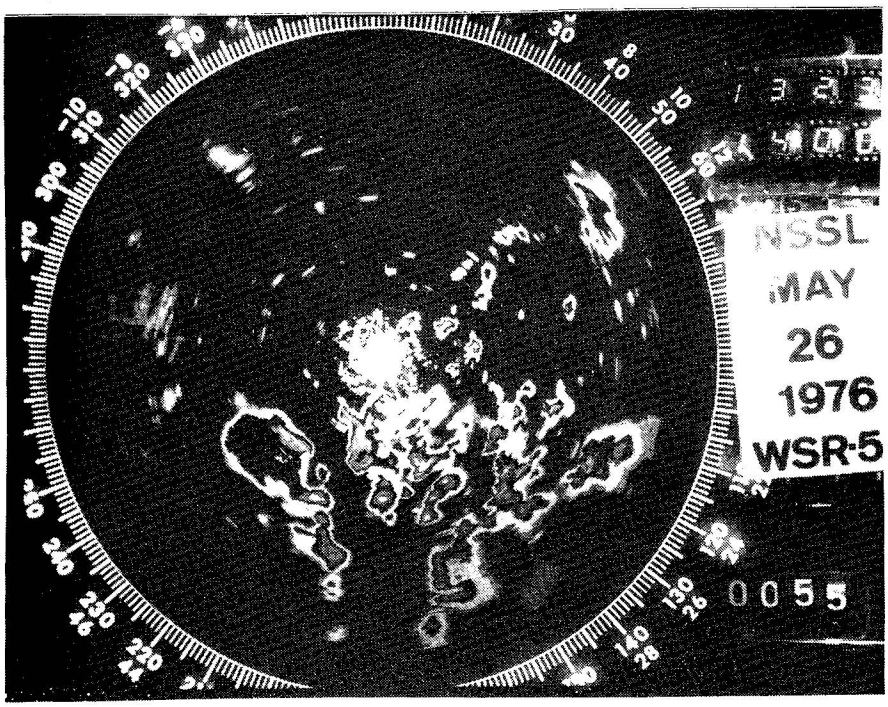

Figure 1.34. WSR-57 radar photo 1323 CST: 26 May 1976. Range interval 40 km, 0° tilt. Compare previous photos.

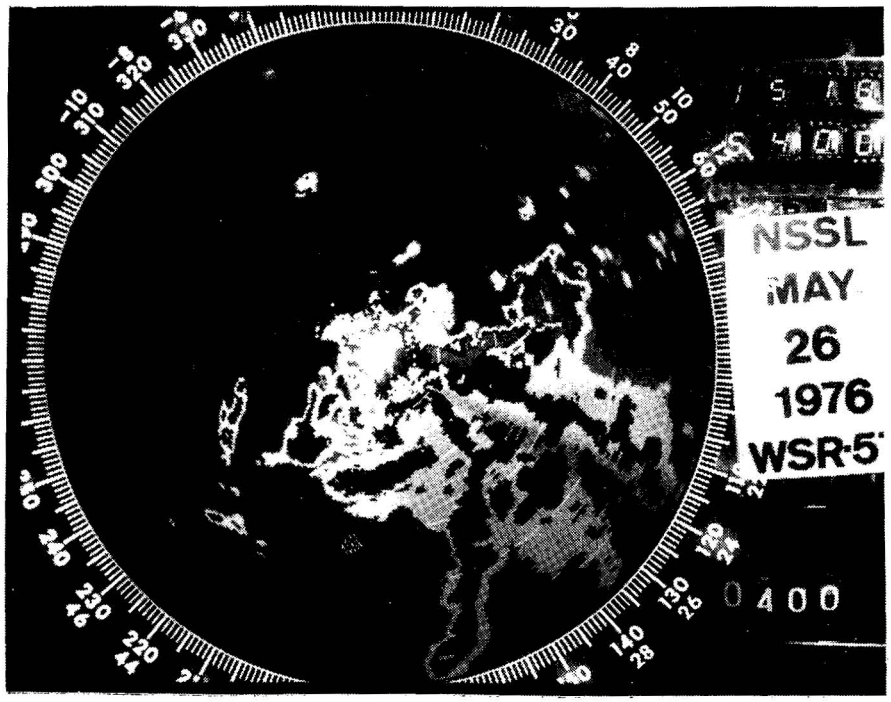

Figure 1.35. WSR-57 radar photo 1518 CST: 26 May 1976. Range interval 40 km, 0° tilt. Compare previou photos.

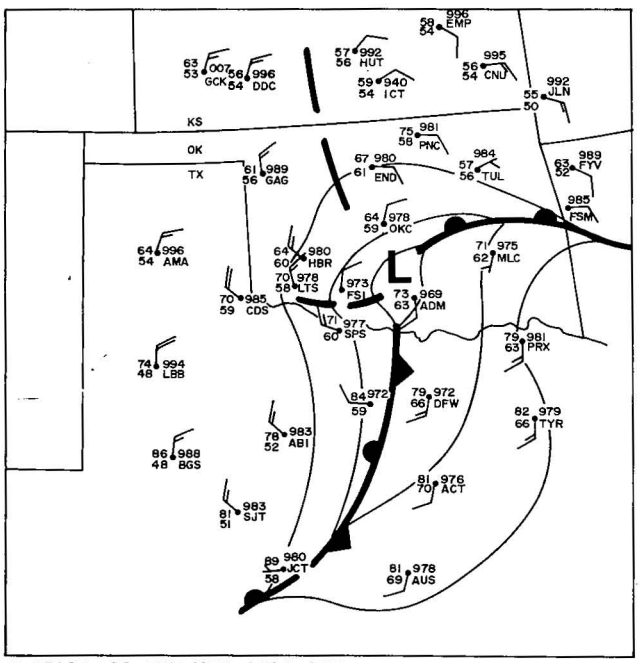

Figure 1.36. Surface analysis 1400 CST: 26 May 1976 Altimeter isobars; analyzed increments in .05".

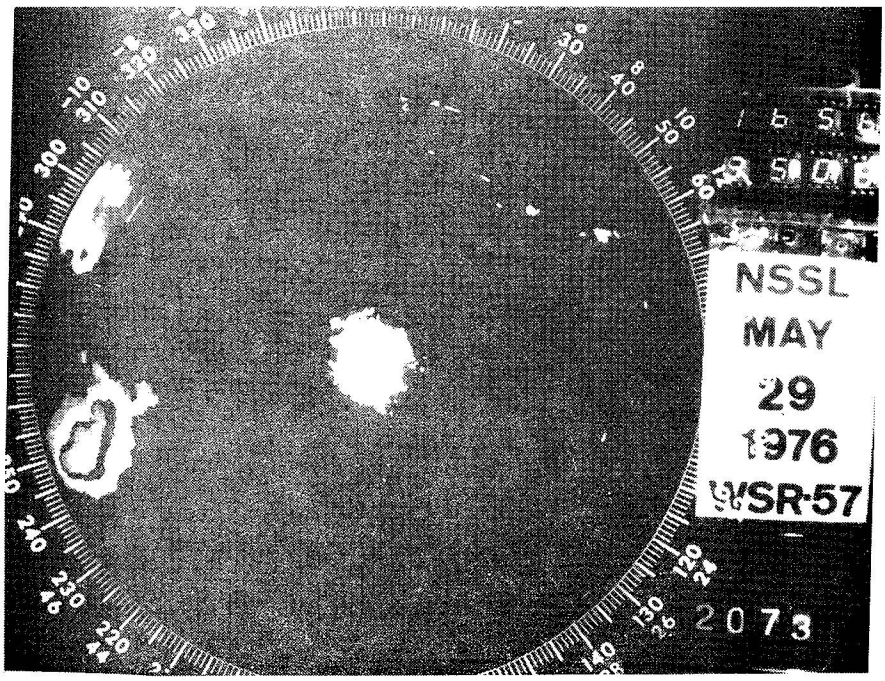

Figure 1.37. WSR-57 radar photo 1656 CST: 29 May 1976. Range interval 40 km, 0° tilt. Storm near Altus, Oklahoma (250° at 220 km).

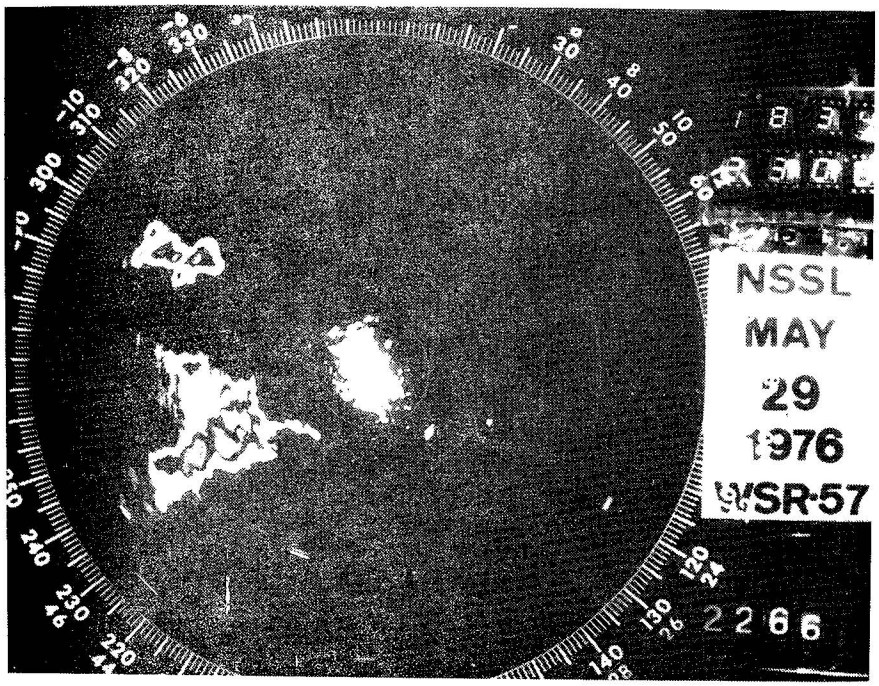

Figure 1.38. WSR-57 radar photo 1834 CST: 29 May 1976. Range interval 40 km, 0° tilt. Circulation "notch" at 240° at 140 km.

Figure 1.39. Hennessey, Oklahoma (HEN) sounding 1901 CST: 29 May 1976, plotted on Skew T - Log P diagram. Temperature (T) and dewpoint (DP) traces so indicated. Sounding prior to "heat burst".

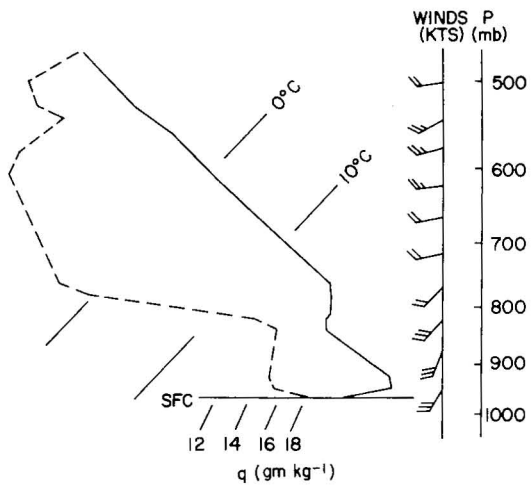

Figure 1.40. HEN sounding 2200 CST: 29 May 1976, plotted on Skew T - Log P diagram. Temperature (T) and dewpoint (DP) traces so indicated. Post "heat burst".

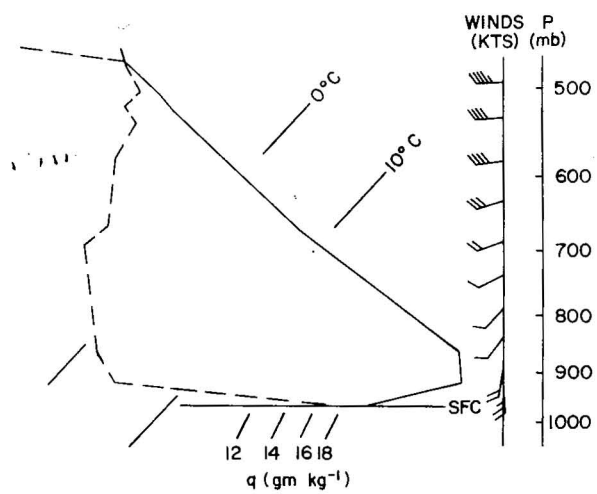

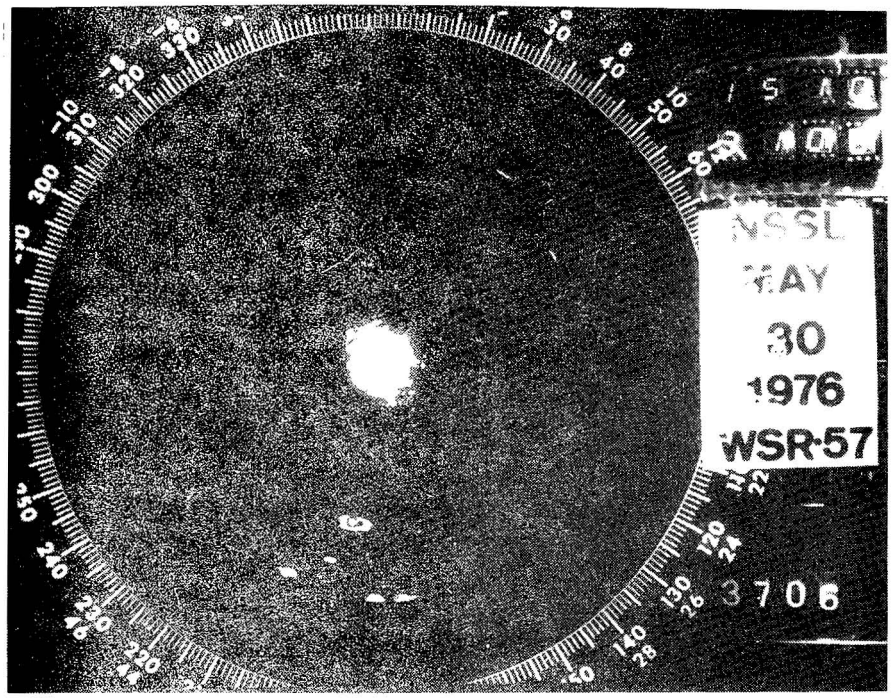

Figure 1.42. WSR-57 radar photo 1510 CST: 30 May 1976. Range interval missing, 0° tilt. Note rapid growth of Ringling cell, compare Fig. 1.41.

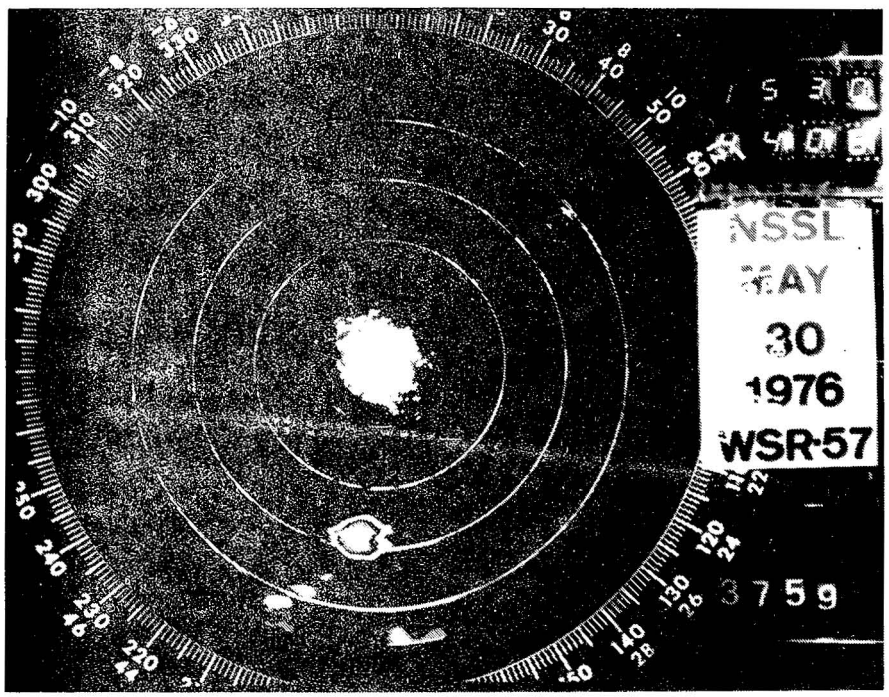

Figure 1.43. WSR-57 radar photo 1530 CST: 30 May 1976. Range interval 40 km, 0° tilt. Compare Figs. 1.41, 1.42.

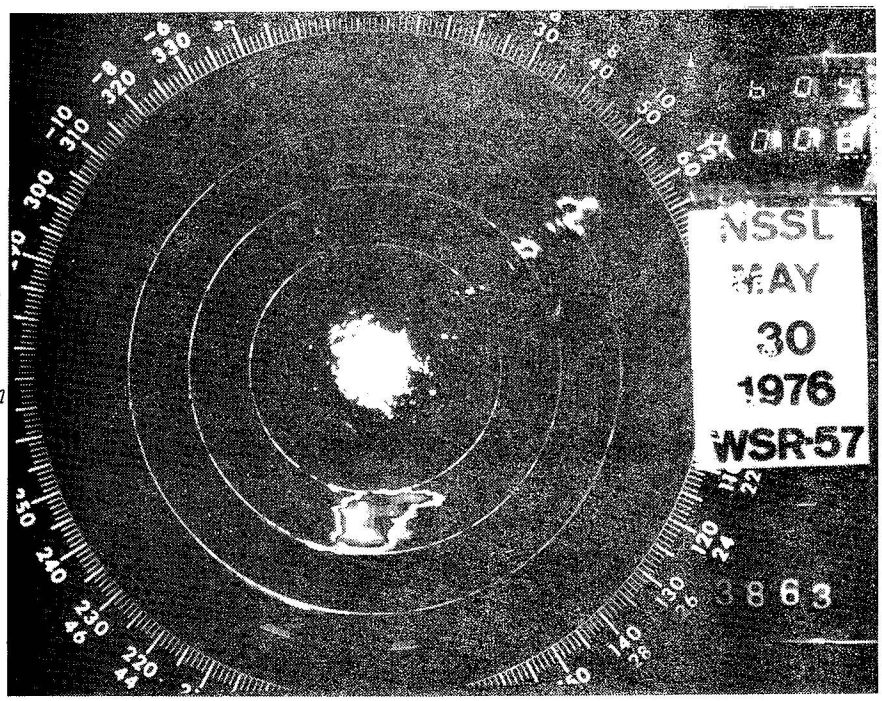

Figure 1.44. WSR-57 radar photo 1604 CST: 30 May 1976. Range interval 40 km, 0° tilt. Ringling storm begins to split.

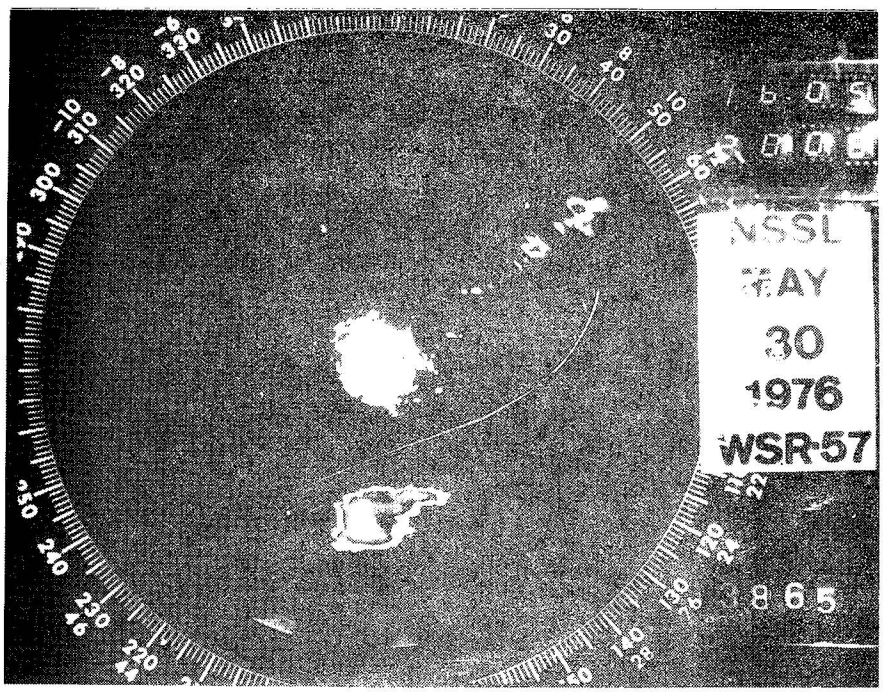

Figure 1.45. WSR-57 radar photo 1605 CST: 30 May 1976. Range interval 40 km, 0° tilt. Compare previous figure.

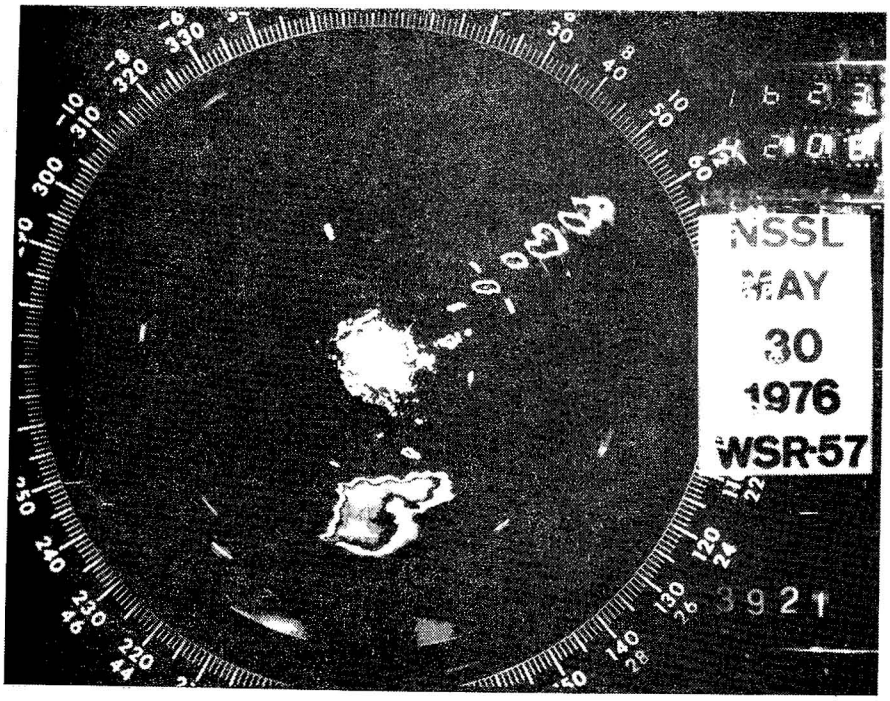

Figure 1.46. WSR-57 radar photo 1623 CST: 30 May 1976. Range interval 40 km, 0° tilt. Compare Figs. 1.44, 1.45.

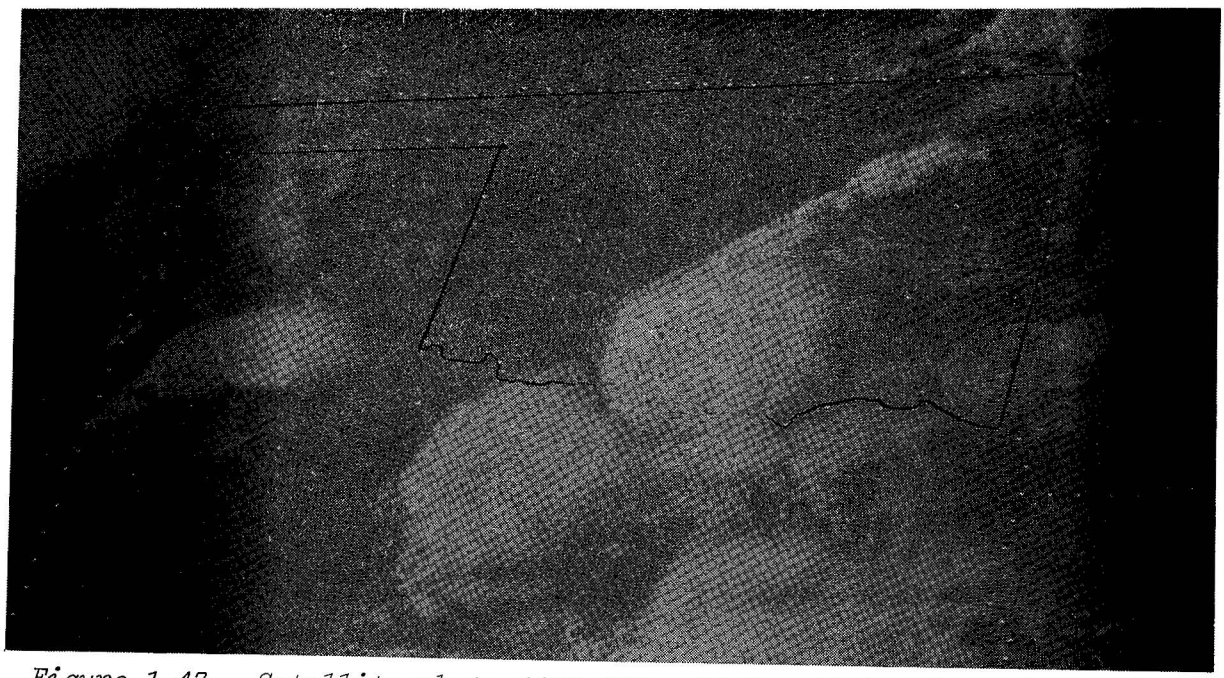

Figure 1.47. Satellite photo 1630 CST: 30 May 1976. Storm in southern Oklahoma near time of the Waurika Tornado.

Figure 1.48. Waurika wall cloud 1624 CST: 30 May 1976. 3.6 miles west of Waurika looking east.

Figure 1.49. Waurika wall cloud 1626: 30 May 1976. 8 miles east of Waurika looking west.

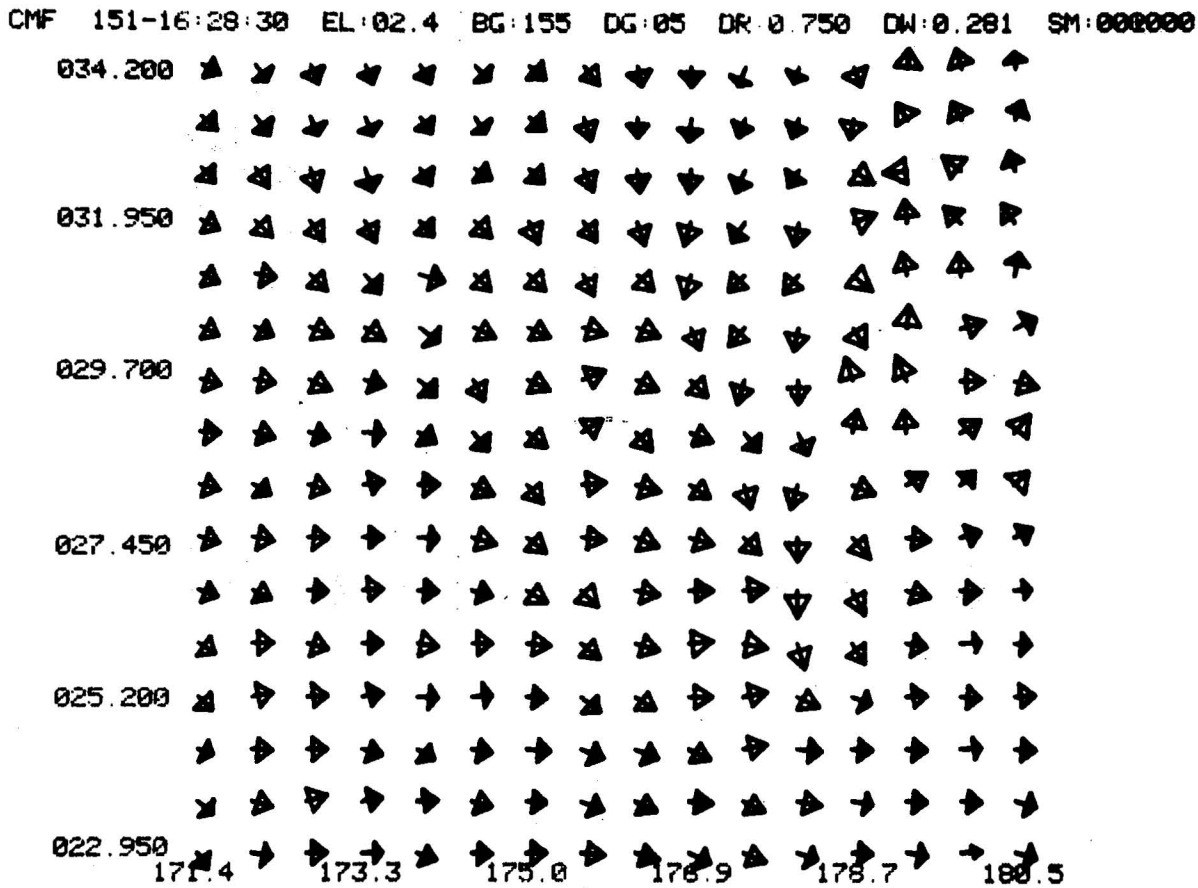

Figure 1.50. Multimoment display 1628 CST: 30 May 1976. Abcissa is the azimuth from Cimarron (CIM) radar; ordinate value plus 115 km is range from CIM in km. Arrow direction is proportional to wind speed with clockwise deflection from the right representing flow toward the radar over the range 0-34 MPS and counterclockwise deflections from the right representing flow away over the same range of values. Arrow length is proportional to reflectivity. For further clarification the reader is referred to Burgess et al. (1976). Note the indications of cyclonic circulation in the upper right portion of the figure and the tornado vortex signature at 179° at 147 km (shown on ordinate as 32).

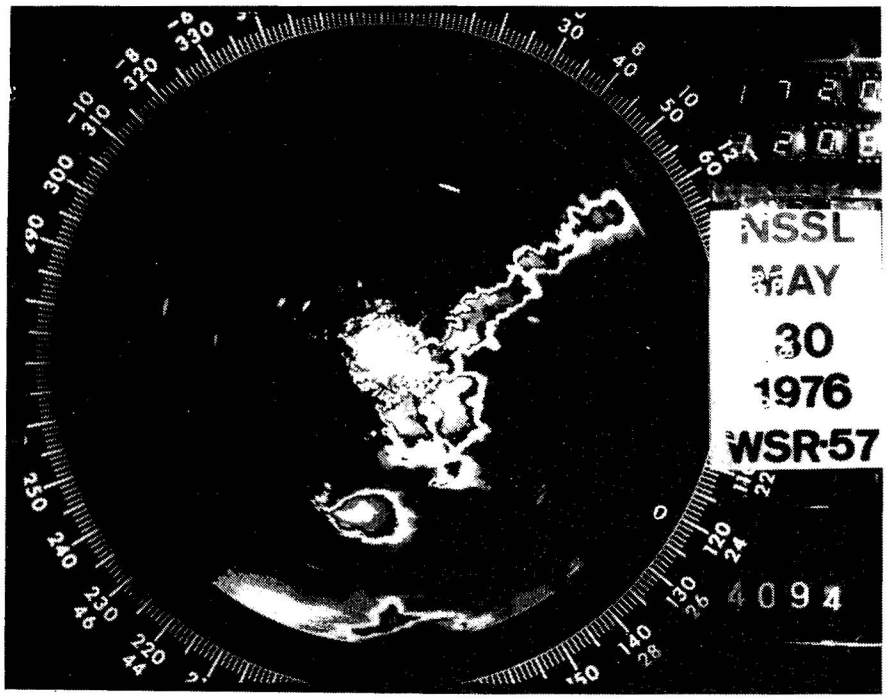

Figure 1.51. WSR-57 radar photo 1720 CST: 30 May 1976. Range interval 40 km, 0° tilt. Thunderstorm activity near time of Norman wall cloud.

June 12, 1976

A strong blocking pattern, which had persisted for nearly two weeks, was beginning to erode as an upper trough approached slowly from the west. 500 mb cooling, and substantial PVA, were expected over the study area by mid afternoon. A low level moisture ridge was situated over central Texas and Oklahoma. At the surface, a cold front extended through central Kansas, western Oklahoma and southwestern Texas and was expected to begin moving eastward along its northern extent by early afternoon. A frontal wave was predicted to form in southwestern Oklahoma in response to the upper system. The air mass was very unstable (LI -7) over most of the area of interest, however, a strong capping inversion (5°C negative buoyancy at cloud base) existed at all Oklahoma RAOB sites. Vertical wind profiles were favorable for severe storm development.

The forecast was for severe storms to development in southwestern Oklahoma, if the surface low materialized in sufficient strength to overcome the inversion. Late afternoon activity was expected.

Intercept teams and aircraft monitored high-based thundershowers which formed in northwest Oklahoma at 1445 CST, however, the storms dissipated soon after. No severe storm data were obtained.

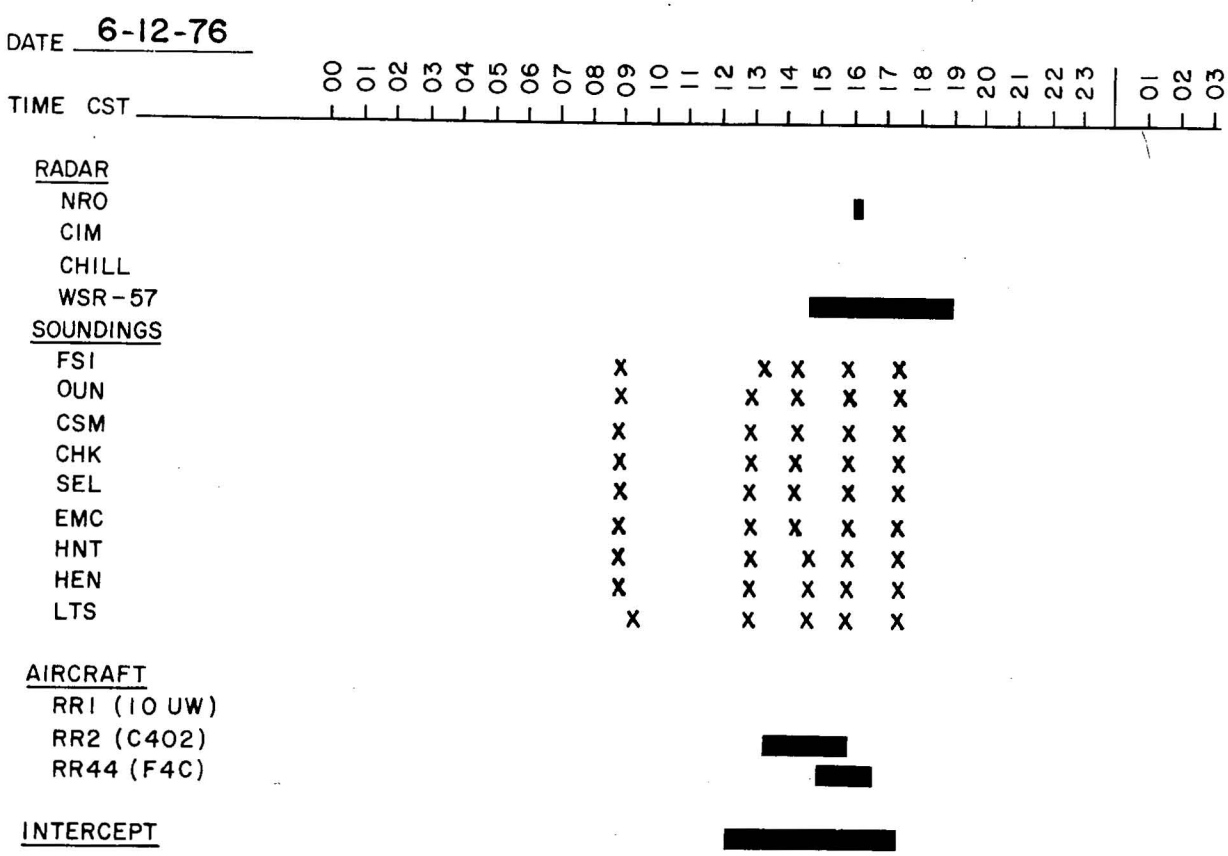

June 13, 1976

A surface front had retreated from western Oklahoma into the Texas Panhandle in response to an advancing shortwave whose axis was situated between Utah and Arizona at 0600 CST. The 700 mb "no change" line was in eastern New Mexico and, at 850 mb, moist air predominated over most of Texas and Oklahoma. Soundings indicated an unstable air mass (LI -10) over the study area and upper winds were favorable. There remained a capping inversion at cloud base level, but not as strong as that of the previous day.

The morning forecast admitted the possibility of thunderstorms anywhere in Oklahoma, but favored the areas near the front and along a surface trough line running from Gage to Altus, Oklahoma to Brownwood, Texas at 0900 CST.

The storms which occurred during the day were characterized by substantial vertical development (some tops in excess of 60,000 ft), 1/2" hail and strong outflow. No tornadic activity was reported. First trip, dual-Doppler data were obtained on a relatively strong storm to the west of Norman from about 1800 to 1915 CST (Figs. 1.52 and 1.53). A gust front passed the KTVY instrumented tower at 2008 CST, but no supportive radar data were collected.

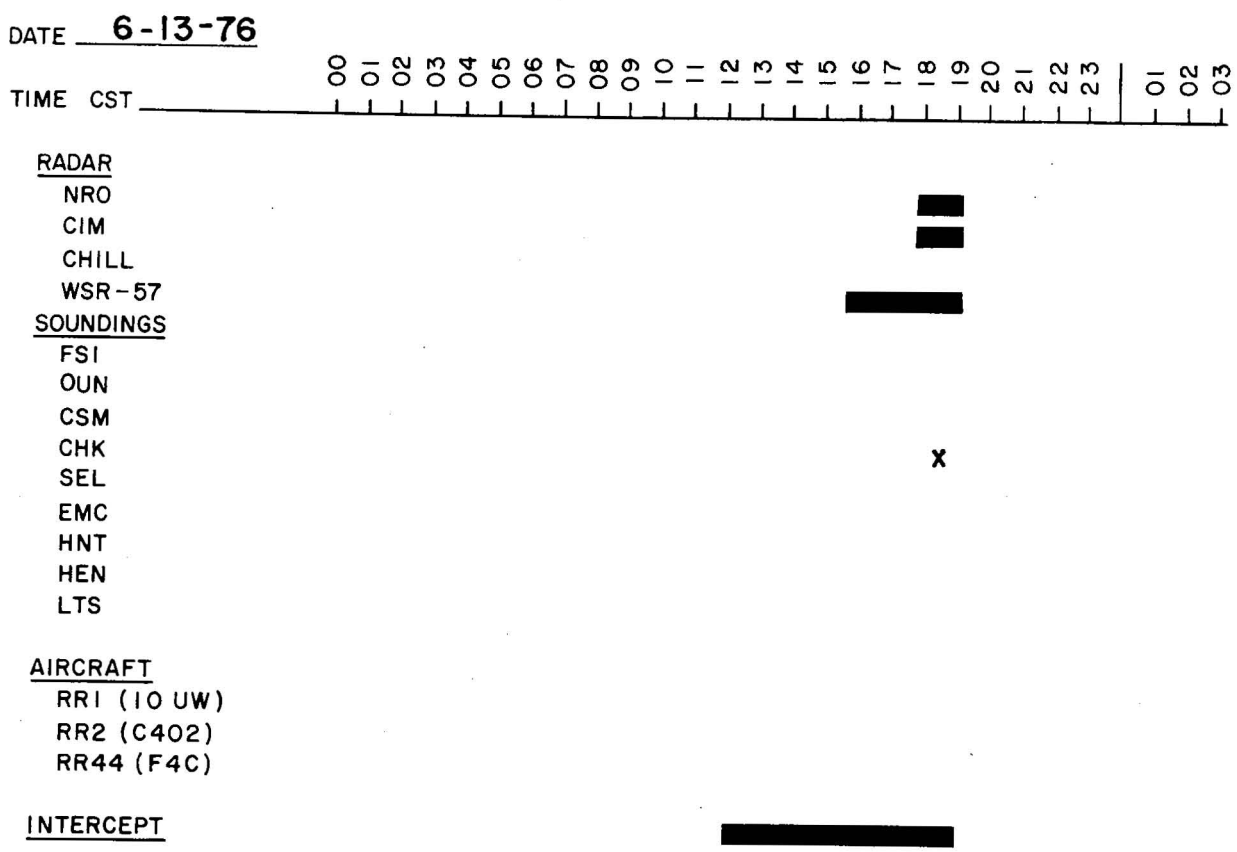

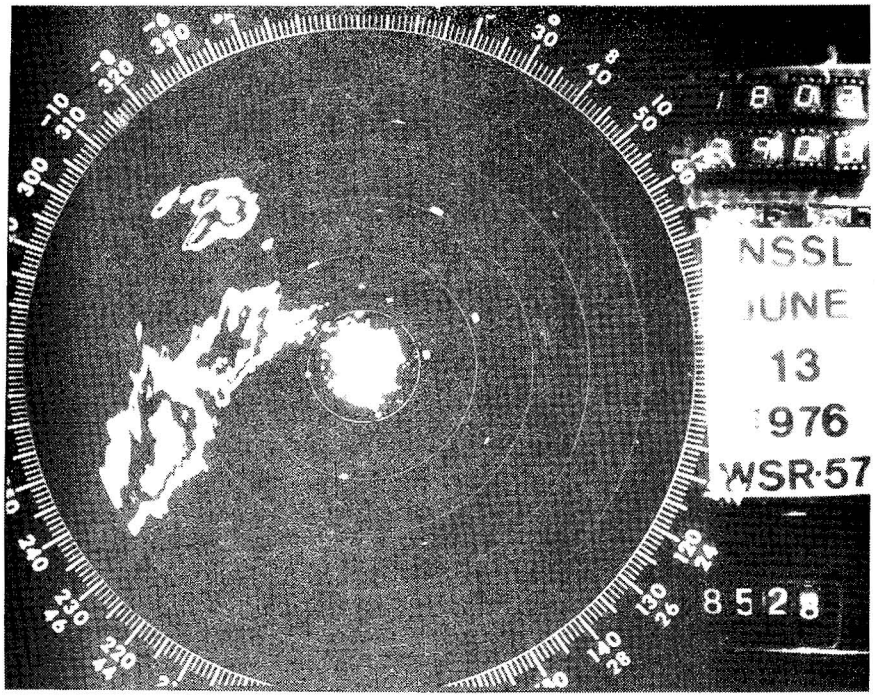

Figure 1.52. WSR-57 radar photo 1802 CST: 13 June 1976. Range interval 40 km, 0° tilt. Activity west.

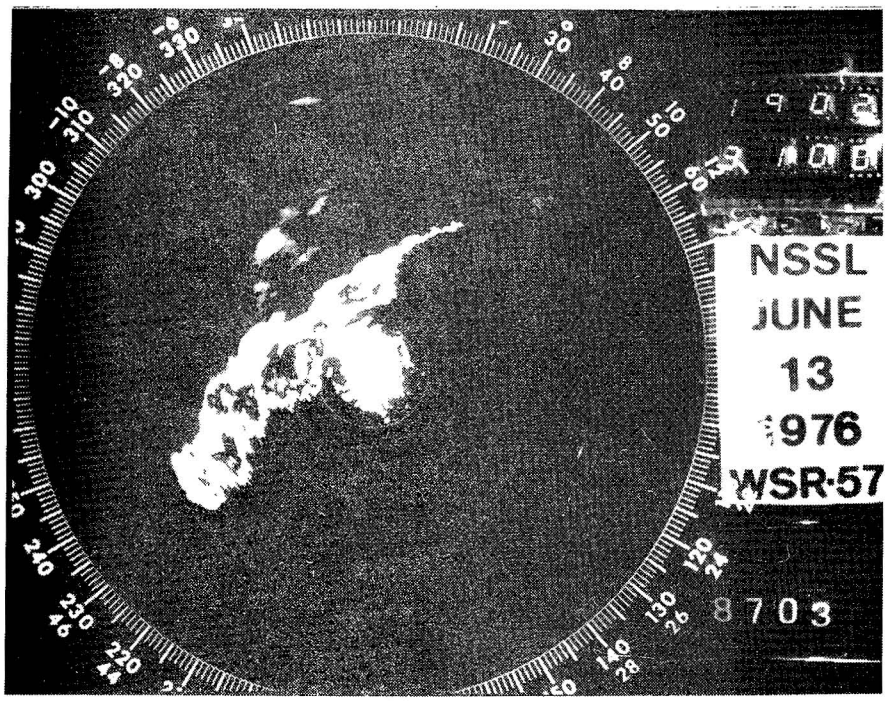

Figure 1.53. WSR-57 radar photo 1902 CST: 13 June 1976. Range interval 40 km, 0° tilt. Compare Fig. 1.52.

June 14, 1976

A major shortwave (height falls 100 m) in western Colorado was sliding rapidly southeastward. A surface front in central Kansas and the northern Texas Panhandle intersected a dry air boundary near Guymon, Oklahoma. The front, along with this intersection point (or, triple point) was expected to move southeastward with the approaching shortwave. A major problem, regarding storm formation, was that the air mass over Oklahoma was only moderately unstable (LI -3) and mid-cloud winds were weak. Furthermore, while upper winds were quite strong (exceeding 120 knots above 40,000 ft), all winds below 35,000 ft. were 40 knots or less. The potential effect of this "sudden shear" was unknown.

The forecast problem was one of timing. In Kansas, where the air mass and dynamics were best, early passage of the surface front could effectively eliminate chances for severe storms. On the other hand, the Oklahoma air mass awaited arrival of the shortwave for necessary destabilization.

At approximately 1300 CST, a storm began to develop near triple point in northwestern Oklahoma. Intercept teams observed this storm for several hours, but saw no severe activity. This storm was peculiar in that it grew to an altitude over 40,000 ft. all the while maintaining a long, skinny structure both on satellite photos and on radar (Figs. 1.54 and 1.55). Horizontal dimensions of the visual cloud at approximately 1430 CST were roughly 20 km in width by 160 km in length.

The triple point storm dissipated before sunset; however, a moderately strong squall line formed along the surface front at 1900 CST and was observed for several hours by both NRO and CIM Dopplers.

DATE 6-14-76

TIME CST	00	01	02	03	04	05	06	07	08	09	10	11	12	13	14	15	16	17	18	19	20	21	22	23	01	02	03
RADAR																											
NRO																			■	■	■	■			■	■	
CIM																			■	■	■	■		■	■	■	
CHILL																											
WSR-57																	■	■	■	■	■	■	■	■	■	■	
SOUNDINGS																											
FSI																	X	X	X	X	X	X	X	X	X		
OUN																	X	X	X	X	X	X	X	X	X		
CSM																	X	X	X	X	X	X	X	X	X		
CHK																	X	X	X	X	X	X	X	X	X		
SEL														X			X	X	X	X	X	X	X	X	X		
EMC														X	X		X	X	X	X	X	X	X	X			
HNT																	X	X	X	X	X	X	X	X	X		
HEN																	X	X	X	X	X	X	X	X	X		
LTS																	X	X	X	X	X	X	X	X	X		
AIRCRAFT																											
RR1 (10 UW)																											
RR2 (C402)																		■	■								
RR44 (F4C)																											
INTERCEPT											■	■	■	■	■	■	■	■	■								

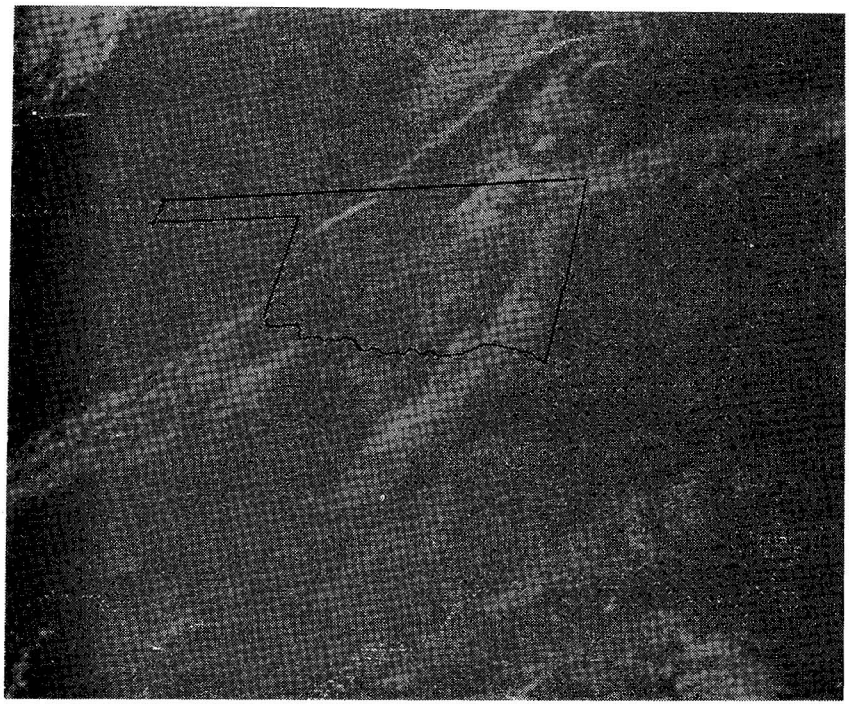

Figure 1.54. Satellite photo 1430 CST: 14 June 1976. Note long, narrow thunderstorm in western Oklahoma.

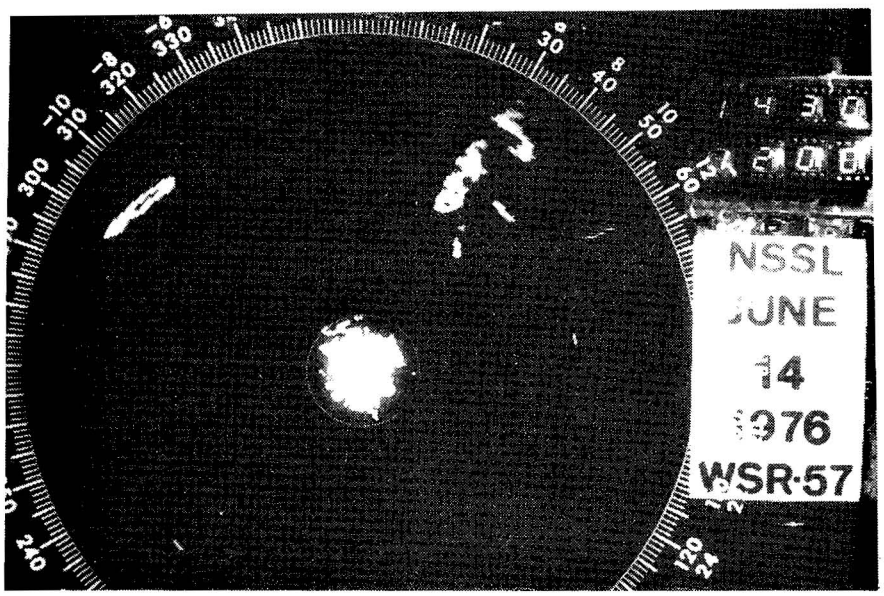

Figure 1.55. WSR-57 radar photo 1430 CST: 14 June 1976. Range interval 40 km, 0° tilt. Radar echo corresponding to satellite photo, Fig. 1.54.

June 17, 1976

Numerical guidance suggested that a weak shortwave over central New Mexico would move into western Oklahoma by late afternoon and would interact with a surface cold front extending through western Kansas and the northern Texas Panhandle and a dryline which extended from the northern Panhandle into southeastern New Mexico.

Several factors diminished chances of tornadic storms. Morning soundings indicated only moderate instability and mid-level winds were light. Moisture was limited and some question existed as to the probability of sufficient advection. The morning outlook foresaw only a slight chance for severe storms in the eastern Texas Panhandle and western Oklahoma.

Thunderstorms began forming at 1230 CST in extreme western Texas and activity continued to build northeastward toward central Kansas. Large hail was reported at 1735 CST near Canadian, Texas. No tornadoes occurred. Doppler radars observed storms as they moved into northwestern Oklahoma.

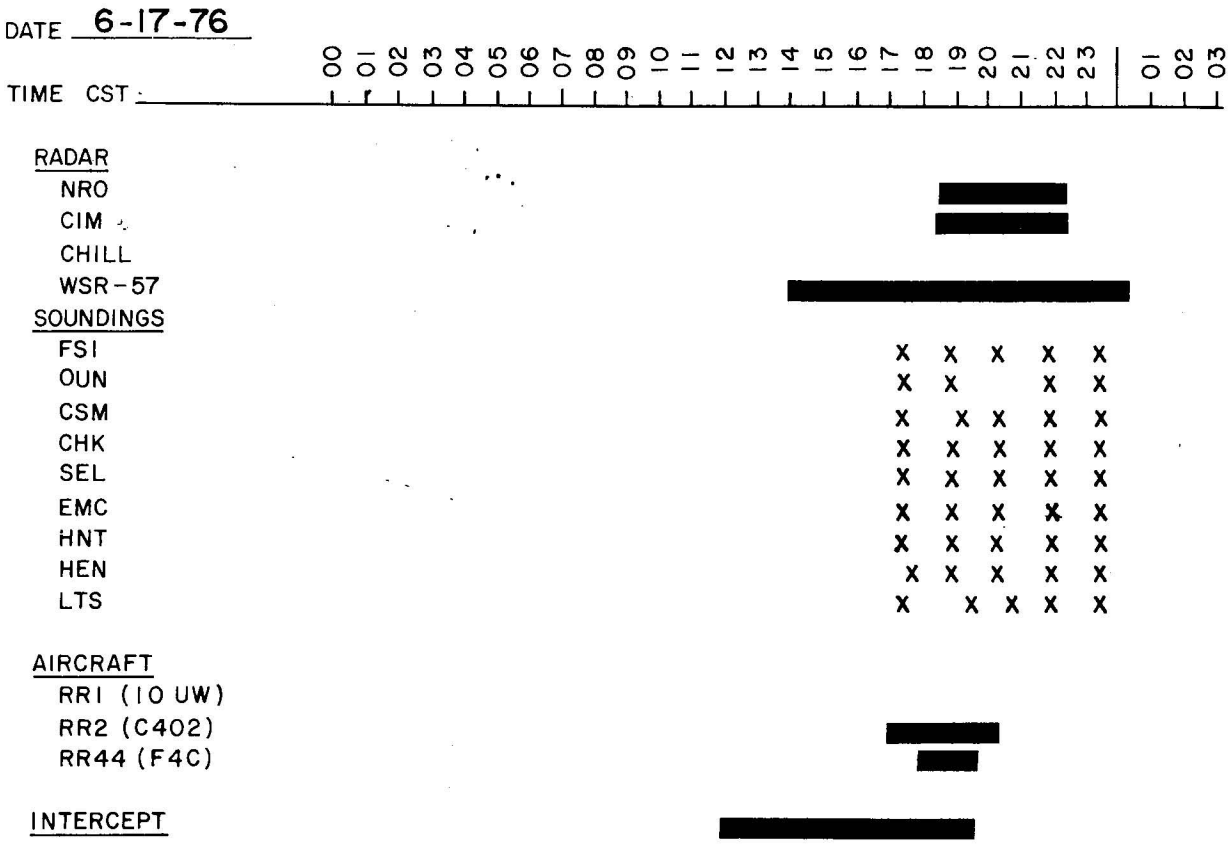

APPENDIX "A"

Radar Logs

RADAR LOGS

NRO			CIM			CHILL		WSR-57	
DATE	SECTOR ANGLE	TIME (CST)	DATE	SECTOR ANGLE	TIME (CST)	DATE	TIME (CST)	DATE	TIME (CST)
4-15-76	130° - 285°	2136 - 2146	4-15-76	135° - 275°	2116 - 2123	4-15-76	1540 - 1927	4-15-76	1150 - 1350
-------	----------	----------	4-15-76	130° - 230°	2136 - 2142	-------	----------	4-15-76	1418 - 2145
4-19-76	330° - 025°	1622 - 1634	4-19-76	230° - 270°	2111 - 2116	4-19-76	1925 - 2359	4-19-76	1520 - 1731
4-19-76	210° - 250°	2031 - 2036	4-19-76	170° - 200°	2136 - 2141	-------	----------	4-19-76	1814 - 1845
4-19-76	240° - 285°	2111 - 2118	4-19-76	050° - 090°	2339 - 2341	-------	----------	4-19-76	1854 - 1911
4-19-76	190° - 230°	2136 - 2143	-------	----------	----------	-------	----------	4-19-76	1920 - 2234
4-19-76	340° - 030°	2339 - 2344	-------	----------	----------	-------	----------	4-19-76	2240 - 2359
4-20-76	250° - 330°	0006 - 0014	4-20-76	200° - 320°	0007 - 0015	4-20-76	0000 - 0014	4-20-76	0000 - 0024
-------	----------	----------	-------	----------	----------	-------	----------	4-23-76	1622 - 1900
5-05-76	220° - 310°	1819 - 1824	5-05-76	210° - 230°	2028 - 2030	5-05-76	1921 - 2035	5-05-76	1254 - 2104
5-05-76	320° - 130°	1824 - 1846	5-05-76	195° - 230°	2056 - 2102	5-05-76	2037 - 2054	5-05-76	2110 - 2300
5-05-76	FULL PPI	1846 - 2002	5-05-76	190° - 230°	2114 - 2115	5-05-76	2116 - 2140	-------	----------
5-05-76	190° - 290°	2002 - 2103	5-05-76	180° - 250°	2124 - 2125	-------	----------	-------	----------
5-05-76	220° - 280°	2114 - 2130	5-05-76	170° - 240°	2130 - 2150	-------	----------	-------	----------
5-05-76	210° - 280°	2130 - 2139	5-05-76	160° - 280°	2157 - 2159	-------	----------	-------	----------
5-05-76	210° - 290°	2157 - 2207	5-05-76	160° - 280°	2205 - 2208	-------	----------	-------	----------
5-05-76	210° - 290°	2217 - 2221	5-05-76	160° - 280°	2218 - 2221	-------	----------	-------	----------
5-05-76	210° - 290°	2228 - 2230	5-05-76	160° - 280°	2228 - 2230	-------	----------	-------	----------
5-09-76	240° - 290°	2135 - 2141	5-09-76	300° - 325°	2223 - 2226	5-09-76	1655 - 1843	5-09-76	2020 - 2359

NRO			CIM			CHILL		WSR-57	
DATE	SECTOR ANGLE	TIME (CST)	DATE	SECTOR ANGLE	TIME (CST)	DATE	TIME (CST)	DATE	TIME (CST)
5-09-76	280° - 330°	2258 - 2302	5-09-76	300° - 325°	2237 - 2245	5-09-76	1850 - 2149	--------	----------
5-09-76	290° - 330°	2318 - 2322	5-09-76	270° - 320°	2259 - 2306	5-09-76	2150 - 2359	--------	----------
5-09-76	300° - 320°	2335 - 2342	5-09-76	260° - 320°	2318 - 2323	-------	----------	--------	----------
-------	----------	----------	5-09-76	250° - 320°	2342 - 2345	-------	----------	--------	----------
5-10-76	300° - 320°	0009 - 0012	5-10-76	290° - 350°	0031 - 0036	5-10-76	0000 - 0203	5-10-76	0000 - 0212
5-10-76	300° - 320°	0030 - 0033	5-10-76	285° - 030°	0114 - 0120	-------	----------	--------	----------
5-10-76	290° - 010°	0132 - 0143	5-10-76	280° - 060°	0132 - 0137	-------	----------	--------	----------
5-10-76	280° - 020°	0150 - 0156	5-10-76	280° - 090°	0138 - 0146	-------	----------	--------	----------
-------	----------	----------	5-10-76	260° - 100°	0150 - 0158	-------	----------	--------	----------
5-12-76	240° - 295°	1251 - 1254	5-12-76	200° - 250°	1251 - 1254	5-12-76	1310 - 1330	5-12-76	0706 - 1002
5-12-76	RHI 262°	1309 - 1332	5-12-76	RHI 201°	1309 - 1332	-------	----------	5-12-76	1010 - 1324
5-12-76	RHI 310°	1348 - 1352	5-12-76	RHI 130°	1348 - 1352	-------	----------	5-12-76	1335 - 1831
5-12-76	100° - 190°	1412 - 1430	-------	----------	----------	-------	----------	--------	----------
5-12-76	100° - 220°	1430 - 1523	-------	----------	----------	-------	----------	--------	----------
5-12-76	220° - 270°	1526 - 1541	-------	----------	----------	-------	----------	--------	----------
5-12-76	230° - 260°	1544 - 1608	-------	----------	----------	-------	----------	--------	----------
-------	----------	----------	-------	----------	----------	-------	----------	5-21-76	1247 - 2240
5-22-76	260° - 280°	1838 - 1854	5-22-76	240° - 295°	1808 - 1814	5-22-76	1420 - 2015	5-22-76	0150 - 0910
5-22-76	260° - 310°	1854 - 1911	5-22-76	230° - 305°	1844 - 1852	5-22-76	2020 - 2045	5-22-76	1537 - 2235
5-22-76	250° - 290°	1913 - 1921	5-22-76	250° - 270°	1913 - 1915	5-22-76	2046 - 2320	5-22-76	2239 - 2324

NRO			CIM			CHILL		WSR-57	
DATE	SECTOR ANGLE	TIME (CST)	DATE	SECTOR ANGLE	TIME (CST)	DATE	TIME (CST)	DATE	TIME (CST)
5-22-76	260° - 290°	1930 - 2034	5-22-76	240° - 270°	1936 - 1952	--------	----------	--------	----------
5-22-76	240° - 300°	2035 - 2107	5-22-76	240° - 275°	2000 - 2019	--------	----------	--------	----------
5-22-76	220° - 290°	2116 - 2136	5-22-76	230° - 285°	2020 - 2044	--------	----------	--------	----------
5-22-76	180° - 360°	2147 - 2155	5-22-76	160° - 280°	2133 - 2140	--------	----------	--------	----------
5-22-76	160° - 190°	2208 - 2224	5-22-76	160° - 180°	2147 - 2155	--------	----------	--------	----------
-------	----------	----------	5-22-76	060° - 080°	2200 - 2234	--------	----------	--------	----------
5-24-76	110° - 140°	1535 - 1543	5-24-76	110° - 135°	1539 - 1544	5-24-76	1535 - 1620	5-24-76	1350 - 1631
5-24-76	110° - 140°	1600 - 1611	5-24-76	120° - 140°	1610 - 1611	--------	----------	5-24-76	1700 - 1702
5-24-76	110° - 140°	1620 - 1624	5-24-76	120° - 140°	1620 - 1622	--------	----------	--------	----------
5-24-76	120° - 150°	1626 - 1635	5-24-76	120° - 140°	1630 - 1631	--------	----------	--------	----------
5-25-76	240° - 300°	2315 - 2320	5-25-76	160° - 340°	2315 - 2338	5-25-76	2142 - 2313	5-25-76	0536 - 1311
5-25-76	240° - 300°	2331 - 2353	5-25-76	160° - 280°	2338 - 2359	5-25-76	2315 - 2359	5-25-76	1320 - 2244
5-25-76	240° - 300°	2357 - 2359	-------	----------	----------	--------	----------	5-25-76	2250 - 2359
5-26-76	240° - 300°	0000 - 0003	5-26-76	140° - 280°	0000 - 0004	5-26-76	0000 - 0130	5-26-76	0000 - 0113
5-26-76	340° - 010°	0020 - 0028	5-26-76	060° - 080°	0020 - 0028	--------	----------	5-26-76	0120 - 0141
5-26-76	120° - 200°	0040 - 0046	5-26-76	090° - 170°	0040 - 0046	--------	----------	--------	----------
5-26-76	RHI 310°	0102 - 0104	5-26-76	RHI 130°	0102 - 0104	--------	----------	--------	----------
5-26-76	RHI 310°	0111 - 0112	5-26-76	RHI 130°	0111 - 0112	--------	----------	--------	----------
5-26-76	230° - 320°	0120 - 0124	5-26-76	175° - 240°	0120 - 0128	--------	----------	--------	----------
5-26-76	100° - 170°	0922 - 1009	5-26-76	100° - 160°	0922 - 0933	5-26-76	1110 - 1237	5-26-76	0620 - 1415

NRO			CIM			CHILL		WSR-57	
DATE	SECTOR ANGLE	TIME (CST)	DATE	SECTOR ANGLE	TIME (CST)	DATE	TIME (CST)	DATE	TIME (CST)
5-26-76	140° - 220°	1057 - 1139	5-26-76	100° - 150°	0935 - 0950	5-26-76	1238 - 1358	5-26-76	1430 - 1744
5-26-76	140° - 210°	1140 - 1149	5-26-76	090° - 140°	0951 - 1007	5-26-76	1359 - 1504	5-26-76	1753 - 2100
5-26-76	110° - 220°	1150 - 1154	5-26-76	090° - 180°	1145 - 1153	-------	----------	-------	----------
5-26-76	110° - 200°	1155 - 1229	5-26-76	090° - 180°	1155 - 1418	-------	----------	-------	----------
5-26-76	090° - 210°	1245 - 1319	5-26-76	090° - 180°	1430 - 1433	-------	----------	-------	----------
5-26-76	190° - 250°	1335 - 1337	5-26-76	090° - 180°	1445 - 1449	-------	----------	-------	----------
5-26-76	160° - 250°	1340 - 1353	5-26-76	090° - 180°	1500 - 1504	-------	----------	-------	----------
5-26-76	140° - 250°	1353 - 1357	5-26-76	090° - 180°	1515 - 1519	-------	----------	-------	----------
5-26-76	110° - 210°	1405 - 1419	5-26-76	090° - 180°	1530 - 1534	-------	----------	-------	----------
5-26-76	110° - 210°	1430 - 1434	5-26-76	090° - 180°	1546 - 1551	-------	----------	-------	----------
5-26-76	110° - 210°	1445 - 1449	5-26-76	090° - 180°	1600 - 1602	-------	----------	-------	----------
5-26-76	110° - 210°	1500 - 1504	5-26-76	090° - 180°	1615 - 1618	-------	----------	-------	----------
5-26-76	110° - 210°	1515 - 1519	5-26-76	090° - 180°	1630 - 1633	-------	----------	-------	----------
5-26-76	110° - 210°	1530 - 1535	5-26-76	050° - 190°	1645 - 1651	-------	----------	-------	----------
5-26-76	110° - 210°	1547 - 1551	5-26-76	050° - 190°	1700 - 1706	-------	----------	-------	----------
5-26-76	050° - 180°	1600 - 1604	5-26-76	050° - 190°	1718 - 1723	-------	----------	-------	----------
5-26-76	050° - 180°	1718 - 1720	5-26-76	040° - 190°	1730 - 1736	-------	----------	-------	----------
5-26-76	010° - 180°	1730 - 1736	5-26-76	040° - 190°	1745 - 1751	-------	----------	-------	----------
5-26-76	010° - 180°	1745 - 1751	5-26-76	040° - 190°	1800 - 1806	-------	----------	-------	----------
5-26-76	010° - 180°	1800 - 1806	-------	----------	----------	-------	----------	-------	----------

NRO			CIM			CHILL		WSR-57	
DATE	SECTOR ANGLE	TIME (CST)	DATE	SECTOR ANGLE	TIME (CST)	DATE	TIME (CST)	DATE	TIME (CST)
5-29-76	230° - 270°	1801 - 1836	5-29-76	200° - 250°	1813 - 1818	5-29-76	1750 - 1859	5-29-76	1500 - 2047
5-29-76	230° - 280°	1848 - 1859	5-29-76	200° - 250°	1845 - 1858	5-29-76	1901 - 1935	5-29-76	2055 - 2322
5-29-76	220° - 280°	1900 - 1908	5-29-76	210° - 230°	1900 - 1907	5-29-76	1936 - 2009	5-29-76	2330 - 2359
5-29-76	230° - 250°	1909 - 1919	5-29-76	200° - 250°	1910 - 1918	5-29-76	2010 - 2053	-------	----------
5-29-76	210° - 260°	1920 - 1941	5-29-76	200° - 240°	1920 - 1931	5-29-76	2054 - 2141	-------	----------
5-29-76	190° - 260°	1950 - 2008	5-29-76	200° - 235°	1931 - 1933	-------	----------	--------	----------
5-29-76	170° - 260°	2012 - 2024	5-29-76	190° - 230°	1935 - 1941	-------	----------	--------	----------
5-29-76	150° - 240°	2030 - 2034	5-29-76	170° - 230°	1950 - 2002	-------	----------	--------	----------
5-29-76	150° - 240°	2040 - 2044	5-29-76	160° - 230°	2002 - 2009	-------	----------	--------	----------
5-29-76	150° - 180°	2051 - 2103	5-29-76	150° - 190°	2012 - 2015	-------	----------	--------	----------
5-29-76	130° - 200°	2105 - 2108	5-29-76	150° - 190°	2020 - 2022	-------	----------	--------	----------
5-29-76	120° - 190°	2120 - 2123	5-29-76	145° - 185°	2030 - 2032	-------	----------	--------	----------
5-29-76	110° - 180°	2130 - 2133	5-29-76	140° - 180°	2040 - 2042	-------	----------	--------	----------
5-29-76	110° - 170°	2140 - 2142	5-29-76	135° - 175°	2051 - 2107	-------	----------	--------	----------
-------	----------	----------	5-29-76	125° - 155°	2120 - 2121	-------	----------	--------	----------
-------	----------	----------	-------	----------	----------	-------	----------	5-30-76	0000 - 0115
5-30-76	180° - 200°	1530 - 1541	5-30-76	160° - 190°	1545 - 1550	5-30-76	1542 - 1716	5-30-76	1520 - 1713
5-30-76	170° - 210°	1545 - 1602	5-30-76	160° - 190°	1556 - 1616	5-30-76	1720 - 1816	5-30-76	1720 - 2044
5-30-76	170° - 200°	1602 - 1605	5-30-76	160° - 190°	1620 - 1650	5-30-76	1817 - 1932	5-30-76	2100 - 2359
5-30-76	160° - 200°	1606 - 1612	5-30-76	150° - 185°	1650 - 1711	5-30-76	2031 - 2130	-------	----------

NRO			CIM			CHILL		WSR-57	
DATE	SECTOR ANGLE	TIME (CST)	DATE	SECTOR ANGLE	TIME (CST)	DATE	TIME (CST)	DATE	TIME (CST)
5-30-76	180° - 200°	1613 - 1617	5-30-76	140° - 185°	1712 - 1718	5-30-76	2135 - 2246	------	----------
5-30-76	150° - 200°	1620 - 1633	5-30-76	140° - 195°	1725 - 1729	5-30-76	2247 - 2325	------	----------
5-30-76	170° - 200°	1634 - 1646	5-30-76	165° - 195°	1729 - 1759	5-30-76	2326 - 2359	------	----------
5-30-76	150° - 210°	1648 - 1654	5-30-76	165° - 195°	1805 - 1809	-------	----------	------	----------
5-30-76	180° - 210°	1655 - 1707	5-30-76	090° - 180°	1819 - 1824	-------	----------	------	----------
5-30-76	040° - 210°	1709 - 1712	5-30-76	090° - 180°	1830 - 1840	-------	----------	------	----------
5-30-76	150° - 210°	1713 - 1731	5-30-76	165° - 200°	1850 - 1855	-------	----------	-------	----------
5-30-76	170° - 220°	1735 - 1740	5-30-76	165° - 200°	1906 - 1922	-------	----------	-------	----------
5-30-76	170° - 220°	1750 - 1800	5-30-76	160° - 200°	1930 - 1933	-------	----------	-------	----------
5-30-76	170° - 230°	1805 - 1811	5-30-76	225° - 250°	2210 - 2235	-------	----------	-------	----------
5-30-76	240° - 160°	1819 - 1824	5-30-76	180° - 270°	2245 - 2255	-------	----------	-------	----------
5-30-76	160° - 230°	1824 - 1829	5-30-76	160° - 280°	2310 - 2316	-------	----------	-------	----------
5-30-76	170° - 290°	1830 - 1838	5-30-76	160° - 280°	2325 - 2344	-------	----------	-------	----------
5-30-76	170° - 220°	1850 - 1855	-------	----------	----------	-------	----------	-------	----------
5-30-76	170° - 220°	1905 - 1910	-------	----------	----------	-------	----------	-------	----------
5-30-76	180° - 210°	1911 - 1923	-------	----------	----------	-------	----------	-------	----------
5-30-76	170° - 210°	1931 - 1934	-------	----------	----------	-------	----------	-------	----------
5-30-76	220° - 270°	2210 - 2220	-------	----------	----------	-------	----------	-------	----------
5-30-76	240° - 260°	2221 - 2229	-------	----------	----------	-------	----------	-------	----------
5-30-76	220° - 270°	2232 - 2237	-------	----------	----------	-------	----------	-------	----------

NRO			CIM			CHILL		WSR-57	
DATE	SECTOR ANGLE	TIME (CST)	DATE	SECTOR ANGLE	TIME (CST)	DATE	TIME (CST)	DATE	TIME (CST)
5-30-76	200° - 290°	2245 - 2254	------	----------	----------	-------	----------	------	----------
5-30-76	200° - 290°	2308 - 2317	------	----------	----------	-------	----------	------	----------
5-30-76	200° - 290°	2325 - 2341	------	----------	----------	-------	----------	------	----------
5-31-76	300° - 340°	0000 - 0004	5-31-76	310° - 350°	0000 - 0009	5-31-76	0000 - 0026	5-31-76	0000 - 0058
5-31-76	290° - 340°	0016 - 0021	5-31-76	310° - 350°	0016 - 0019	-------	----------	-------	----------
5-31-76	340° - 010°	0049 - 0051	5-31-76	050° - 090°	0049 - 0052	-------	----------	-------	----------
6-12-76	350° - 020°	1606 - 1617	-------	----------	----------	-------	----------	-------	----------
6-13-76	250° - 320°	1757 - 1805	6-13-76	230° - 310°	1757 - 1803	-------	----------	6-13-76	1554 - 1922
6-13-76	250° - 310°	1809 - 1825	6-13-76	230° - 310°	1809 - 1812	-------	----------	-------	----------
6-13-76	FULL PPI	1832 - 1834	6-13-76	220° - 310°	1820 - 1829	-------	----------	-------	----------
6-13-76	240° - 320°	1848 - 1856	6-13-76	FULL PPI	1848 - 1901	-------	----------	-------	----------
6-13-76	240° - 320°	1905 - 1913	6-13-76	FULL PPI	1906 - 1919	-------	----------	-------	----------
6-14-76	310° - 020°	1815 - 1825	6-14-76	350° - 030°	1815 - 1818	-------	----------	6-14-76	1610 - 2359
6-14-76	310° - 020°	1830 - 1836	6-14-76	330° - 030°	1830 - 1834	-------	----------	-------	----------
6-14-76	310° - 020°	1850 - 1852	6-14-76	330° - 030°	1845 - 1850	-------	----------	-------	----------
6-14-76	300° - 020°	1900 - 1909	6-14-76	310° - 030°	1900 - 1905	-------	----------	-------	----------
6-14-76	300° - 020°	1920 - 1930	6-14-76	300° - 010°	1921 - 1931	-------	----------	-------	----------
6-14-76	290° - 020°	1940 - 1959	6-14-76	300° - 010°	1942 - 1945	-------	----------	-------	----------
6-14-76	300° - 020°	2003 - 2010	6-14-76	300° - 350°	1951 - 1955	-------	----------	-------	----------
6-14-76	300° - 350°	2016 - 2020	6-14-76	300° - 350°	2003 - 2007	-------	----------	-------	----------

NRO			CIM			CHILL		WSR-57	
DATE	SECTOR ANGLE	TIME (CST)	DATE	SECTOR ANGLE	TIME (CST)	DATE	TIME (CST)	DATE	TIME (CST)
6-14-76	300° - 350°	2030 - 2034	6-14-76	300° - 350°	2016 - 2020	-------	----------	-------	----------
6-14-76	310° - 350°	2040 - 2043	6-14-76	310° - 355°	2025 - 2033	-------	----------	-------	----------
6-14-76	310° - 350°	2055 - 2059	6-14-76	310° - 355°	2040 - 2043	-------	----------	-------	----------
6-14-76	320° - 010°	2103 - 2115	6-14-76	310° - 355°	2055 - 2059	-------	----------	-------	----------
6-14-76	320° - 010°	2120 - 2134	6-14-76	325° - 355°	2103 - 2105	-------	----------	-------	----------
6-14-76	230° - 270°	2356 - 2359	6-14-76	325° - 355°	2110 - 2112	-------	----------	-------	----------
-------	----------	----------	6-14-76	325° - 350°	2120 - 2122	-------	----------	-------	----------
-------	----------	----------	6-14-76	325° - 350°	2130 - 2132	-------	----------	------	----------
------	----------	----------	6-14-76	230° - 250°	2244 - 2250	--------	----------	-------	----------
------	----------	----------	6-14-76	225° - 245°	2300 - 2304	--------	----------	--------	----------
------	----------	----------	6-14-76	225° - 245°	2310 - 2314	--------	----------	--------	----------
------	----------	----------	6-14-76	225° - 245°	2320 - 2325	--------	----------	--------	----------
-----	----------	----------	6-14-76	225° - 245°	2340 - 2346	--------	----------	--------	----------
6-15-76	230° - 270°	0000 - 0015	6-15-76	215° - 240°	0003 - 0013	--------	----------	6-15-76	0000 - 0022
6-15-76	230° - 270°	0020 - 0024	6-15-76	205° - 240°	0021 - 0025	--------	----------	6-15-76	0030 - 0143
6-15-76	230° - 270°	0030 - 0034	6-15-76	205° - 230°	0030 - 0033	--------	----------	--------	----------
6-15-76	230° - 270°	0040 - 0045	6-15-76	205° - 230°	0040 - 0043	--------	----------	--------	----------
6-15-76	210° - 270°	0101 - 0108	6-15-76	190° - 230°	0101 - 0106	-------	----------	--------	----------
6-15-76	210° - 270°	0118 - 0129	6-15-76	175° - 200°	0118 - 0122	-------	----------	--------	----------
6-15-76	200° - 260°	0130 - 0133	6-15-76	175° - 200°	0130 - 0134	--------	----------	--------	----------
6-15-76	200° - 260°	0140 - 0143	6-15-76	155° - 190°	0140 - 0143	-------	----------	--------	----------

NRO			CIM			CHILL		WSR-57	
DATE	SECTOR ANGLE	TIME (CST)	DATE	SECTOR ANGLE	TIME (CST)	DATE	TIME (CST)	DATE	TIME (CST)
6-17-76	260° - 290°	1840 - 1844	6-17-76	270° - 010°	1817 - 1824	-------	----------	6-17-76	1412 - 2042
6-17-76	260° - 290°	1849 - 1859	6-17-76	230° - 275°	1840 - 1845	-------	----------	6-17-76	2100 - 2359
6-17-76	270° - 280°	1907 - 1916	6-17-76	230° - 020°	1918 - 1930	-------	----------	--------	----------
6-17-76	270° - 340°	1923 - 1931	6-17-76	230° - 030°	1936 - 1951	------	----------	--------	----------
6-17-76	280° - 340°	1936 - 1952	6-17-76	280° - 340°	1959 - 2005	------	----------	--------	----------
6-17-76	290° - 350°	1955 - 1959	6-17-76	280° - 350°	2009 - 2024	-------	----------	--------	----------
6-17-76	290° - 350°	2009 - 2023	6-17-76	280° - 350°	2030 - 2047	-------	----------	--------	----------
6-17-76	290° - 350°	2030 - 2041	6-17-76	290° - 010°	2050 - 2109	------	----------	--------	----------
6-17-76	290° - 360°	2041 - 2108	6-17-76	290° - 355°	2120 - 2128	-------	---------	--------	----------
6-17-76	290° - 010°	2108 - 2109	6-17-76	280° - 355°	2146 - 2152	-------	--------	-------	----------
6-17-76	290° - 020°	2120 - 2128	6-17-76	260° - 010°	2215 - 2225	-------	--------	-------	---------
6-17-76	290° - 020°	2147 - 2155	------	----------	----------	-------	--------	-------	--------
6-17-76	300° - 030°	2215 - 2222	------	----------	----------	-------	--------	--------	----------
-------	----------	----------	------	---------	----------	--------	--------	6-18-76	0000 - 0031

SECTION II

DOPPLER RADAR DATA QUALITY CONTROL SUMMARY

D. Sirmans, J. T. Dooley, and B. Bumgarner

DOPPLER RADAR DATA QUALITY CONTROL SUMMARY

D. Sirmans, J. T. Dooley, and B. Bumgarner

1. INTRODUCTION

This is the second comprehensive data quality summary and is the first to include the hardwired velocity estimators. It includes a brief description of the checks made on those estimators but does not repeat any of the general data test descriptions in the Summary for 1975. The data user may refer to the previous summary or supplemental references to understand testing methods and interpretation of results.

The summary's intention parallels the previous summary, i.e., a tabulation of radar system characteristics, data parameters, subjective evaluations of data quality, and listing of known problems in the data (image suppression, maximum velocity bias, ect.). Examples of the quality control testing outputs are given.

1.1 Doppler Radar System Characteristics

Basic radar system characteristics are given in Table 1. This supersedes the Table of Characteristics for 1975 and represents system configurations during the 1976 acquisition season. Certain radar parameters such as transmitter power and receiver noise level are subject to variation and should be determined from the daily log.

Detection performance of the Norman system (NRO) is illustrated in Fig. 1.1 for both the low ("A") and high ("B") PRF channels. The curves for NRO "A" is also applicable to Cimarron (CIM) since the return power, P_r, for a given reflectivity (Z) and slant range of the CIM system is about 5 dB less than NRO "A" due to lower antenna gain, larger waveguide loss, and lower transmitter power. The log Z, log P_r relationship for NRO "A" (or CIM) is given in Fig. 1.2 for a normalization range of 100 km (the value used for the real time reflectivity displays). A range normalized intensity display calibration is shown in Table 2. Recorded intensity was <u>not</u> range normalized.

The isotach display parameters given in Table 3 are valid for the entire season. Photographic records of the mean velocity (V) are available. The spectrum width estimate (W) was not compensated in real time for noise influence.

The data acquisition timing sequence is shown in Fig. 1.3a for NRO and in Fig. 1.3b for CIM. Practically all normal PRF data was taken with 64 time series samples, 128 pulse pair velocity samples and 127 intensity samples (exponential time window with time constant of 64 radar system periods). High PRF data was taken with 128 time series samples. The 128 pulse pair velocity samples and 127 intensity samples were at an equivalent PRF of 870 Hz (every third radar pulse) in the high PRF mode.

TABLE 1 NSSL Doppler Radar Characteristics (1976)

PARAMETER	CIMARRON (CIM)	NORMAN (NRO)	NRO Hi PRF
Antenna			
Shape	Parabolic	Parabolic	Parabolic
Diameter	9.15 m	9.15 m	9.15 m
Half-Power Beam Width	0.85 deg	0.81 deg	0.81 deg
Gain	46 dB	46.8 dB	46.8 dB
First Side Lobe Level	21 dB	21 dB	21 dB
Polarization	Horizontal	Vertical	Vertical
RMS Surface Deviation	2.5 mm	2.8 mm	2.8 mm
Transmitter			
Wavelength	10.94 cm	10.52 cm	10.52 cm
Frequency	2735 MHz	2850 MHz	2850 MHz
Pulse Repetition Time	768 μsec	768 μsec	288 μsec
Pulse Width	1 μsec (150 m)	1 μsec (150 m)	0.30 μsec (52 m)
* Peak Power	500 kW	750 kW	200 kW
Receiver			
*/**System Noise Figure	4 dB	4 dB	4 dB
Transfer Function	Doppler - linear Intensity - logarithmic	Doppler - linear Intensity - logarithmic	Doppler - linear Intensity - logarithmic
* Dynamic Range	70 dB	80 dB	80 dB
Band Width: 3 dB; 6 dB	.6; .85 MHz	.6; .85 MHz	.45; .63 MHz
Intermediate Frequency	30 MHz	30 MHz	30 MHz
* Min. Detectable Signal (SNR = 1)	-105 dBm	-108 dBm	-107 dBm
Doppler Time Series Data Acquisition			
No. of Simultaneous Range Gates	16	16	6
No. of Blocks Along Radial	Unlimited	8	8
Range Gate Spacing	300, 450,...1200, 1350 m	150, 300, 600, 1200 m	150, 300, 600, 1200 m
Azimuthal Sample Spacing	0.1 to 9.9 deg	0.1 to 9.9 deg	0.1 to 9.9 deg
Automatic Elevation Increment	0.5 to 9.9 deg	0.1 to 9.9 deg	0.1 to 9.9 deg
***Number of Samples in Time Series	2^n; n = 1, 2,...13	2^n; n = 1, 2,...13	2^n; n = 1, 2,...13
Complex Video Digital Word Length	10 bits (binary)	12 bits (binary)	12 bits (binary)

*Representative value.
**Measured at receiver calibration port.
***Practically all data taken with n = 6, i.e., 64 samples for normal PRF and n = 7, i.e., 128 samples for Hi PRF.

TABLE 1 (Continued).

PARAMETER	CIMARRON (CIM)	NORMAN (NRO)	NRO Hi PRF
Mean Velocity and Spectrum Width			
Data Acquisition			
No. of Range Gates	762	762	192
Range Gate Spacing	150 m	150 m	225
*****Number of Samples in Estimate	2^n; n = 5, 6, 7, 8	2^n; n = 5, 6, 7, 8	2^n; n = 5, 6, 7, 8
Recorded Word Length			
Velocity	6 bits (2's comp)	6 bits (2's comp)	6 bits (2's comp)
Width	6 bits, 0-32 (binary)	6 bits, 0-32 (binary)	6 bits, 0-32 (binary)
Intensity Data Acquisition			
No. of Range Gates	762	762	192
Range Gate Spacing	150 m	150 m	225 m
******Number of Samples in Estimate	$2^n - 1$ (exp); 2^n (linear) n = 3, 4,...10	$2^n - 1$; 2^n n = 3, 4,...10	$2^n - 1$; 2^n n = 3, 4,...10
Time Window Function	Linear or exponential	Linear or exponential	Linear or exponential
Recorded Word Length	6 bits (binary)	6 bits (binary)	6 bits (binary)
General Features			
Azimuthal Antenna Rotation Rate	0.1 to 24.0 deg sec^{-1}	0.1 to 10 deg sec^{-1}	0.1 to 10 deg sec^{-1}
****Maximum Unambiguous Range	115 km	115 km	43 km
Maximum Unambiguous Velocity	±35.6 m sec^{-1}	±34.2 m sec^{-1}	±91 m sec^{-1}
PPI Capability	Yes	Yes	Yes
RHI Capability	Yes	Yes	Yes
Coplane Capability	No	No	No

****High PRF real time estimates are with an equivalent PRF of 870 Hz; Vm = 22.7 m s^{-1}

*****Practically all data taken with n = 7, i.e., 128 samples in estimate.

******Practically all data taken in exponential mode with n = 7, i.e., 127 samples in two time constants.

TABLE 1 (Continued).

CALIBRATION AND TIMING PARAMETERS	CIM	NRO	NRO Hi PRF
Radome Loss (2 way)	2.0 dB	2.0 dB	2.0 dB
Waveguide Loss (2 way, from cal port to antenna feed assembly)	3.6 dB	2 dB	2 dB
Cir-TR Loss (Rx Port)	0.8 dB	1.7 dB	1.7 dB
*Rx detection Loss	2.7 dB	2.7 dB	8.4 dB
Signal Generator Cable Loss	6.7 dB	9.5 dB	9.5 dB
Directional Coupler Loss (FWD PWR)	36.5 dB	36.2 dB	36.2 dB
**Delay to Tx Pulse	4.5 μs	4.2 μs	4.5 μs
**PPP INT Delay	4.4 μs/4.2 μs	2.3 μs	2.3 μs
Waveguide Delay	0.33 μs	0.1 μs	0.1 μs
Doppler Sample Hold Aperture	0.07 μs	0.4 μs	0.4 μs
Doppler Sample Hold Time Constant	0.04 μs	0.15 μs	0.15 μs
PPP-INT Sample Hold Aperture	0.04 μs	0.04 μs	0.04 μs
PPP-INT Sample Hold Time Constant	0.01 μs	0.01 μs	0.01 μs
Rx Initial Delay	1.2 μs	1.2 μs	1.4 μs
Rx Nominal Delay	1.6 μs	1.6 μs	2.2 μs
Rx Rise Time	1.0 μs	1.0 μs	1.4 μs

*See Memo for Record, "Reflectivity Equation for NSSL's WDS-71 10 cm Doppler Radar", 21 Feb 1973, R. J. Doviak and D. Sirmans.

**Delay from system pre-trigger to first sample-hold operation.

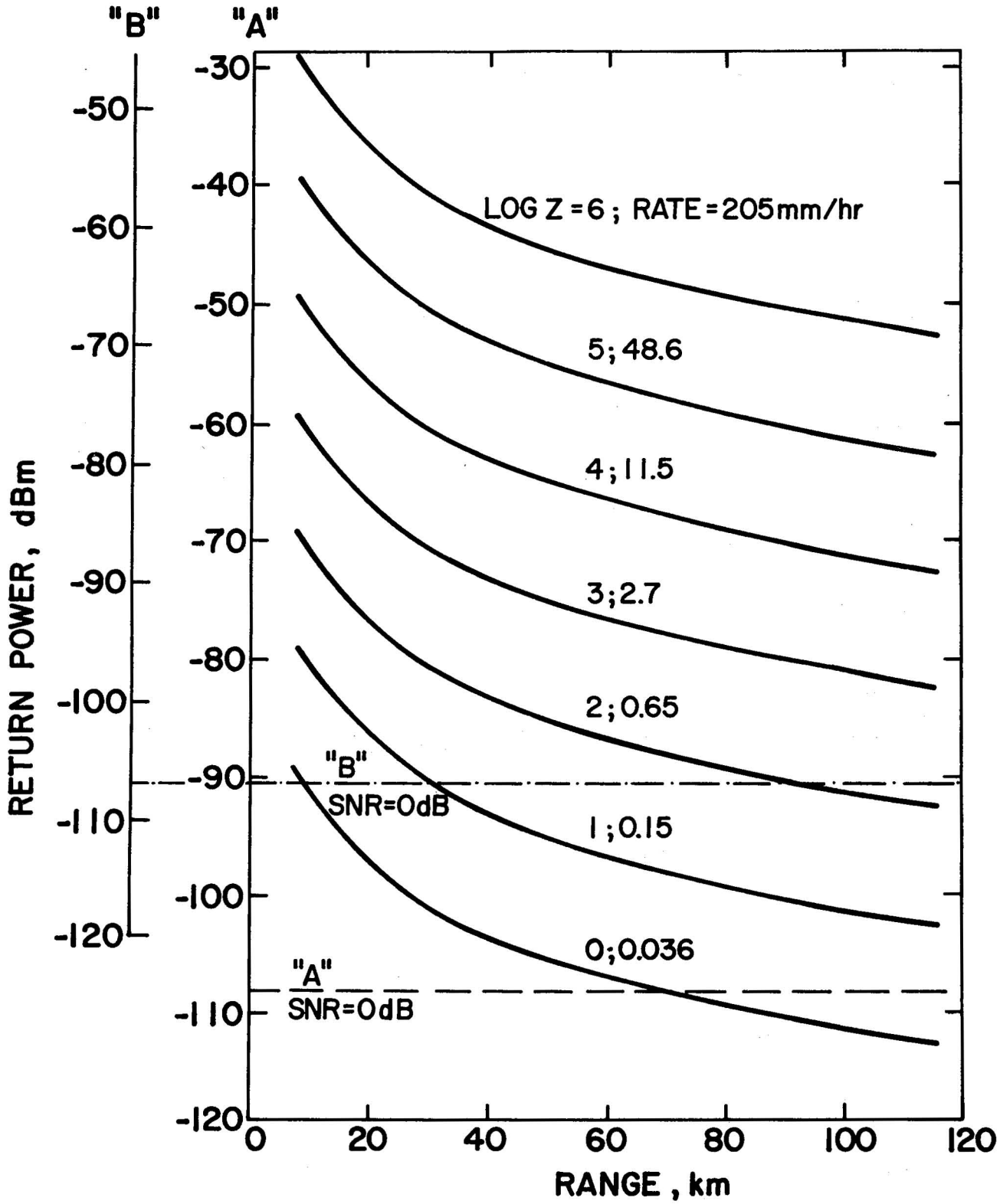

Figure 1.1. Reflectivity detection performance of NRO "A" and "B". Curves for NRO "A" are applicable to CIM with a 5 dB reduction of return power. The curves were calculated using a Z-r relationship of $Z=200r^{1.6}$ and the radar system parameters given in Fig. 1.2.

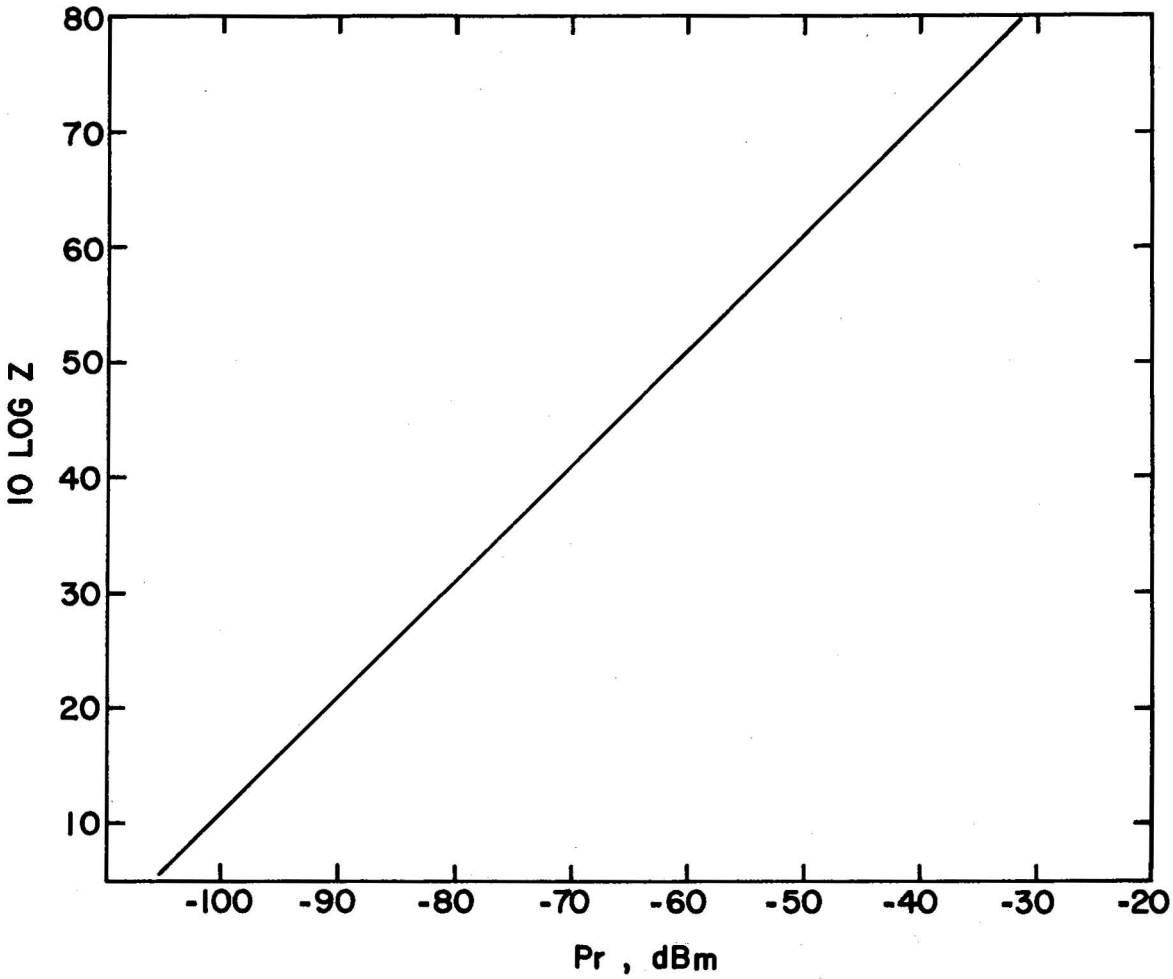

Figure 1.2. Return power, 10 log Z relationship for NRO "A" and a normalization range of 100 km. Curve applicable to CIM with a reduction of P_r by 5 dB.

System parameters for Fig. 1.1 and 1.2 are:

PARAMETER	A CHANNEL	B CHANNEL
Antenna Gain	46.8 dB	46.8 dB
Antenna Beamwidth	0.81 deg	0.81 deg
Transmitter Pulse Length	1 μs	0.3 μs
Transmitter Peak Power	750 KW	200 KW
Radome Loss (two way)	2 dB	2 dB
Waveguide Loss (two way)	2 dB	2 dB
Detection Loss	2.7 dB	8.4 dB

TABLE 2 *A Typical Reflectivity Display Calibration (3-22-76). Calibration for a particular data set (day) should be determined from the receiver calibration (Section 6) and Fig. 1.2.*

Intensity Display "A" NRO - Normalization Range = 100 km

Integrator Digit	Contour Number	Shade	Reflectivity ≤ Log Z	<
8 - 15	1	DIM	1.0	2.1
16 - 23	2	BRT	2.1	3.25
24 - 31	3	OFF	3.25	4.4
32 - 35	4	DIM	4.4	5.0
36 - 43	5	BRT	5.0	6.05
44 - 52	6	OFF	6.05	7.05
52 - 59	7	DIM	7.05	8.4
60 - 63	8	BRT	8.4	∞

Relationships between integrator digit, contour number, and shade were constant for the entire season.

TABLE 3 *Mean Velocity and Spectrum Width Display Categories. Only velocities associated with a digital integrator value of 8 and above are displayed. The typical SNR threshold is 1 dB. Actual signal to noise ratio can be determined from receiver calibration (6.1) for a particular data set.*

Velocity Display "A" NRO

Contour	Shade	V (Magnitude)*	W
1	DIM	0 - 12.8 m s^{-1}	.9 - 3.85 m s^{-1}
2	MED	12.8 - 23.5 m s^{-1}	3.85 - 7.7 m s^{-1}
3	BRT	23.5 - 34.4 m s^{-1}	7.7 - 15.4 m s^{-1}

*Velocities away from the radar are strobed in range at 600 m intervals.

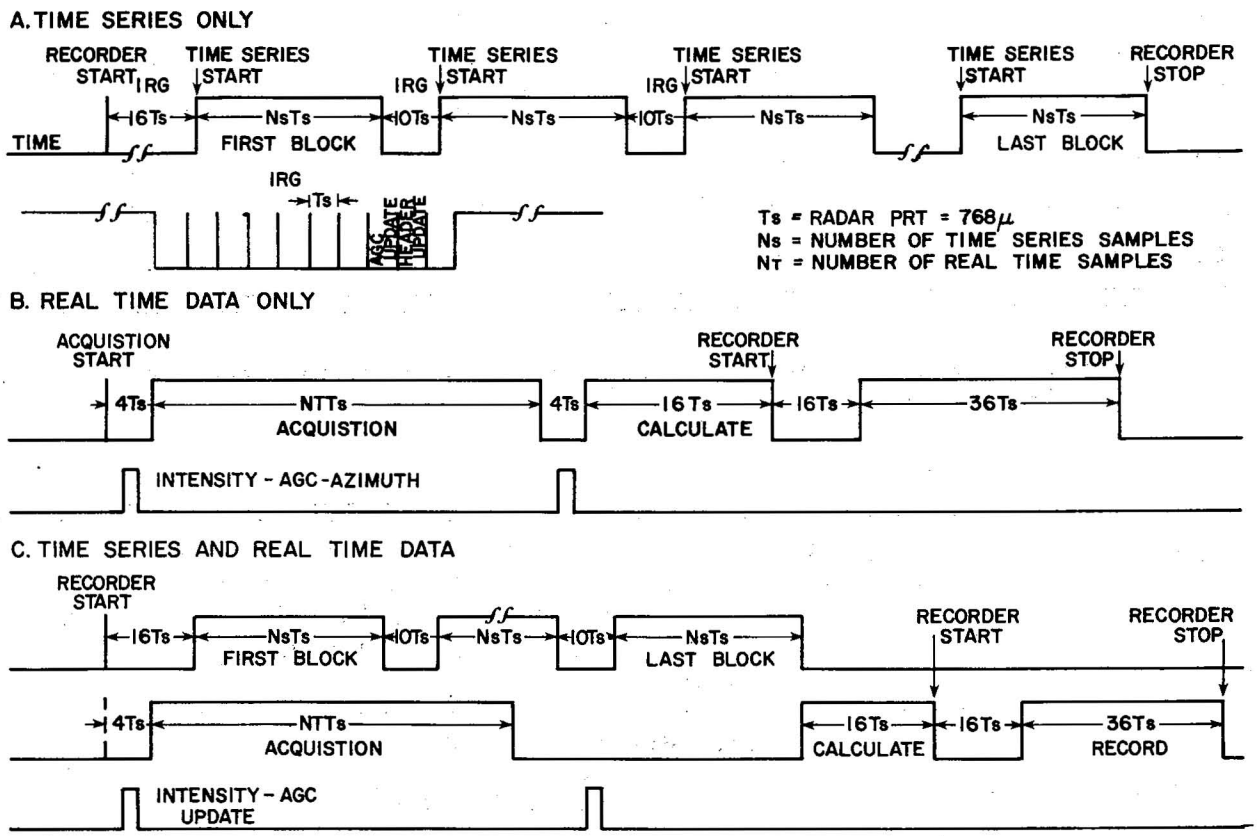

Figure 1.3a. Data acquisition timing for NRO system.

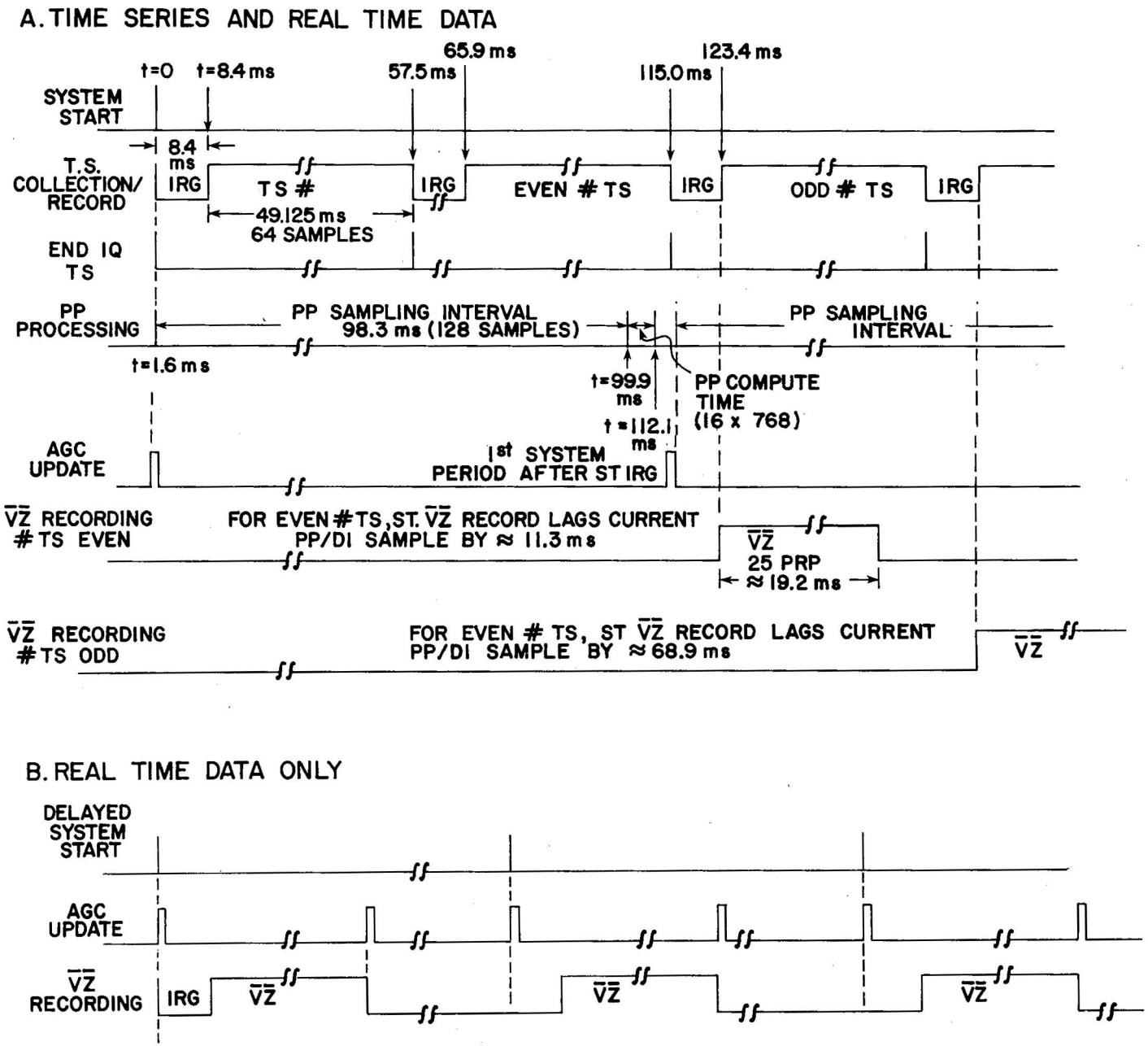

Figure 1.3b. Data acquisition timing for CIM system.

2. RADAR SYSTEM GENERAL PERFORMANCE PARAMETERS

Some general performance characteristics of the Doppler radars are given in Tables 4 through 6.

2.1 Antenna Orientation Checks

Results of antenna orientation checks by sun scan are shown in Figs. 2.1 and 2.2. Enough data is available to establish a systematic correction for NRO azimuth (θ) and fixed corrections for NRO elevation and CIM azimuth and elevation.

Unless otherwise requested the additive corrections made during data archival will be:

Parameter	Correction
NRO Azimuth	$1° \cos \theta$
NRO Elevation	0.3°
CIM Azimuth	-0.1°
CIM Elevation	-0.1°

For case studies over a limited azimuth and time, the user is encouraged to use the cross correlation of the intensity fields of the two radars to determine relative orientation. Details of this scheme can be found in the Master's Thesis "Comparison of Simutaneous Doppler Radar Fields" by C. T. Jobson.

2.2 Doppler Receiver Transfer Function

Doppler receiver input power-output voltage (digit) transfer characteristics is given in Table 4. This information may be needed for studies requiring the spectral density functional form as well as "fine" corrections to the second and higher order moments of the spectral density estimates.

TABLE 4 Doppler Receiver Transfer.

NRO "A"	NRO "B"	CIM
$V = a\ P^{\beta}$	$V = b\ P^{\beta}$	$V = b\ P^{\beta}$
$\beta = 0.465$	$\beta = 0.465$	$\beta = .46$

V = output voltage
P = input power
a,b = units conversion constants

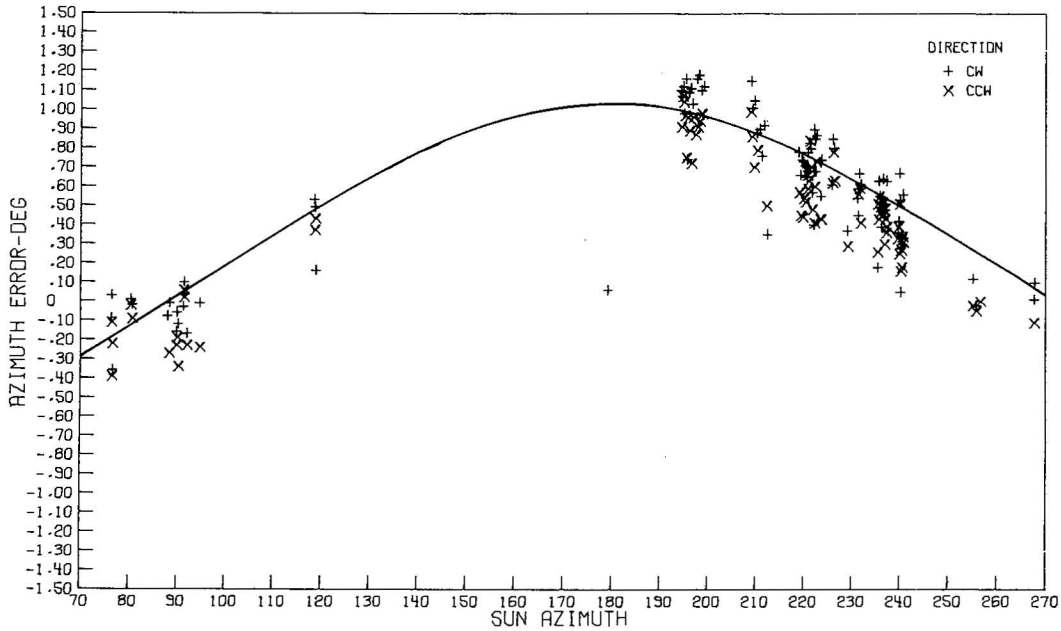

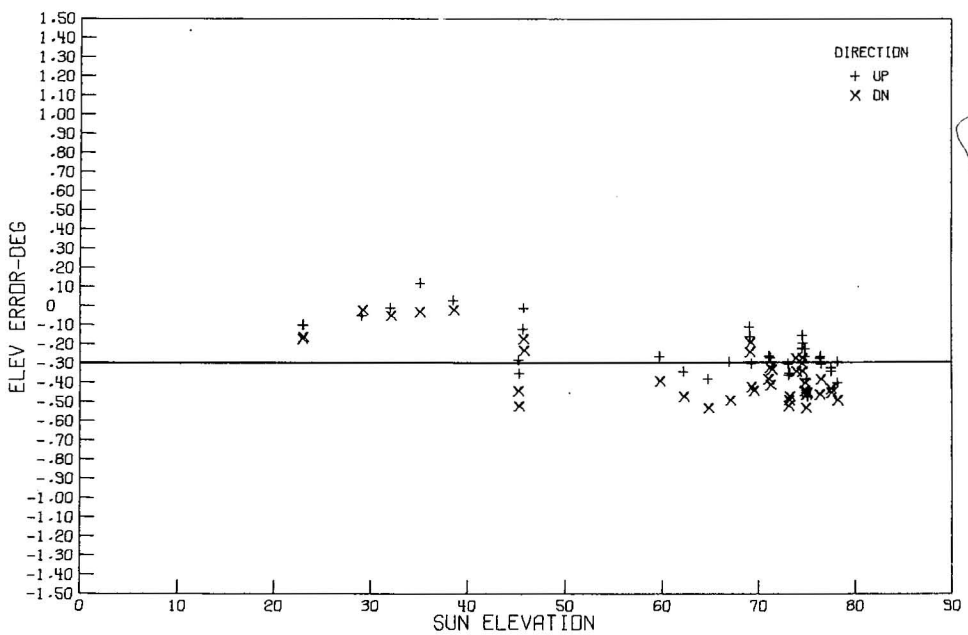

Figure 2.1. Error versus true sun position for the NRO system. Data taken between April 16, 1976 and June 24, 1976. Solid line is the assumed error function.

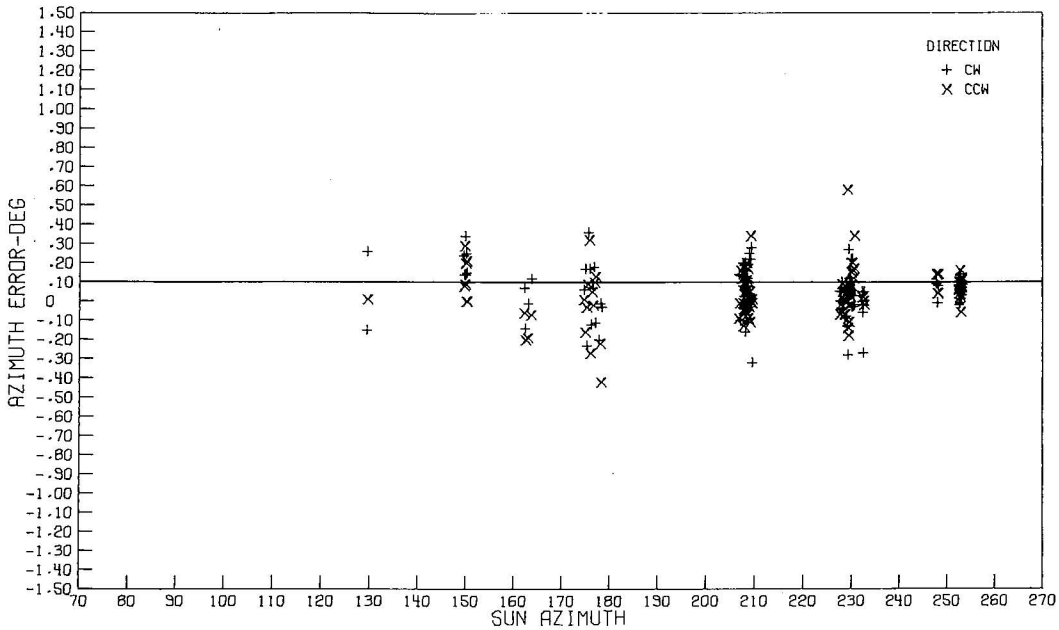

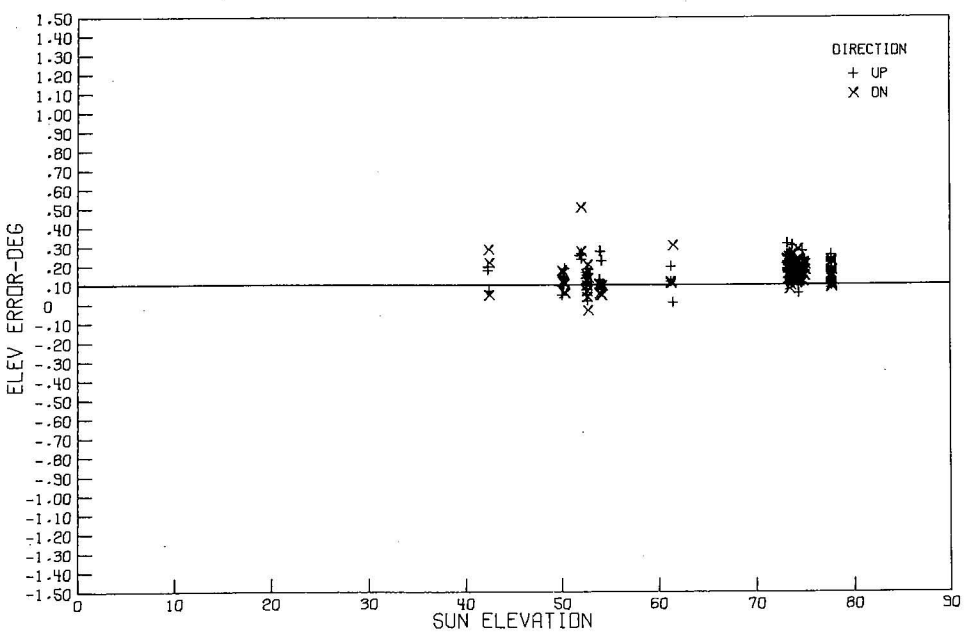

Figure 2.2. Error sun versus true sun position for the CIM system. Data taken between April 2, 1976 and June 22, 1976. Solid line is the assumed error function.

2.3 Complex Video ADC Performance

Measured performance of the time series Analog to Digital Converters (ADC) is given in Table 5. The testing scheme is given in the 1975 Quality Control Summary. Of particular interest is the quantization noise increase over ideal converter (Entry 5) which is the adjustment needed in theoretical calculations to specify the noise in the real data.

TABLE 5a ADC Characteristics.

Site - Norman	Unit - Datel # 11044
1. Non-zero classes.	2985
2. Number of equivalent bits based on non-zero classes.	11.545
3. Equivalent quantization noise width.	2216
4. Number of equivalent bits based on noise.	11.114
5. Quantization noise increase over ideal 12 bit converter.	5.329 dB

TABLE 5b ADC Characteristics.

Site - Cimarron	Unit I-Com Lab # 304074 I	Unit Q-Com Lab # 504152 Q
1. Non-zero classes.	1022	1022
2. Number of equivalent bits based on non-zero classes.	9.997	9.997
3. Equivalent quantization noise width.	1015	1015
4. Number of equivalent bits based on noise.	9.988	9.988
5. Quantization noise increase over ideal 10 bit converter.	0.57 dB	0.57 dB

3. PARAMETERS PERTAINING TO INTENSITY MEASUREMENT

The quantities given in this section were taken from the intensity testing calibration checks and provide a quantitative summary of system performance.

3.1 Radar Peak Power Log

Transmitter peak power for selected data days is given in Table 6. An effort was made to standardize NRO at 750 kw and CIM at 500 kw. Power for other days can be obtained from the Doppler Meteorologist's Log or from the Radar System Log.

TABLE 6 Doppler Radar Peak Power - 1976.

Date	4-19	5-05	5-12	5-22	5-26	5-29	5-30
Norman A	600 KW	750 KW	750 KW	750 KW	750 KW	750 KW	750 KW
Cimarron	500 KW	500 KW	500 KW	500 KW	500 KW	500 KW	500 KW

3.2 Logarithmic Receiver Parameters

Three parameters pertaining to the logarithmic receiver calibration are given in Figs. 3.1, 3.2, and 3.3. A description of the testing and calibration procedure is given in the 1975 Quality Control Summary. Collectively, these parameters provide a index of calibration stability and performance. The logging constant is the slope of the integrator digital output-input power transfer characteristic. The noise digit, as the name implies, is the integrator digital output for noise alone. Noise power is derived by the technique described in the 1975 Summary and is not measured directly.

3.3 Intensity Calibration Drift

The intensity receiver calibration drift is given in Table 7. Drift (D) is defined as the absolute difference (dB) between pre- and post-collection calibrations. The drift range given in the table brackets the magnitude at digital output integrator values of 16, 24, 32, 40, 48, and 56.

TABLE 7 Intensity Calibration Drift.

Date	NRO "A"	CIM
4-19-76	0.1 dB $\leq$ D $\leq$ 1.1 dB	1.7 dB $\leq$ D $\leq$ 2.7 dB
5-05-76	1.5 dB $\leq$ D $\leq$ 1.8 dB	0.7 dB $\leq$ D $\leq$ 3.7 dB
5-12-76	0.1 dB $\leq$ D $\leq$ 0.3 dB	1.0 dB $\leq$ D $\leq$ 3.4 dB
5-22-76	0.1 dB $\leq$ D $\leq$ 1.1 dB	0.2 dB $\leq$ D $\leq$ 3.9 dB
5-25-76	0.5 dB $\leq$ D $\leq$ 0.7 dB	2.9 dB $\leq$ D $\leq$ 6.4 dB
5-26-76	0.9 dB $\leq$ D $<$ 1.3 dB	0.7 dB $\leq$ D $\leq$ 3.2 dB
5-29-76	0 $\leq$ D $<$ 0.5 dB	4.0 dB $\leq$ D $\leq$ 6.3 dB
5-30-76	0.8 dB $\leq$ D $\leq$ 1.3 dB	0.7 dB $\leq$ D $\leq$ 1.3 dB

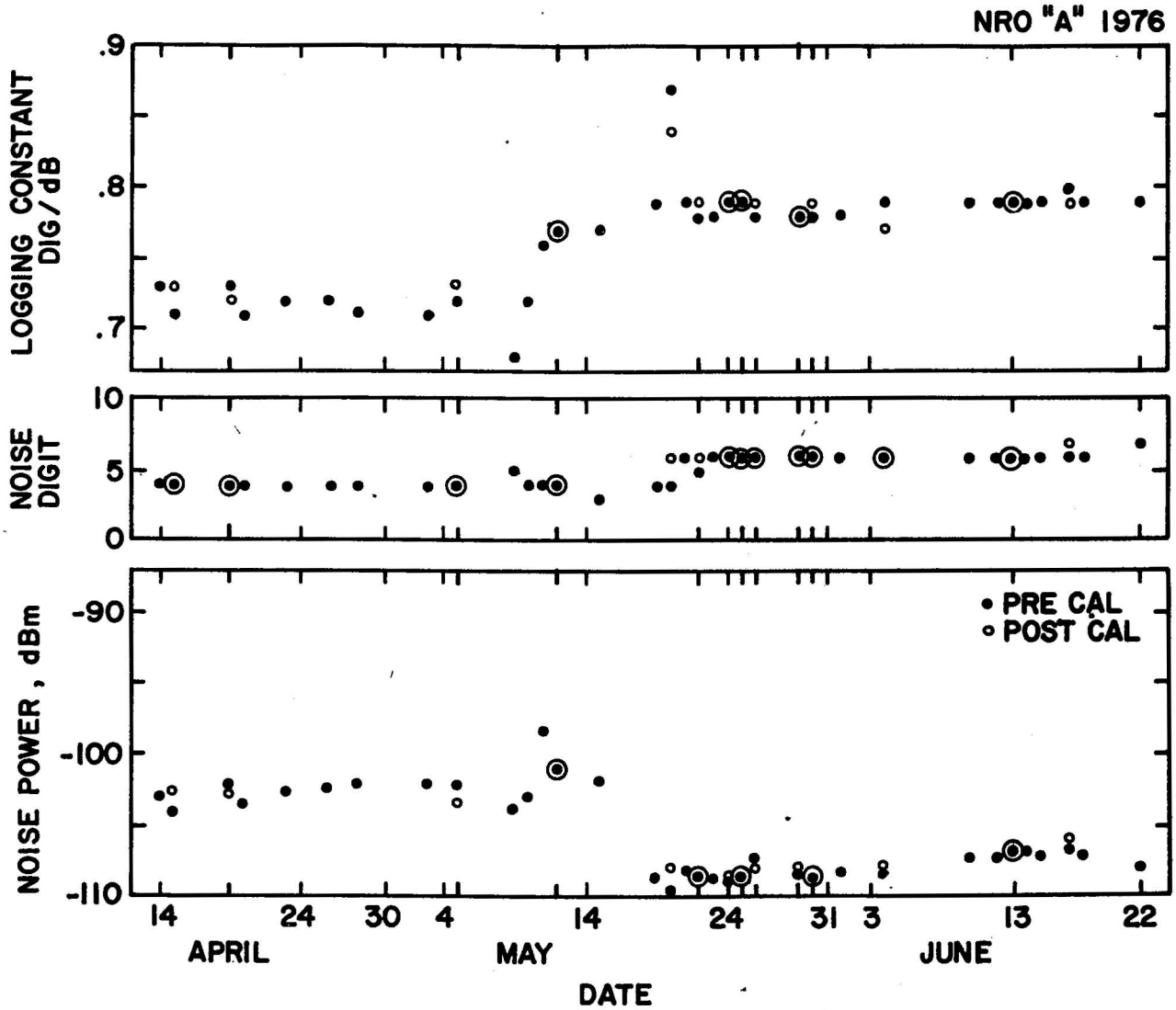

Figure 3.1. Parameters monitoring logarithmic receiver performance and the constancy of the intensity calibrations. NRO "A".

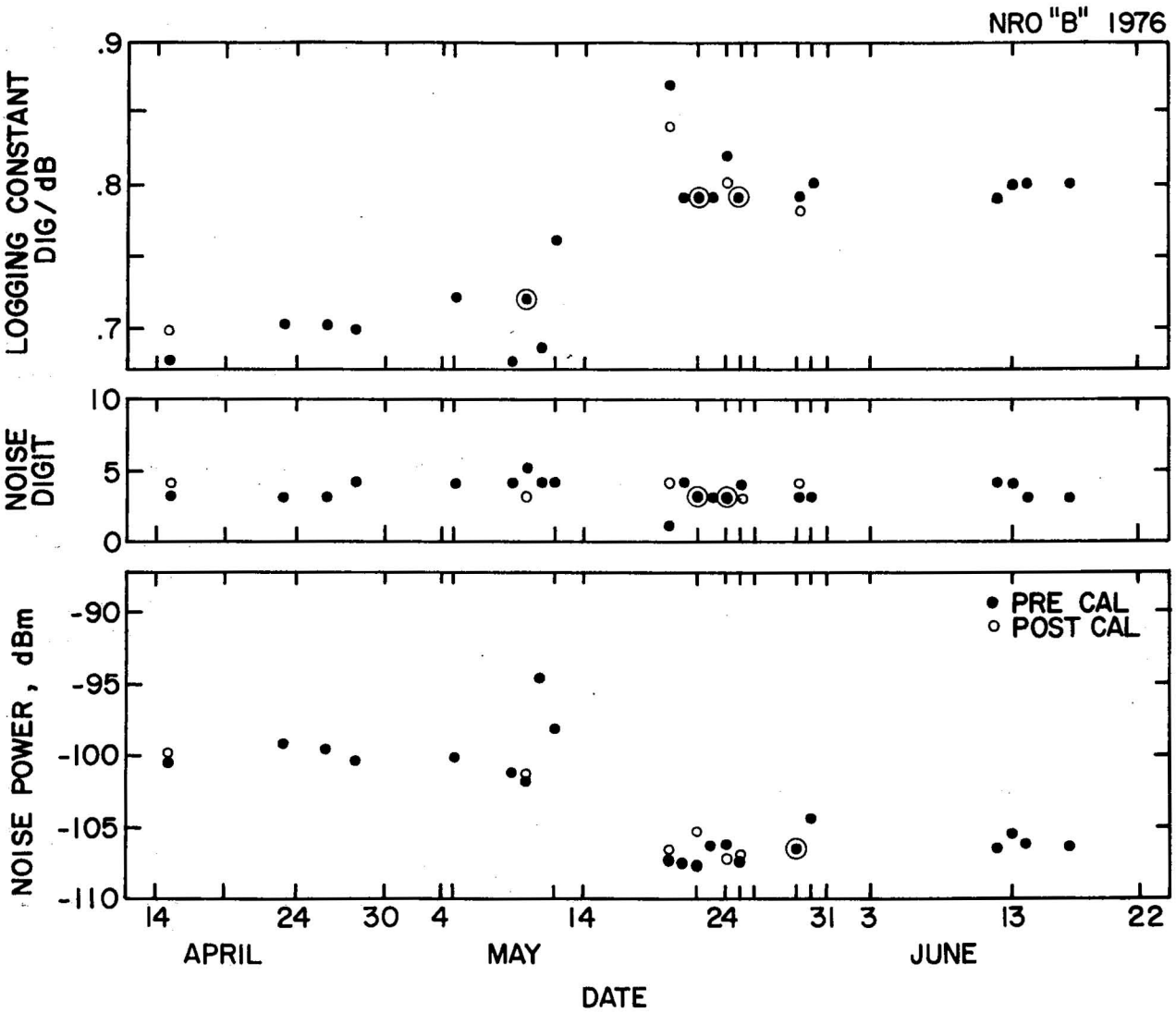

Figure 3.2. Parameters monitoring logarithmic receiver performance and the constancy of the intensity calibrations. NRO "B".

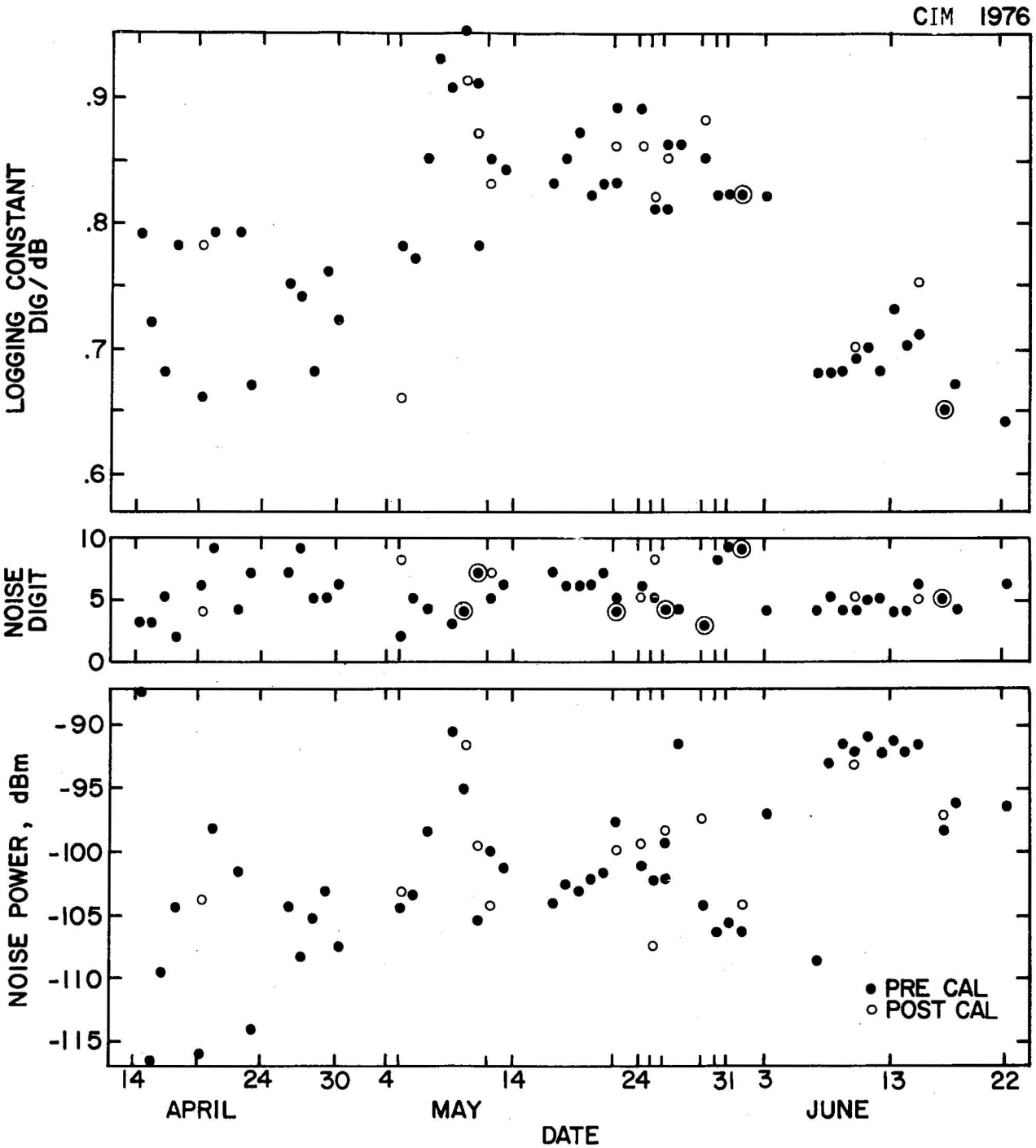

Figure 3.3. Parameters monitoring logarithmic receiver performance and the constancy of the intensity calibrations. CIM.

4. PARAMETERS PERTAINING TO MEAN VELOCITY AND SPECTRUM WIDTH MEASUREMENTS

In this section, we examine quantities related to the velocity measurement. Examination is divided into two parts; Section 4.1 presents results of test and calibration checks and Section 4.2 gives results of data quality control spot checks.

4.1 Test and Calibration Parameters

The quantities tabulated in Tables 8 and 9 are some of the quantities examined in test and calibration checks. Information which may be gained from these listings include but are not limited to the following:

(a) Integrator Digital Range is taken from the integrator-digital intensity calibration (Fig. 6.1) and is the digital span of the integrator output on a scale of 0-63. Minimum values of 2 or less indicate a questionable intensity calibration and receiver noise determination. A maximum value of 63 could indicate receiver ADC saturation rather than in the logarithmic IF or the parametric amplifier.

(b) Time Series (ADC) Digital Range is taken from the AGC time series analog to digital converter amplitude transfer (Fig. 6.3) and is the variation in digital RMS amplitude across the receiver dynamic range during the intensity calibration. Maximum values greater than 1024 for NRO and 256 for CIM indicate a harmonic power generation by clipping within 28 dB of spectrum mode. A minimum value less than 8 (either system) indicates a significant increase in quantization noise and harmonic generation by truncation.

(c) Time Series Offset is taken from the ADC histogram (Fig. 6.4) and is the dc offset (in digits) of the complex video. A value larger than 256 for NRO and 64 for CIM limits the effective dynamic range of the ADC.

(d) Noise Digit - Calibration/Noise are taken from the receiver calibration and are the noise digit values measured during the intensity calibration (Fig. 6.1) and during the receiver noise alone testing (Fig. 6.11). The two values should differ by less than two digits. A calibration value significantly larger than the value for noise alone could indicate a questionable receiver noise power value.

(e) Pulse Pair Processor (PPP) Noise Statistics Mode to Null Ratio is taken from the histogram of mean velocity estimates with noise alone (Fig. 6.12) and is the ratio of the mode to the skirt or minimum of this histogram. This provides a qualitative (quantitative if the signal digital RMS is noted) index of the maximum bias due to dc offset in the hardwired mean velocity estimate. The relationship between mode to skirt ratio and maximum bias is shown in Fig. 4.1.

TABLE 8 Test and Calibration Parameters - NRO Radar

DATE	PARAMETERS	PRECAL.	POSTCAL.
4/19	Integrator Digital Range	4-62	
	Time Series AGC Digital Range	550-300	
	*Time Series Offset	+256	**
	Noise Digit - Calibration/Noise	4, 3	
	PPP Noise Statistics Mode to Null Ratio	300:1	
5/5	Integrator Digital Range	4-62	4-62
	Time Series AGC Digital Range	600-300	560-280
	Time Series Offset	+200	+128
	Noise Digit - Calibration/Noise	4, 4	4, 4
	PPP Noise Statistics Mode to Null Ratio	7:1	12:1
5/12	Integrator Digital Range	3-62	4-62
	Time Series AGC Digital Range	700, 350	900-450
	Time Series Offset	0	0
	Noise Digit - Calibration/Noise	3+, 3+	4, 3+
	PPP Noise Statistics Mode to Null Ratio	1.64:1	1.4:1
5/22	Integrator Digital Range	4-62	5-62
	Time Series AGC Digital Range	680-220	280-120
	Time Series Offset	-128	-128
	Noise Digit - Calibration/Noise	5, 5	
	PPP Noise Statistics Mode to Null Ratio	2:1	2.25:1
5/25	Integrator Digital Range	6-62	6-62
	Time Series AGC Digital Range	800-300	880-360
	Time Series Offset	-64	-64
	Noise Digit - Calibration/Noise	6, 6	6, 5+
	PPP Noise Statistics Mode to Null Ratio	1.5:1	2:1
5/26	Integrator Digital Range	6-62	5-63
	Time Series AGC Digital Range	560-240	960-440
	Time Series Offset	-64	-64
	Noise Digit - Calibration/Noise	6, 5+	5+, 5+
	PPP Noise Statistics Mode to Null Ratio	2.7:1	1.33:1
5/29	Integrator Digital Range	5-62	5-62
	Time Series AGC Digital Range	680-320	560-240
	Time Series Offset	+128	+128
	Noise Digit - Calibration/Noise	5, 5	6, 5+
	PPP Noise Statistics Mode to Null Ratio	2.5:1	1.55:1
5/30	Integrator Digital Range	5-62	5-62
	Time Series AGC Digital Range	700-350	560-240
	Time Series Offset	+128	+128
	Noise Digit - Calibration/Noise	5+, 5	6-, 5+
	PPP Noise Statistics Mode to Null Ratio	1.33:1	1.2:1

*I and Q composite

**Available but not tabulated

TABLE 9 Test and Calibration Parameters - CIM Radar.

DATE	PARAMETERS	PRECAL.	POSTCAL.
5/5	Integrator Digital Range	1-60	No cal.
	Time Series AGC Digital Range	350-20	Missing
	Time Series Offset	I -8; Q +8	I -8; Q -8
	Noise Digit - Calibration/Noise	2, 3	4, 20
	PPP Noise Statistics Mode to Null Ratio	Missing Categories	Missing
5/12	Integrator Digital Range		6-61
	Time Series AGC Digital Range		180-80
	Time Series Offset		I -8; Q -8
	Noise Digit - Calibration/Noise		7, 4
	PPP Noise Statistics Mode to Null Ratio		4.7:1
5/22	Integrator Digital Range	3-61	3-61
	Time Series AGC Digital Range	140-60	130-50
	Time Series Offset	I -8; Q -8	I 0; Q 0
	Noise Digit - Calibration/Noise	4, 3	4, 3
	PPP Noise Statistics Mode to Null Ratio	2.5:1	2.7:1
5/25	Integrator Digital Range	4-61	7-62
	Time Series AGC Digital Range	140-50	140-40
	Time Series Offset	I -8; Q -8	I -16; Q -8
	Noise Digit - Calibration/Noise	5, 4	7, 4
	PPP Noise Statistics Mode to Null Ratio	4.7:1	6.7:1
5/26	Integrator Digital Range	4-61	3-62
	Time Series AGC Digital Range	150-60	160-60
	Time Series Offset	I -16; Q -8	I -16; Q -8
	Noise Digit - Calibration/Noise	4, 3	3, 4
	PPP Noise Statistics Mode to Null Ratio	18.8:1	10:1
5/29	Integrator Digital Range	2-62	2-62
	Time Series AGC Digital Range	160-60	Not Printed Out
	Time Series Offset	I 0; Q 0	I -8; Q -8
	Noise Digit - Calibration/Noise	3, 2	2, 3
	PPP Noise Statistics Mode to Null Ratio	3.3:1	9.6:1
5/30	Integrator Digital Range	7-62	7-62
	Time Series AGC Digital Range	140-60	180-70
	Time Series Offset	I -16; Q -8	I 0; Q 0
	Noise Digit - Calibration/Noise	8, 7	7, 8
	PPP Noise Statistics Mode to Null Ratio	1:1	14.3:1

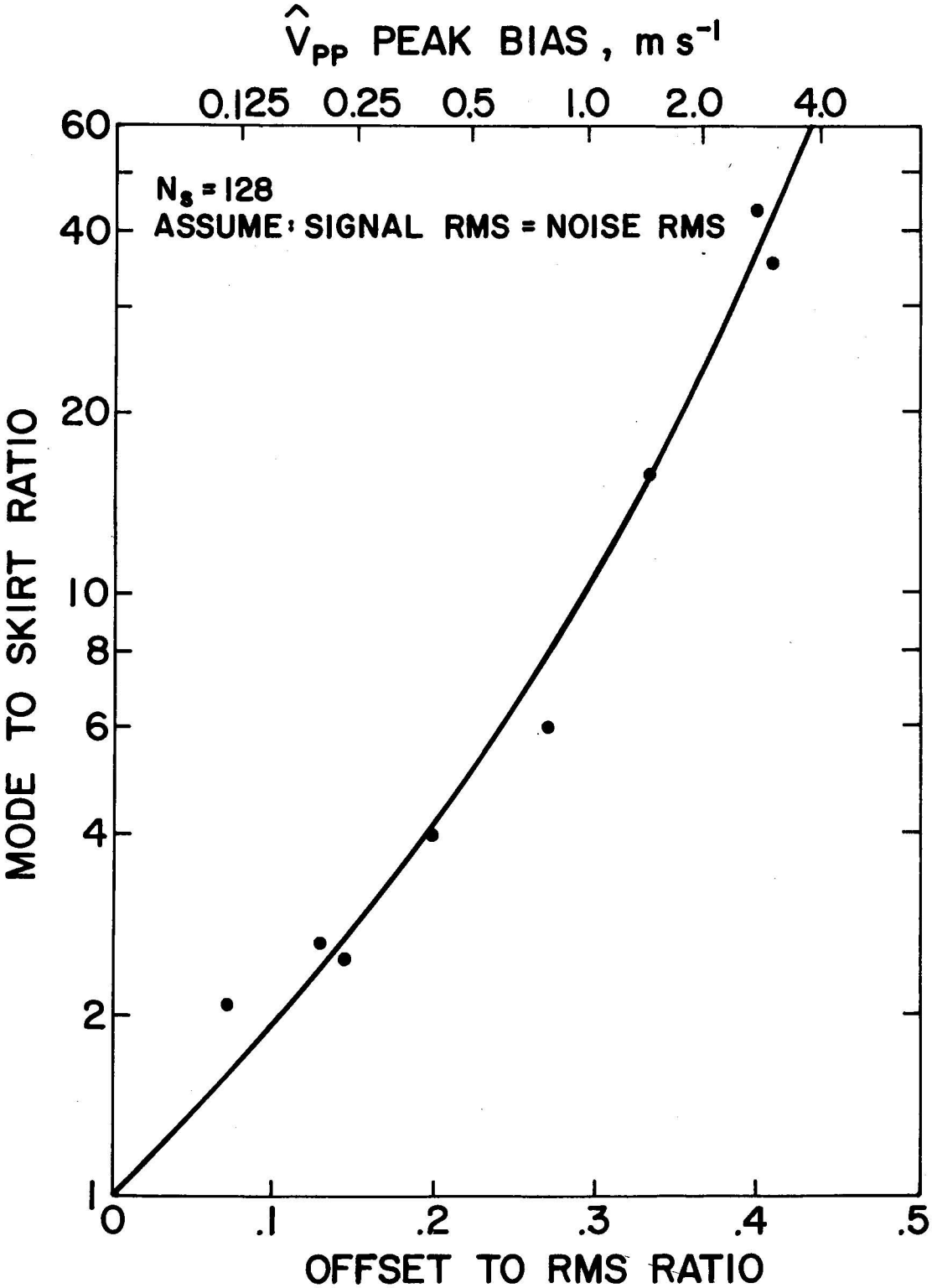

Figure 4.1. Relationship between noise alone V histogram mode to null ratio and peak bias of the mean velocity estimate. Valid for 128 sample estimate and signal RMS equal to noise RMS. Dots are experimental values.

4.2 Weather Data Quality Control Spot Check Results

Tables 10 and 12 contain selected quantities derived from the quality control testing. Methods of derivation and implication of these parameters are:

(a) Image Suppression is estimated from the image suppression histogram (Fig. 6.15) at SNR > 15 dB and provides a measure of the time series complex video amplitude and phase balance (1975 Summary).

(b) Integrator Value (AGC) in the Time Series Record Header (INT_D) versus Corresponding Integrator Value in the Integrator Record (INT) Regression Width is estimated from Integrator versus Doppler Header intensity scattergram (Fig. 6.4). Regression width is defined as the distance between the 50% mode values of the regression histogram. The parameter provides a measure of the validity of the extrapolated AGC values.

(c) $\hat{W}_{FFT}$ is the spectrum width estimate by FFT/15 dB. The value given in the table is the mean estimated from the FFT width versus Integrator Scattergram (Fig. 6.17) for the region of SNR > 15 dB.

(d) $\hat{W}_{pp}$ is the spectrum width estimate by the hardwired calculator. The value given in the table is the mean estimated from the width estimate by hardwire versus Integrator Scattergram - SNR > 0 dB (Fig. 6.19) for the region of SNR > 15 dB.

(e) $\hat{V}_{FFT}$ and $\hat{V}_{pp}$ are the mean velocity estimates by FFT/15 dB and by the hardwired device. The upper regression width is estimated from $\hat{V}_{pp}$ versus $\hat{V}_{FFT}$ Scattergram, 0 dB < SNR < 15 dB (Fig. 6.20). The lower regression width is estimated from $\hat{V}_{pp}$ versus $\hat{V}_{FFT}$ Scattergram SNR > 15 dB (Fig. 6.21). These regression widths provide a measure of the consistency of the two estimators as well as the spacial variation of the velocity field.

(f) $\hat{V}_{pp}$ Maximum Bias is defined as the deviation (at the Nyquist Interval midpoint) of $\hat{V}_{pp}$ from a linear regression against $\hat{V}_{FFT}$. The value given in the table is estimated from Fig. 6.20 or Fig. 6.21, whichever shows the larger bias.

5. DATA QUALITY ENGINEERING SUMMARY

Known data problems associated with the hardware, given in Table 12, are probably not exhaustive since problems of a more subtle nature might appear in detailed data analysis. However, it is not anticipated that detailed analysis will reveal any major problems. A list of manipulations and software corrections between raw and archive data tapes other than antenna orientation corrections is also given.

TABLE 10 Results of Quality Control Spot Check - NRO

DATE	TIME - CST	IMAGE SUPPRESSION dB BELOW MODE	INT_D vs INT REGRESSION WIDTH*	W_{FFT}	W_{PP}	V_{FFT} vs V_{PP} REGRESSION WIDTH*	V_{PP} MAXIMUM BIAS
4/19	2030:00 2035:50	21 dB	1 digit	2.5 m s^{-1}	6.5 m s^{-1}	3 m s^{-1} 2 m s^{-1}	1 m s^{-1}
	2339:12 2344:01	23 dB	3 digits	1.5 m s^{-1}	5.5 m s^{-1}	3 m s^{-1} 4 m s^{-1}	2 m s^{-1}
5/05	2204:54 2228:54	22 dB	1 digit	1.5 m s^{-1}	4.5 m s^{-1}	6 m s^{-1} 5 m s^{-1}	5 m s^{-1}
	2114:43 2115:16	21 dB	1 digit	1.5 m s^{-1}	5 m s^{-1}	5 m s^{-1} 5 m s^{-1}	5 m s^{-1}
5/12	1348:04 1351:48	21 dB	3 digits	1 m s^{-1}	2 m s^{-1}	1 m s^{-1} 1 m s^{-1}	1 m s^{-1}
5/22	2240:00 **2240:40	19 dB	3 digits	1.5 m s^{-1}		——·—— 2 m s^{-1}	1 m s^{-1}
	2030:10 **2034:32	19 dB	2 digits	4 m s^{-1}	4.5 m s^{-1}	——·—— ——·——	
5/25	1343:10 1347:20	21 dB	4 digits	1.5 m s^{-1}	2.5 m s^{-1}	1 m s^{-1} 1 m s^{-1}	1 m s^{-1}
5/26	0019:45 0028:16	22 dB	4 digits	1.5 m s^{-1}	2.5 m s^{-1}	1 m s^{-1} 1 m s^{-1}	1 m s^{-1}
5/29	1903:45 1907:37	19 dB	10 digits	2 m s^{-1}	3 m s^{-1}	3 m s^{-1} 2 m s^{-1}	1 m s^{-1}
5/30	1819:01 **1823:40	22 dB	5 digits	1.5 m s^{-1}	2 m s^{-1}	——·—— 3 m s^{-1}	1 m s^{-1}

*Regression width is the distance between the 50% mode values of the regression histogram.

**Data taken in intense ground clutter.

TABLE 11 Results of Quality Control Spot Check - CIM

DATE	TIME - CST	IMAGE SUPPRESSION dB BELOW MODE	INT_D vs INT REGRESSION WIDTH*	W_{FTT}	V_{FFT} vs V_{PP} REGRESSION WIDTH*	V_{PP} MAXIMUM BIAS
4/19	2046:45 2053:35	**	**	5 m s^{-1}	6 m s^{-1} 5 m s^{-1}	2 m s^{-1}
5/05	1924:08 1928:30	20 dB	***	4 m s^{-1}	—·— 3 m s^{-1}	3 m s^{-1}
	2217:50 2230:11	20 dB	****	****	****	****
5/12	1348:04 1351:46	28 dB	6 digits	2 m s^{-1}	2 m s^{-1} 2 m s^{-1}	1 m s^{-1}
5/25	2316:00 2344:15	28 dB	5 digits	1.5 m s^{-1}	3 m s^{-1} 3 m s^{-1}	1 m s^{-1}
	0944:31 0945:58	27 dB	3 digits	4.5 m s^{-1}	5 m s^{-1} 4 m s^{-1}	1 m s^{-1}
5/26	0019:48 0027:30	29 dB	6 digits	1 m s^{-1}	—·— 3 m s^{-1}	1 m s^{-1}
5/29	1910:06 1925:23	27 dB	5 digits	2.5 m s^{-1}	6 m s^{-1} 3 m s^{-1}	1 m s^{-1}
5/30	2337:00 2343:48	25 dB	4 digits	2 m s^{-1}	3 m s^{-1} 3 m s^{-1}	1 m s^{-1}

*Regression width is the distance between the 50% mode values of the regression histogram.

**Integrator failure (see Table 13).

***Header intensity transfer malfunction (see Table 13).

****Real time estimator failure (see Table 13).

TABLE 12 Comments and Malfunctions

DATE	NRO "A"	CIM
4/19	———·———	Integrator output is stratified at 4 bit levels.
5/05	Excessive maximum bias (≈ 5 m s^{-1}) in hardwired V estimate. Should probably not be used without correction.	Significant maximum bias (≈ 3 m s^{-1}) in hardwired V estimate. Real time estimator failure. No data after about 2200 CST.
5/12	———·———	1
5/22	———·———	1
5/25	———·———	1
5/26	———·———	1
5/29	———·———	1
5/30	———·———	1

General

CIM

[1]No hardwired width estimate from this system. Recorded width set to zero during archival.

Intensity listing has intermittent range displacement of one location. Problem was present from 5/9/76 through 5/30/76. Hardwired V, W listings displaced by 2,4 locations relative to I. Corrections made in software during archival.

NRO

Hardwired V listing is displaced in range by one location relative to I and W (hardware logic). Correction made in software during archival.

6. EXAMPLES OF QUALITY CONTROL PROGRAM OUTPUTS

This section contains examples of quality control program outputs. The user is encouraged to utilize these routines to examine data sets prior to analysis. Other routines are available for special testing.

6.1 Intensity Calibration

Data taken during intensity calibrations can also be used to test coherent signal processing even though the intensity calibration signal is incoherent. Receiver noise and the incoherent calibration signal can be used to test for the presence and distribution of the digits (velocity, spectrum width and intensity) as well as the signal handling and recording process. Examples are given in Figs. 6.1 through 6.9. Interpretation of the testing is given in section 4.1.

STA NRO	CHAN	BNTIME	ENTIME	TAPE	DATE	CALAJ	TXPOW
	4	135145	135335	7673	51576	9.5	750.

AVERAGE INTENSITY INTEGER(GATES 10-762)

STA	DAY	TIME	AZM	ELEV	RNG	XBAR	REC	TAPE	DATE
1	114.5	135145	222.5	7.5	163.	2.9934	1	7673	51576
1	113.5	135150	239.1	7.5	163.	3.0080	2	7673	51576
1	112.5	135153	249.2	7.5	163.	3.0053	3	7673	51576
***** SEQUENCE ERROR, CHECK ARRAYS. *****									
1	111.5	135154	252.6	7.5	163.	3.0319	4	7673	51576
1	110.5	135155	256.0	7.5	163.	3.0677	5	7673	51576
1	109.5	135156	259.3	7.5	163.	3.1979	6	7673	51576
1	108.5	135157	262.6	7.5	163.	3.3506	7	7673	51576
1	107.5	135158	265.9	7.5	163.	3.7238	8	7673	51576
1	106.5	135159	269.3	7.5	163.	3.9296	9	7673	51576
1	105.5	135200	272.6	7.5	163.	4.2470	10	7673	51576
1	104.5	135201	275.9	7.5	163.	4.6600	11	7673	51576
1	103.5	135202	279.2	7.5	163.	5.0345	12	7673	51576
1	102.5	135203	282.5	7.5	163.	5.7543	13	7673	51576
1	101.5	135204	285.7	7.5	163.	6.3426	14	7673	51576
1	100.5	135205	289.0	7.5	163.	7.1208	15	7673	51576
1	99.5	135206	292.3	7.5	163.	8.0664	16	7673	51576
1	98.5	135207	295.6	7.5	163.	8.9668	17	7673	51576
1	97.5	135208	298.9	7.5	163.	9.7530	18	7673	51576
1	96.5	135209	302.4	7.5	163.	10.9363	19	7673	51576
1	95.5	135210	305.7	7.5	163.	11.6627	20	7673	51576
1	94.5	135211	308.9	7.5	163.	12.0544	21	7673	51576
1	93.5	135212	312.1	7.5	163.	13.0013	22	7673	51576
1	92.5	135213	315.4	7.5	163.	14.0000	23	7673	51576
1	91.5	135214	318.7	7.5	163.	14.9987	24	7673	51576
1	90.5	135215	322.1	7.5	163.	15.8837	25	7673	51576
1	89.5	135216	325.4	7.5	163.	16.8000	26	7673	51576
1	88.5	135217	328.8	7.5	163.	16.9894	27	7673	51576
1	87.5	135218	332.1	7.5	163.	17.0638	28	7673	51576
1	86.5	135219	335.4	7.5	163.	18.0000	29	7673	51576
1	85.5	135220	338.7	7.5	163.	19.0000	30	7673	51576
1	84.5	135221	342.1	7.5	163.	20.0000	31	7673	51576
1	83.5	135222	345.4	7.5	163.	20.4196	32	7673	51576
1	82.5	135223	348.8	7.5	163.	21.0000	33	7673	51576
1	81.5	135224	352.2	7.5	163.	22.0000	34	7673	51576
1	80.5	135225	355.6	7.5	163.	22.6932	35	7673	51576
1	79.5	135226	358.9	7.5	163.	23.5073	36	7673	51576
1	78.5	135227	2.1	7.5	163.	24.0000	37	7673	51576
1	77.5	135228	5.4	7.5	163.	25.0000	38	7673	51576
1	76.5	135229	8.7	7.5	163.	26.0000	39	7673	51576
1	75.5	135230	12.1	7.5	163.	26.8433	40	7673	51576
1	74.5	135231	15.4	7.5	163.	27.0000	41	7673	51576
1	73.5	135232	18.7	7.5	163.	28.0000	42	7673	51576
1	72.5	135233	22.1	7.5	163.	28.0000	43	7673	51576
1	71.5	135234	25.4	7.5	163.	29.0000	44	7673	51576
1	70.5	135235	28.7	7.5	163.	30.0000	45	7673	51576
1	69.5	135236	32.1	7.5	163.	30.0000	46	7673	51576
1	68.5	135237	35.4	7.5	163.	31.0000	47	7673	51576
1	67.5	135238	38.8	7.5	163.	32.0000	48	7673	51576
1	66.5	135239	42.2	7.5	163.	33.0000	49	7673	51576
1	65.5	135240	45.4	7.5	163.	34.0000	50	7673	51576
1	64.5	135241	48.8	7.5	163.	34.9894	51	7673	51576
1	63.5	135242	52.2	7.5	163.	35.0000	52	7673	51576
1	62.5	135243	55.5	7.5	163.	36.0000	53	7673	51576
1	61.5	135244	58.8	7.5	163.	36.1474	54	7673	51576
1	60.5	135245	62.3	7.5	163.	37.0000	55	7673	51576
1	59.5	135246	65.6	7.5	163.	38.0000	56	7673	51576
1	58.5	135247	69.0	7.5	163.	39.0000	57	7673	51576
1	57.5	135248	72.3	7.5	163.	40.0000	58	7673	51576
1	56.5	135249	75.7	7.5	163.	40.0805	59	7673	51576
1	55.5	135250	79.1	7.5	163.	42.0000	60	7673	51576
1	54.5	135251	82.5	7.5	163.	42.0584	61	7673	51576
1	53.5	135252	85.9	7.5	163.	43.0000	62	7673	51576
1	52.5	135253	89.2	7.5	163.	44.0000	63	7673	51576
1	51.5	135254	92.5	7.5	163.	44.7928	64	7673	51576
1	50.5	135255	95.8	7.5	163.	45.1806	65	7673	51576
1	49.5	135256	99.1	7.5	163.	46.1009	66	7673	51576
1	48.5	135257	102.5	7.5	163.	47.0000	67	7673	51576
1	47.5	135258	105.7	7.5	163.	48.0000	68	7673	51576
1	46.5	135259	109.0	7.5	163.	49.0000	69	7673	51576
1	45.5	135300	112.4	7.5	163.	50.0000	70	7673	51576
1	44.5	135301	115.7	7.5	163.	51.0000	71	7673	51576
1	43.5	135302	119.0	7.5	163.	52.0000	72	7673	51576
1	42.5	135303	122.3	7.5	163.	53.0000	73	7673	51576
1	41.5	135304	125.6	7.5	163.	54.0000	74	7673	51576
1	40.5	135305	128.9	7.5	163.	55.0000	75	7673	51576
1	39.5	135306	132.2	7.5	163.	55.0213	76	7673	51576
1	38.5	135307	135.5	7.5	163.	56.0000	77	7673	51576
1	37.5	135308	138.8	7.5	163.	56.1700	78	7673	51576
1	36.5	135309	142.1	7.5	163.	57.0000	79	7673	51576
1	35.5	135310	145.4	7.5	163.	57.4090	80	7673	51576
1	34.5	135311	148.7	7.5	163.	58.0000	81	7673	51576
1	33.5	135312	152.1	7.5	163.	58.1673	82	7673	51576
1	32.5	135313	155.4	7.5	163.	59.0000	83	7673	51576
1	31.5	135314	158.8	7.5	163.	59.0000	84	7673	51576
1	30.5	135315	162.3	7.5	163.	59.1673	85	7673	51576
1	29.5	135316	165.5	7.5	163.	59.3758	86	7673	51576
1	28.5	135317	168.9	7.5	163.	60.0000	87	7673	51576
1	27.5	135318	172.4	7.5	163.	60.0000	88	7673	51576
1	26.5	135319	175.8	7.5	163.	60.0013	89	7673	51576
1	25.5	135320	179.1	7.5	163.	60.1673	90	7673	51576
1	24.5	135321	182.5	7.5	163.	60.5976	91	7673	51576
1	23.5	135322	185.8	7.5	163.	61.0000	92	7673	51576
1	22.5	135323	189.0	7.5	163.	61.0000	93	7673	51576
1	21.5	135324	192.4	7.5	163.	61.0000	94	7673	51576
1	20.5	135325	195.7	7.5	163.	61.0000	95	7673	51576
1	19.5	135326	199.1	7.5	163.	61.0000	96	7673	51576
1	18.5	135327	202.5	7.5	163.	61.0000	97	7673	51576
1	17.5	135328	205.8	7.5	163.	61.0000	98	7673	51576
1	16.5	135329	209.2	7.5	163.	61.0000	99	7673	51576
1	15.5	135330	212.5	7.5	163.	61.0013	100	7673	51576
1	14.5	135335	229.1	7.5	163.	61.0040	101	7673	51576
STA	DAY	TIME	AZM	ELEV	RNG	XBAR	REC	TAPE	DATE

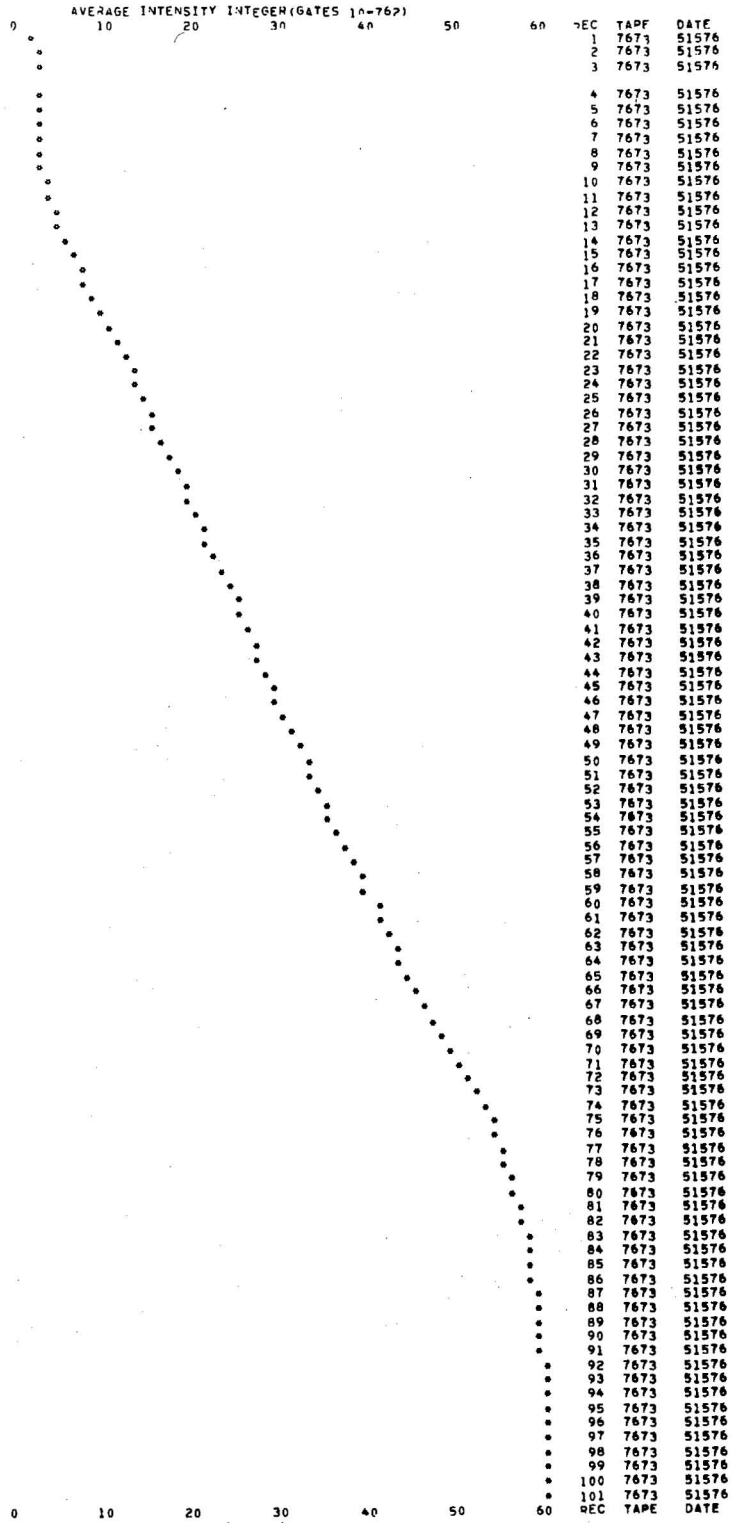

Figure 6.1. Receiver calibration plot of signal generator power in dBm versus mean integrator value. Variable DAY is the calibration power in dBm and XBAR is the average of last 753 integrator gates.

DATE 51576 TIME 135145 STATION NRO CHANNEL A
LOG CONST 0.77 AGC NOISE 3.00 S/N -101.7
TRANS POW 750. CABLE + COUPLER LOSS 9.5

AGC	DBM	SNR	AGC	DBM	SNR
0	-109.1	-7.3	32	-64.5	37.2
1	-109.1	-7.3	33	-63.2	38.5
2	-109.1	-7.3	34	-61.9	39.8
3	-109.1	-7.3	35	-60.6	41.2
4	-104.6	-2.9	36	-59.3	42.4
5	-102.3	-0.6	37	-58.0	43.7
6	-100.4	1.3	38	-56.7	45.0
7	-98.8	2.9	39	-55.5	46.2
8	-97.3	4.4	40	-54.2	47.5
9	-95.9	5.8	41	-53.0	48.7
10	-94.5	7.2	42	-51.7	50.0
11	-93.2	8.5	43	-50.5	51.2
12	-91.8	9.9	44	-49.3	52.4
13	-90.5	11.3	45	-48.2	53.5
14	-89.1	12.6	46	-47.0	54.7
15	-87.8	14.0	47	-45.9	55.8
16	-86.4	15.3	48	-44.8	56.9
17	-85.0	16.7	49	-43.7	58.0
18	-83.7	18.0	50	-42.5	59.2
19	-82.3	19.4	51	-41.3	60.4
20	-81.0	20.7	52	-40.1	61.7
21	-79.6	22.1	53	-38.7	63.0
22	-78.3	23.4	54	-37.3	64.5
23	-76.9	24.8	55	-35.7	66.0
24	-75.5	26.2	56	-33.9	67.8
25	-74.2	27.6	57	-31.8	69.9
26	-72.8	29.0	58	-29.3	72.4
27	-71.4	30.4	59	-26.3	75.4
28	-70.0	31.7	60	-22.2	79.6
29	-68.6	33.1	61	-17.2	84.5
30	-67.3	34.5	62	-17.2	84.5
31	-65.9	35.8	63	-17.2	84.5

Figure 6.2. Final intensity calibration table relating integrator values (AGC) to power received in dBm and signal-to-noise ratio in dB.

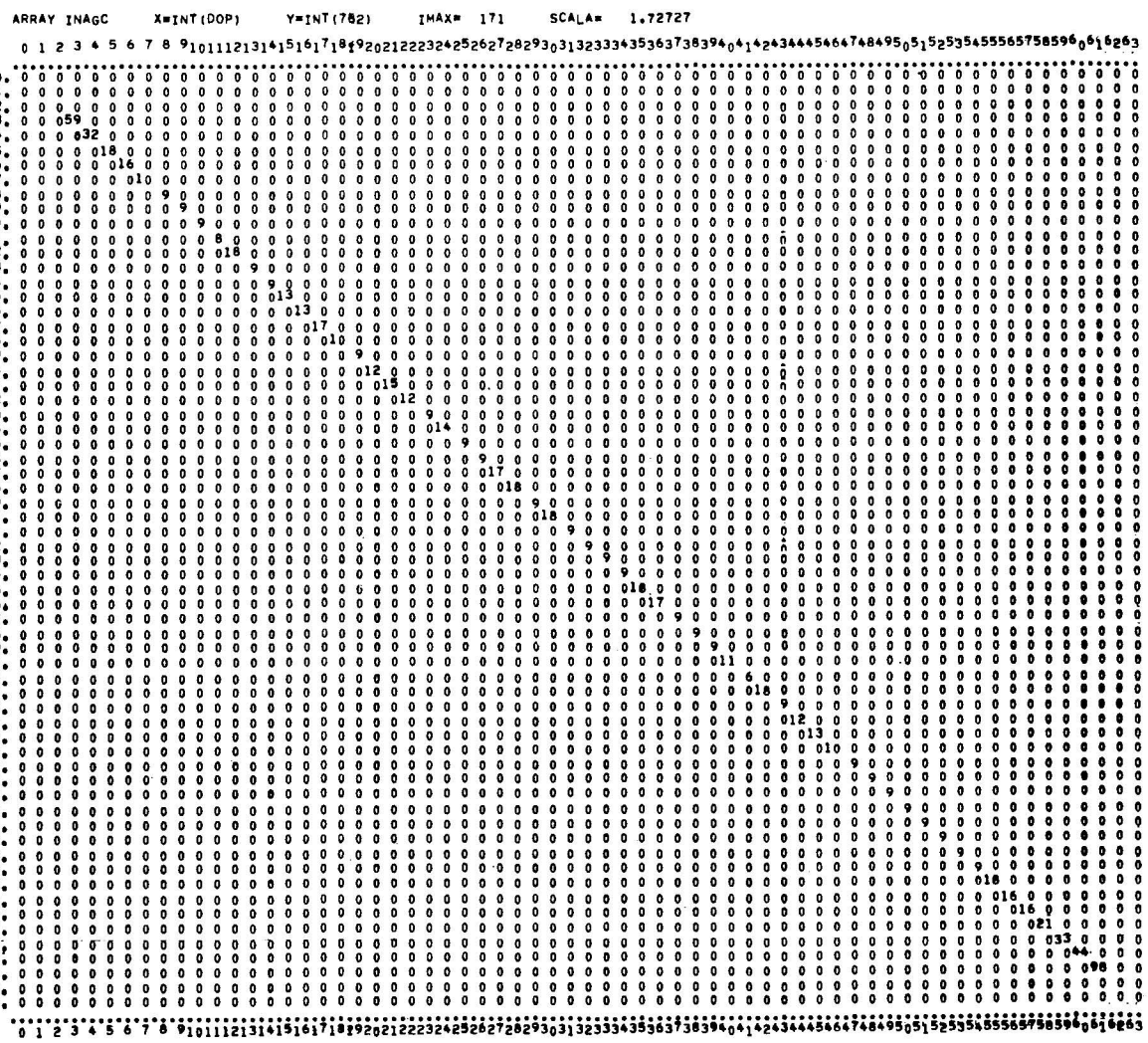

Figure 6.3. Scattergram of integrator value as recorded on 16 gate Doppler record, INT (DOP), and the value of the corresponding location as recorded on the 762 gate integrator record, INT (762). Data taken during intensity calibration.

INPUT DATE AND TIME LIMITS OF TAPE 52976 183151 183954 DATE PROCESSED 09/04/76

AGC	RMS HIGH	RMS LOW
0	-1.	9999.
1	-1.	9999.
2	70.	57.
3	82.	44.
4	92.	45.
5	92.	43.
6	79.	43.
7	81.	49.
8	77.	54.
9	87.	55.
10	90.	68.
11	103.	78.
12	115.	84.
13	121.	76.
14	113.	71.
15	98.	74.
16	115.	87.
17	121.	62.
18	114.	59.
19	100.	70.
20	108.	69.
21	112.	92.
22	93.	64.
23	96.	66.
24	111.	92.
25	120.	101.
26	132.	111.
27	88.	72.
28	103.	87.
29	113.	99.
30	124.	110.
31	142.	120.
32	161.	135.
33	91.	79.
34	106.	88.
35	120.	97.
36	75.	68.
37	91.	70.
38	112.	84.
39	128.	101.
40	88.	77.
41	108.	85.
42	117.	106.
43	144.	107.
44	155.	127.
45	85.	76.
46	103.	77.
47	103.	94.
48	118.	101.
49	87.	68.
50	92.	73.
51	99.	91.
52	122.	102.
53	87.	79.
54	103.	88.
55	117.	96.
56	139.	106.
57	157.	119.
58	113.	94.
59	130.	106.
60	155.	115.
61	154.	116.
62	170.	121.
63	-1.	9999.

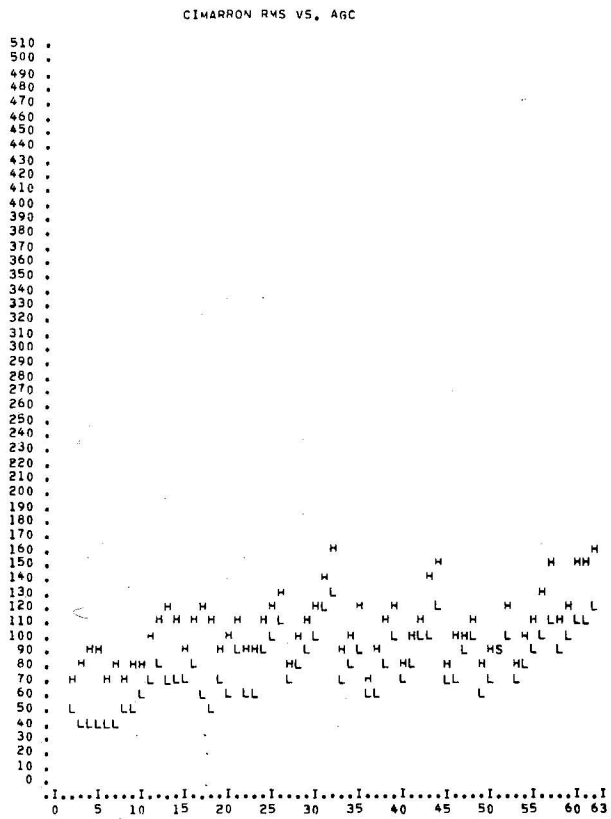

Figure 6.4. Table showing the maximum and minimum root-mean-square (RMS) of the in-phase or quadrature components of the time series data for each integrator class. The plot shows maximum RMS (H) and minimum RMS (L) versus integrator classes. Data taken during intensity calibration.

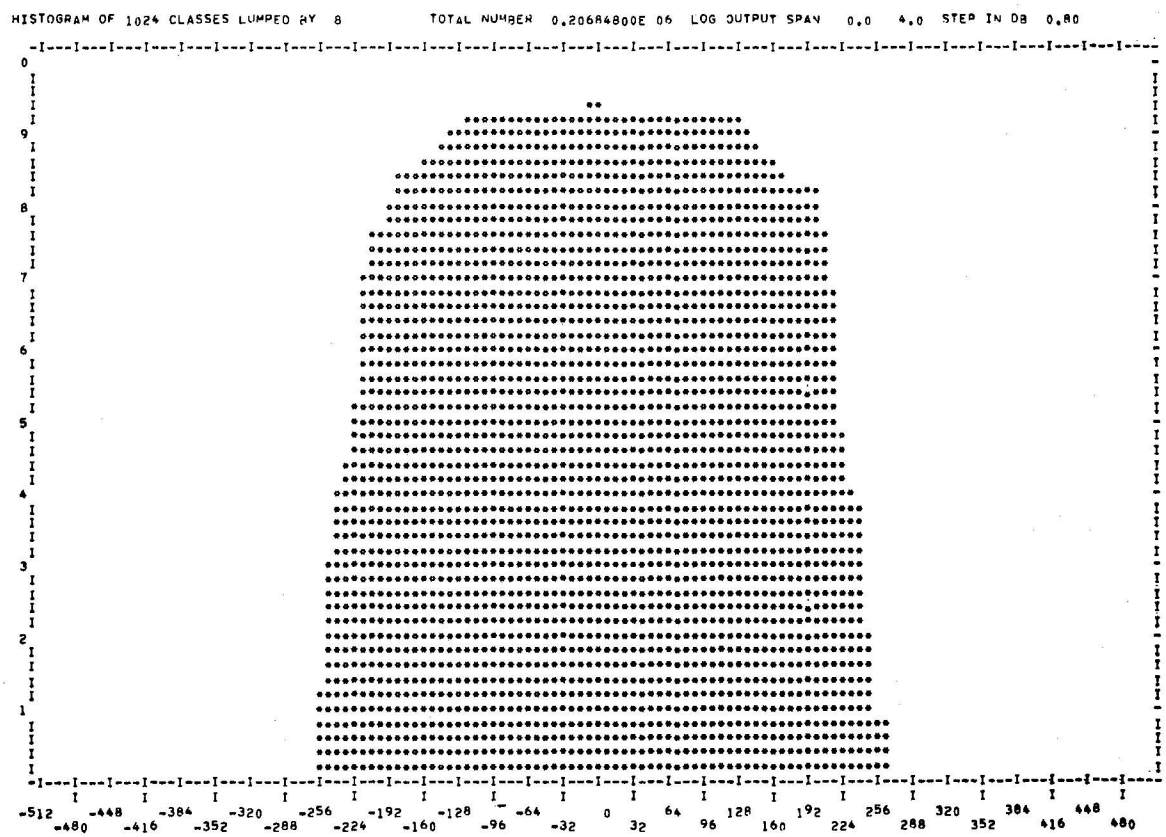

Figure 6.5. Histogram showing relative frequency distribution of each analog-to-digital converter class (-512 to +511 in increments of eight). Data taken during intensity calibration.

NOR DOPPLER RECORD
INTEGRATOR STATISTICS JULIAN DATE 105 TIME 135145 135335 GATES 1 TO 16 RECORDS PROCESSED 101

GATE	1	2	3	4	5	6	7	8	9	10	11	12	13	14	15	16
63	0	0	0	0	0	0	0	0	0	0	0	0	0	0	0	0
62	0	0	0	0	0	0	0	0	0	0	0	0	0	0	0	0
61	11	11	11	11	11	11	10	11	10	10	11	10	10	11	10	10
60	4	5	5	5	5	4	5	4	5	5	5	5	5	5	5	5
59	4	3	3	3	3	4	4	4	4	4	3	4	4	3	4	4
58	2	2	3	3	2	3	2	2	2	2	2	2	2	2	2	2
57	2	2	2	1	2	1	2	2	2	2	2	2	2	2	2	2
56	2	2	1	2	2	2	2	2	2	2	2	2	2	2	2	2
55	2	2	2	2	2	2	2	2	2	2	2	2	2	2	2	2
54	1	1	1	1	1	1	1	1	1	1	1	1	1	1	1	1
53	1	1	1	1	1	1	1	1	1	1	1	1	1	1	1	1
52	1	1	1	1	1	1	1	1	1	1	1	1	1	1	1	1
51	1	1	1	1	1	1	1	1	1	1	1	1	1	1	1	1
50	1	1	1	1	1	1	1	1	1	1	1	1	1	1	1	1
49	1	1	1	1	1	1	1	1	1	1	1	1	1	1	1	1
48	1	1	1	1	1	1	1	1	1	1	1	1	1	1	1	1
47	1	1	1	1	1	1	1	1	1	1	1	1	1	1	1	1
46	1	1	2	1	1	1	1	1	1	1	1	1	1	1	1	1
45	2	2	1	2	2	2	2	1	1	2	1	1	2	1	1	1
44	1	1	1	1	1	1	1	2	2	1	2	2	1	2	2	2
43	1	1	1	1	1	1	1	1	1	1	1	1	1	1	1	1
42	2	2	2	2	2	2	2	2	2	2	2	2	2	2	2	2
41	1	1	1	1	1	1	1	0	0	1	0	0	1	0	0	1
40	1	1	1	1	1	1	1	2	2	1	2	2	1	2	2	1
39	1	1	1	1	1	1	1	1	1	1	1	1	1	1	1	1
38	1	1	1	1	1	1	1	1	1	1	1	1	1	1	1	1
37	1	1	1	1	1	1	1	1	1	1	1	1	1	1	1	1
36	2	2	2	2	2	2	2	2	2	2	2	2	2	2	2	2
35	2	2	2	2	2	2	2	2	2	2	2	2	2	2	2	2
34	1	1	1	1	1	1	1	1	1	1	1	1	1	1	1	1
33	1	1	1	1	1	1	1	1	1	1	1	1	1	1	1	1
32	1	1	1	1	1	1	1	1	1	1	1	1	1	1	1	1
31	1	1	1	1	1	1	1	1	1	1	1	1	1	1	1	1
30	2	2	2	2	2	2	2	2	2	2	2	2	2	2	2	2
29	1	1	1	1	1	1	1	1	1	1	1	1	1	1	1	1
28	2	2	2	2	2	2	2	2	2	2	2	2	2	2	2	2
27	2	2	2	2	2	2	2	2	2	2	2	2	2	1	2	1
26	1	1	1	1	1	1	1	1	1	1	1	1	1	2	1	2
25	1	1	1	1	1	1	1	1	1	1	1	1	1	1	1	1
24	2	1	2	2	2	1	2	1	1	1	1	1	2	1	1	2
23	1	2	1	1	1	1	1	1	2	2	1	1	1	1	2	0
22	1	1	1	1	1	2	1	2	1	1	2	2	1	2	1	2
21	1	1	2	2	1	2	1	1	1	1	2	1	2	1	1	1
20	2	2	1	1	2	1	2	2	2	2	1	2	1	2	2	2
19	1	1	1	1	1	1	1	1	1	1	1	1	1	1	1	1
18	1	1	2	1	2	1	1	1	1	1	1	1	1	1	1	1
17	2	2	1	2	1	2	2	2	2	2	2	2	2	2	2	2
16	1	1	1	1	1	1	1	1	1	1	1	1	1	1	1	1
15	2	2	2	2	2	2	2	2	2	2	2	2	2	2	2	2
14	1	1	1	1	1	1	1	1	1	1	1	1	1	1	1	1
13	1	1	1	1	1	1	1	1	1	1	1	1	1	1	1	1
12	2	1	1	2	1	1	2	1	1	1	1	1	2	1	1	1
11	1	2	2	1	2	2	1	2	2	2	2	2	1	2	2	2
10	0	1	1	1	1	1	1	1	1	0	1	1	1	1	1	1
9	2	1	1	1	1	1	1	1	1	2	1	1	1	1	1	1
8	1	1	1	1	1	1	1	1	1	1	1	1	1	1	1	1
7	1	1	1	2	2	2	1	2	1	2	1	1	1	2	2	2
6	2	2	2	1	1	1	2	1	2	1	1	2	2	1	1	0
5	2	2	4	2	2	1	2	3	2	2	3	2	3	2	2	3
4	3	4	1	4	3	5	3	4	4	5	4	3	3	4	5	3
3	7	6	7	6	7	6	7	5	6	5	6	7	6	6	5	7
2	0	0	0	0	0	0	0	0	0	0	0	0	0	0	0	0
1	0	0	0	0	0	0	0	0	0	0	0	0	0	0	0	0
0	0	0	0	0	0	0	0	0	0	0	0	0	0	0	0	0

Figure 6.6. Frequency distribution of integrator classes for each of the 16 gates as contained in the time series record header. Data taken during intensity calibration.

NOR INTEGRATOR STATISTICS JULIAN DATE 105 TIME 135145 135335 GATES 10 TO 762 RECORDS PROCESSED 101

NUMBER OF CLASSES = 64, TOTAL FREQUENCY COUNT = 0.76053000E 05, EACH ASTERISK WAS A VALUE OF 0.200E 03

INT	FREQ	INT	FREQ
0	0	32	753
1	0	33	753
2	42	34	761
3	4966	35	1493
4	2601	36	1395
5	1569	37	864
6	1104	38	753
7	922	39	753
8	818	40	843
9	965	41	663
10	615	42	1462
11	959	43	797
12	1211	44	909
13	793	45	1214
14	755	46	813
15	1442	47	829
16	824	48	753
17	1450	49	753
18	801	50	753
19	753	51	753
20	1190	52	753
21	1069	53	753
22	984	54	753
23	893	55	1490
24	1135	56	1394
25	753	57	1326
26	871	58	1688
27	1388	59	2729
28	1506	60	3597
29	753	61	8103
30	1506	62	4
31	753	63	0

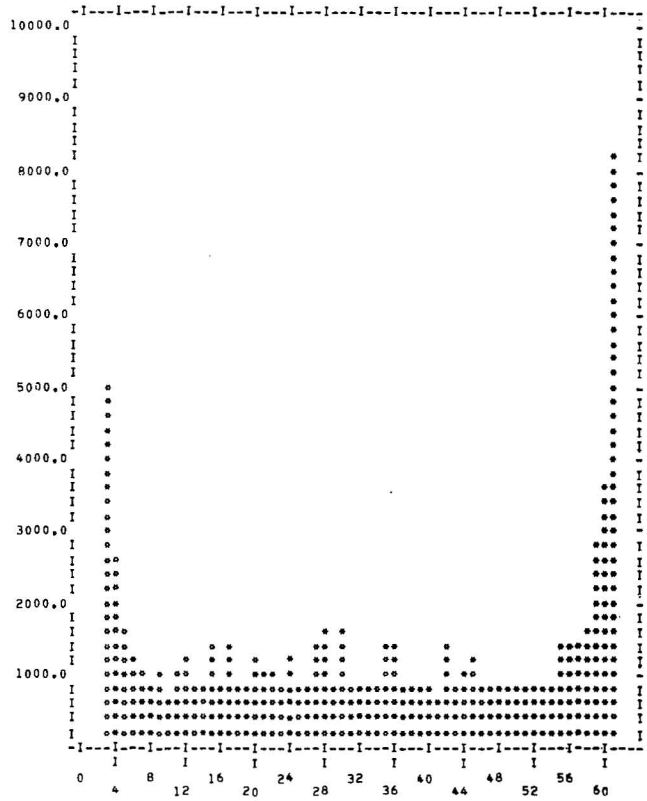

Figure 6.7. Frequency distribution and histogram of the integrator values for gates 10 to 762. Data taken during intensity calibration.

NOR PULSE PAIR VELOCITY STATISTICS JULIAN DATE 105 TIME 135145 135335 GATES 10 TO 762 RECORDS PROCESSED 101

NUMBER OF CLASSES = 64, TOTAL FREQUENCY COUNT = 0.76053000E 05, EACH ASTERISK HAS A VALUE OF 0.400E 02

PPP	FREQ	PPP	FREQ
-32	1994	0	1255
-31	1769	1	1098
-30	1321	2	1087
-29	1213	3	1202
-28	1248	4	1114
-27	1232	5	1229
-26	1610	6	1150
-25	1695	7	1093
-24	1295	8	1065
-23	1103	9	1168
-22	942	10	1411
-21	793	11	1661
-20	898	12	1185
-19	859	13	940
-18	855	14	1027
-17	1050	15	1026
-16	1498	16	1156
-15	1318	17	1294
-14	1242	18	1022
-13	1296	19	1161
-12	1307	20	1401
-11	1364	21	1513
-10	1116	22	1225
-9	761	23	1005
-8	596	24	1146
-7	688	25	1195
-6	948	26	1283
-5	1010	27	1408
-4	1279	28	1458
-3	1071	29	1497
-2	822	30	1278
-1	828	31	1279

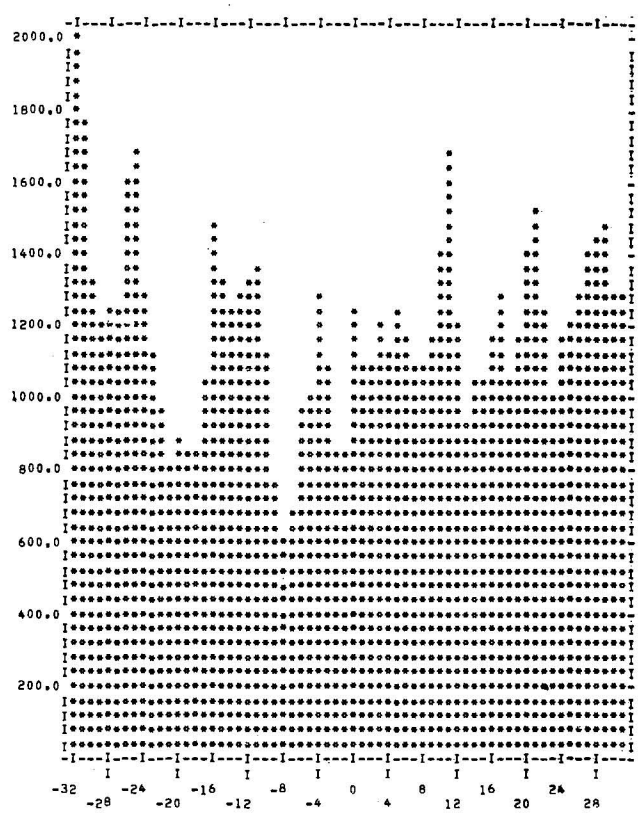

Figure 6.8. Frequency distribution and histogram of the hardwired pulse pair velocity estimator for gates 10 to 762. The classes can be converted to m s^{-1} by multiplying by the Nyquist velocity divided by 32. Data taken during intensity calibration.

NOR PULSE PAIR WIDTH STATISTICS JULIAN DATE 105 TIME 135145 135335 GATES 10 TO 762 RECORDS PROCESSED 101

NUMBER OF CLASSES = 64, TOTAL FREQUENCY COUNT = 0.76053000E 05, EACH ASTERISK HAS A VALUE OF 0.100E 04

WID	FREQ	WID	FREQ
0	0	32	9142
1	0	33	0
2	0	34	0
3	0	35	0
4	0	36	0
5	0	37	0
6	0	38	0
7	0	39	0
8	0	40	0
9	0	41	0
10	0	42	0
11	0	43	0
12	0	44	0
13	0	45	0
14	0	46	0
15	0	47	0
16	0	48	0
17	0	49	0
18	0	50	0
19	0	51	0
20	0	52	0
21	0	53	0
22	0	54	0
23	0	55	0
24	0	56	0
25	0	57	0
26	0	58	0
27	4	59	0
28	132	60	0
29	2111	61	0
30	40262	62	0
31	24402	63	0

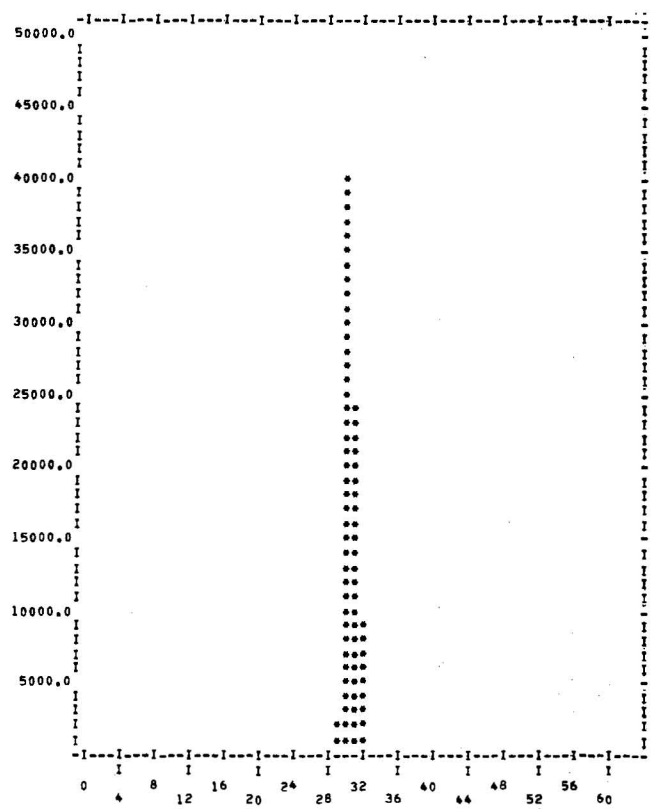

Figure 6.9. Frequency distribution and histogram of the hardwired spectrum width estimator. Only classes 0-32 exist. Data taken during intensity calibration.

6.2 Noise Statistics

Receiver noise with its well behaved statistical properties is useful for testing parts of the signal processing and recording chain, particularly the hardwired mean velocity and spectrum width calculation. Examples of such testing is given in Figs. 6.10 through 6.12. Explanation and test interpretation are given in section 4.1.

NOR INTEGRATOR STATISTICS JULIAN DATE 303 TIME 135422 135432 GATES 10 TO 762 RECORDS PROCESSED 11

NUMBER OF CLASSES = 64, TOTAL FREQUENCY COUNT = 0.82830000E 04, EACH ASTERISK HAS A VALUE OF 0.200E 03

INT	FREQ	INT	FREQ
0	0	32	0
1	0	33	0
2	693	34	0
3	7582	35	0
4	8	36	0
5	0	37	0
6	0	38	0
7	0	39	0
8	0	40	0
9	0	41	0
10	0	42	0
11	0	43	0
12	0	44	0
13	0	45	0
14	0	46	0
15	0	47	0
16	0	48	0
17	0	49	0
18	0	50	0
19	0	51	0
20	0	52	0
21	0	53	0
22	0	54	0
23	0	55	0
24	0	56	0
25	0	57	0
26	0	58	0
27	0	59	0
28	0	60	0
29	0	61	0
30	0	62	0
31	0	63	0

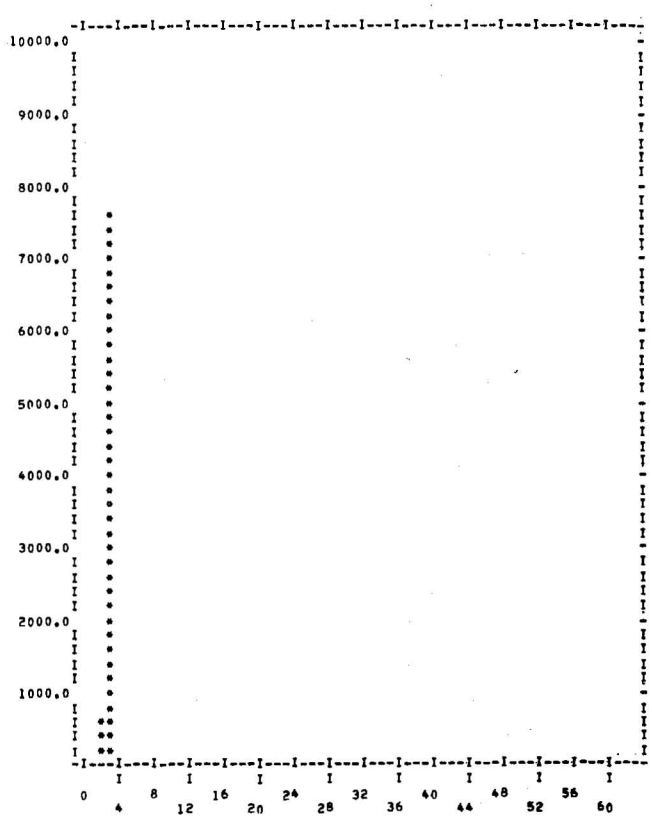

Figure 6.10. Frequency distribution and histogram of the integrator values for noise alone.

NOR PULSE PAIR VELOCITY STATISTICS JULIAN DATE 303 TIME 135422 135432 GATES 10 TO 762 RECORDS PROCESSED 11

NUMBER OF CLASSES = 64, TOTAL FREQUENCY COUNT = 0.82830000E 04, EACH ASTERISK HAS A VALUE OF 0.333E 01

PPP	FREQ	PPP	FREQ
-32	119	0	151
-31	122	1	155
-30	117	2	141
-29	117	3	157
-28	148	4	150
-27	138	5	127
-26	127	6	146
-25	111	7	123
-24	132	8	141
-23	115	9	136
-22	120	10	142
-21	115	11	110
-20	109	12	137
-19	115	13	122
-18	115	14	142
-17	134	15	133
-16	141	16	134
-15	125	17	128
-14	111	18	124
-13	131	19	117
-12	131	20	140
-11	123	21	121
-10	130	22	96
-9	139	23	103
-8	152	24	120
-7	133	25	102
-6	165	26	119
-5	141	27	116
-4	155	28	111
-3	152	29	132
-2	150	30	115
-1	146	31	113

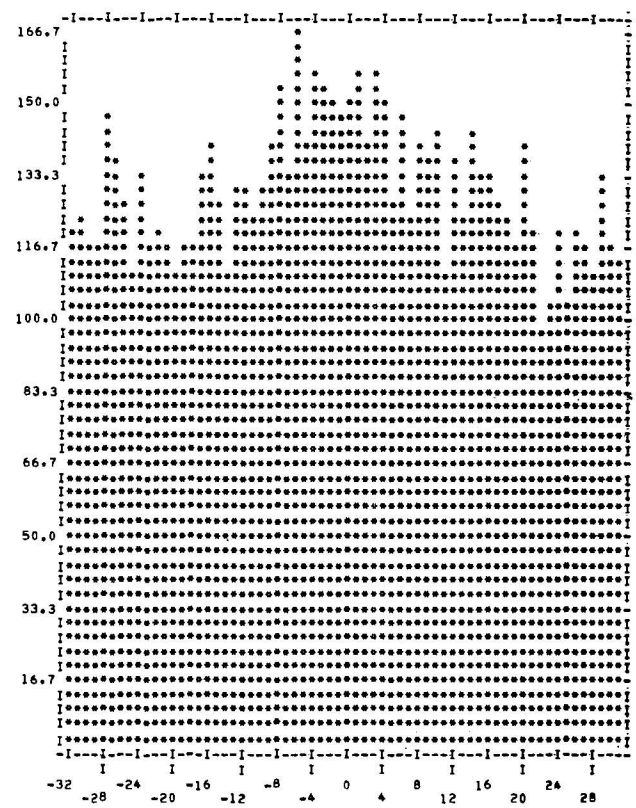

Figure 6.11. Frequence distribution and histogram of the hardwired pulse pair velocity estimator for noise alone.

NOR PULSE PAIR WIDTH STATISTICS JULIAN DATE 303 TIME 135422 135432 GATES 10 TO 762 RECORDS PROCESSED 11

NUMBER OF CLASSES = 64, TOTAL FREQUENCY COUNT = 0.82830000E 04, EACH ASTERISK HAS A VALUE OF 0.100E 03

WID	FREQ	WID	FREQ
0	0	32	1565
1	0	33	0
2	0	34	0
3	0	35	0
4	0	36	0
5	0	37	0
6	0	38	0
7	0	39	0
8	0	40	0
9	0	41	0
10	0	42	0
11	0	43	0
12	0	44	0
13	0	45	0
14	0	46	0
15	0	47	0
16	0	48	0
17	0	49	0
18	0	50	0
19	0	51	0
20	0	52	0
21	0	53	0
22	0	54	0
23	0	55	0
24	0	56	0
25	0	57	0
26	0	58	0
27	1	59	0
28	120	60	0
29	877	61	0
30	3473	62	0
31	2247	63	0

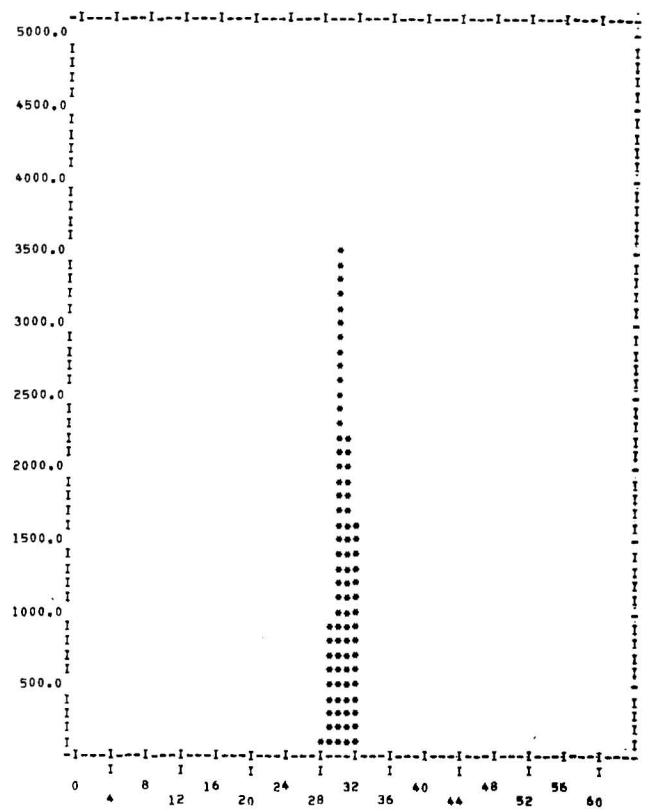

Figure 6.12. Frequency distribution and histogram of the hardwired spectrum width estimator for noise alone.

6.3 Meteorological Data Quality

The most comprehensive evaluation of data quality is made on the basis of the testing of actual data. Examples of this type of testing is given in Figs. 6.13 through 6.23. Interpretation of the testing is explained in section 4.2.

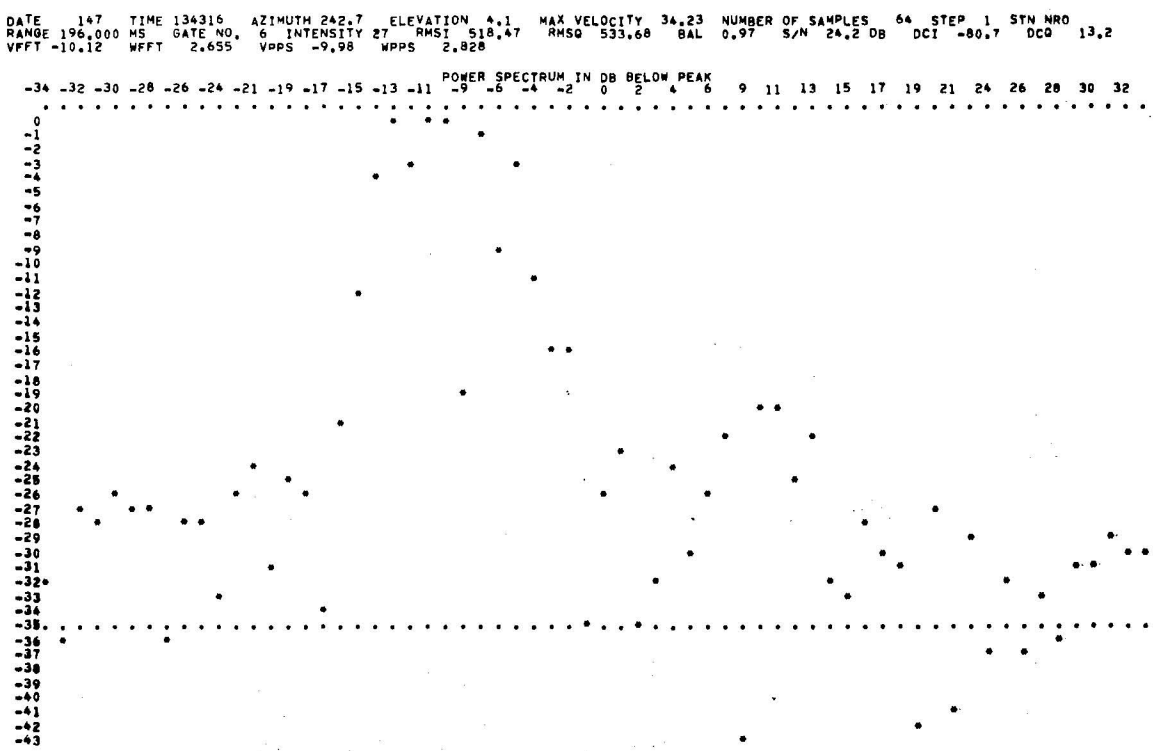

Figure 6.13. Power spectrum plot for one Doppler gate with power displayed in dB below the peak power versus velocity in m s^{-1}. Quality control spectrum plots are automatically selected based on SNR and velocity criteria.

INPUT DATE AND TIME LIMITS OF TAPE 50576 211443 211516 DATE PROCESSED 09/09/76

AGC	RMS HIGH	RMS LOW
0	-1.	9999.
1	-1.	9999.
2	-1.	9999.
3	826.	280.
4	1248.	217.
5	1299.	206.
6	1552.	203.
7	1296.	206.
8	1444.	215.
9	1371.	188.
10	1105.	147.
11	1508.	221.
12	1511.	151.
13	1339.	107.
14	1417.	129.
15	1098.	129.
16	1397.	130.
17	1160.	116.
18	1452.	104.
19	1246.	154.
20	1402.	105.
21	1333.	143.
22	1230.	144.
23	1291.	97.
24	1287.	95.
25	1181.	161.
26	1344.	112.
27	923.	147.
28	1338.	115.
29	1099.	149.
30	734.	145.
31	845.	129.
32	729.	139.
33	1002.	148.
34	892.	176.
35	920.	162.
36	1085.	215.
37	853.	206.
38	742.	193.
39	834.	279.
40	741.	433.
41	468.	405.
42	731.	380.
43	427.	418.
44	-1.	9999.
45	-1.	9999.
46	-1.	9999.
47	-1.	9999.
48	-1.	9999.
49	-1.	9999.
50	-1.	9999.
51	-1.	9999.
52	-1.	9999.
53	-1.	9999.
54	-1.	9999.
55	-1.	9999.
56	-1.	9999.
57	-1.	9999.
58	-1.	9999.
59	-1.	9999.
60	-1.	9999.
61	-1.	9999.
62	-1.	9999.
63	-1.	9999.

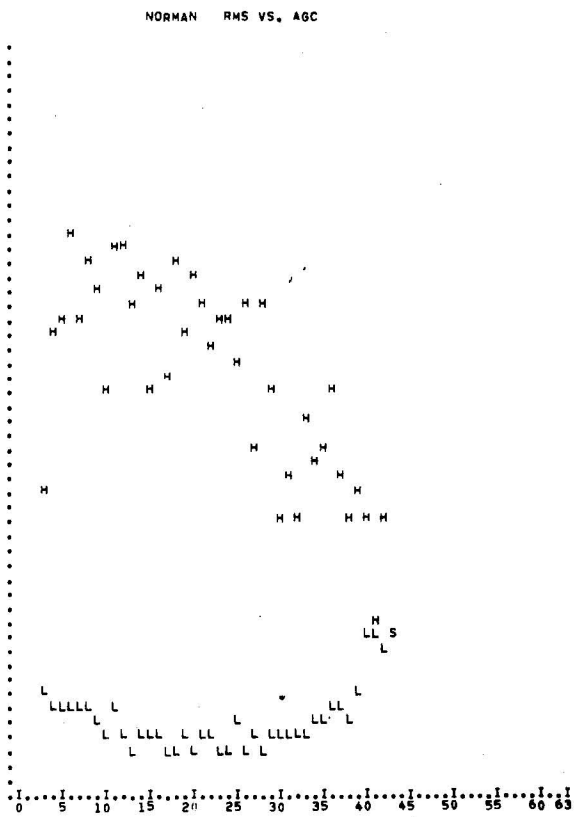

Figure 6.14. Maximum and minimum RMS for weather data. See Fig. 6.4 for explanation of symbols.

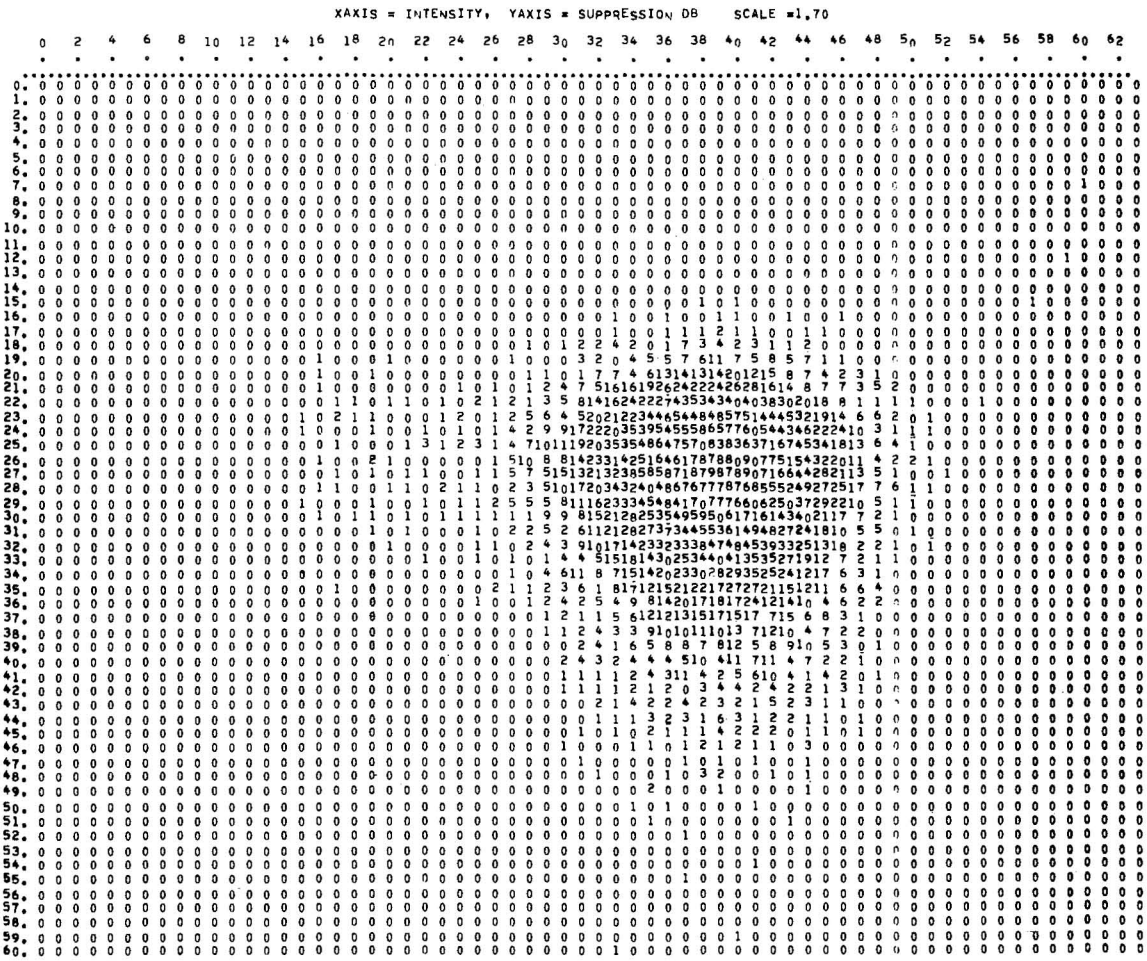

Figure 6.15. Scattergram of image suppression in dB versus integrator digital value. This suppression is derived from the power spectrum. See for example, Fig. 6.13 where the image appears as -19 dB at +11 m s^{-1} which is opposite the peak at -11 m s^{-1}.

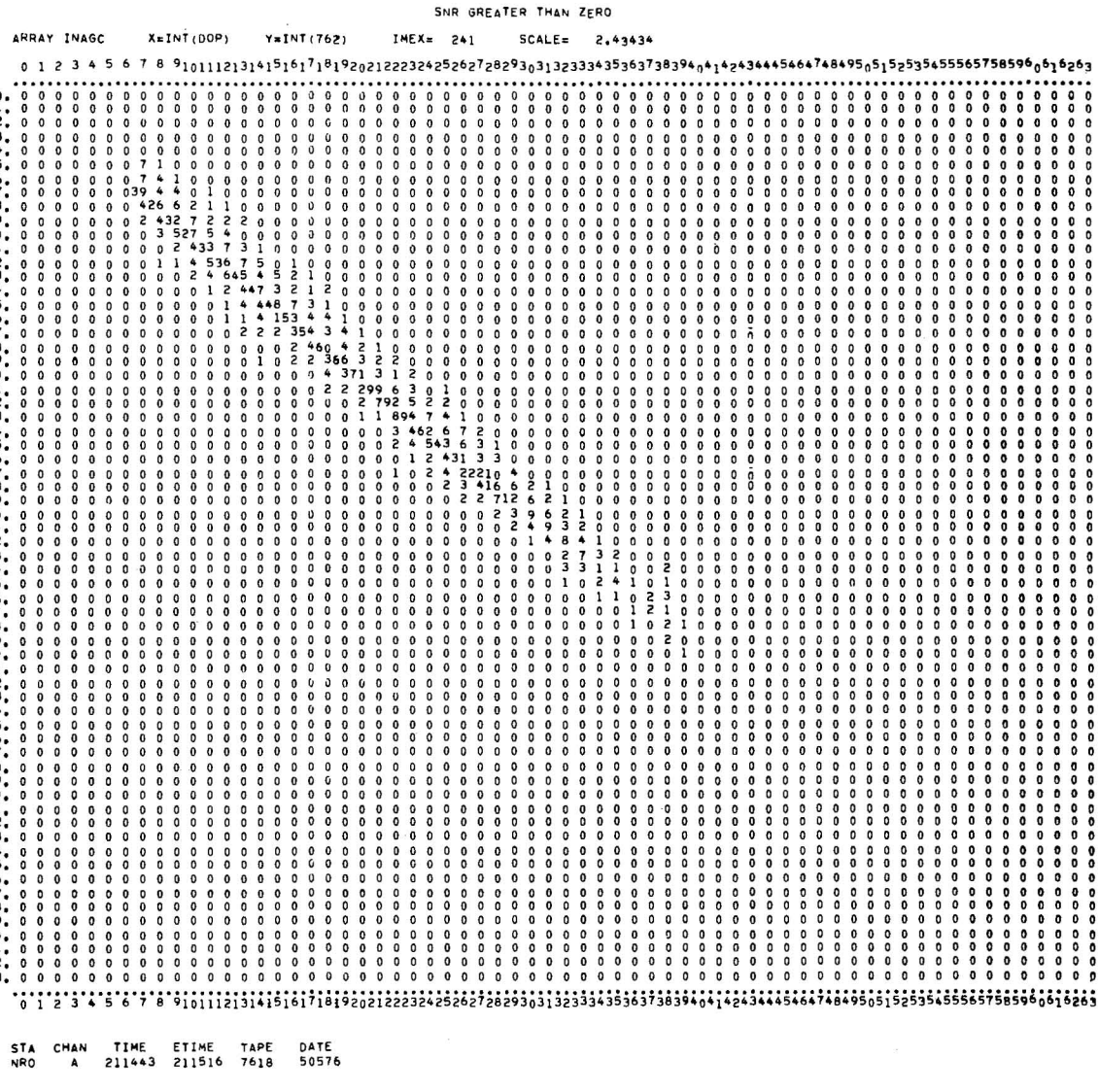

Figure 6.16. Scattergram of Doppler record integrator value and corresponding integrator record value for weather data. Signal-to-noise ratio greater than zero dB. See Fig. 6.3 for symbols and comparison weather and calibration signals.

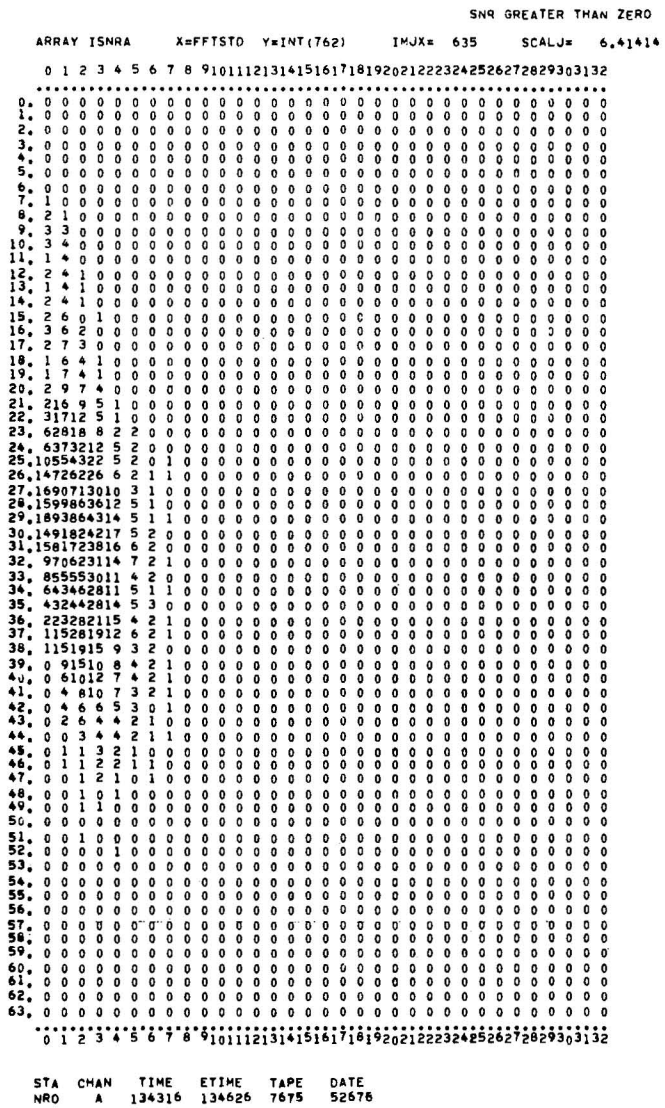

Figure 6.17. Scattergram of spectral width derived from power spectrum (W_{FFT}) and corresponding integrator value from the integrator record.

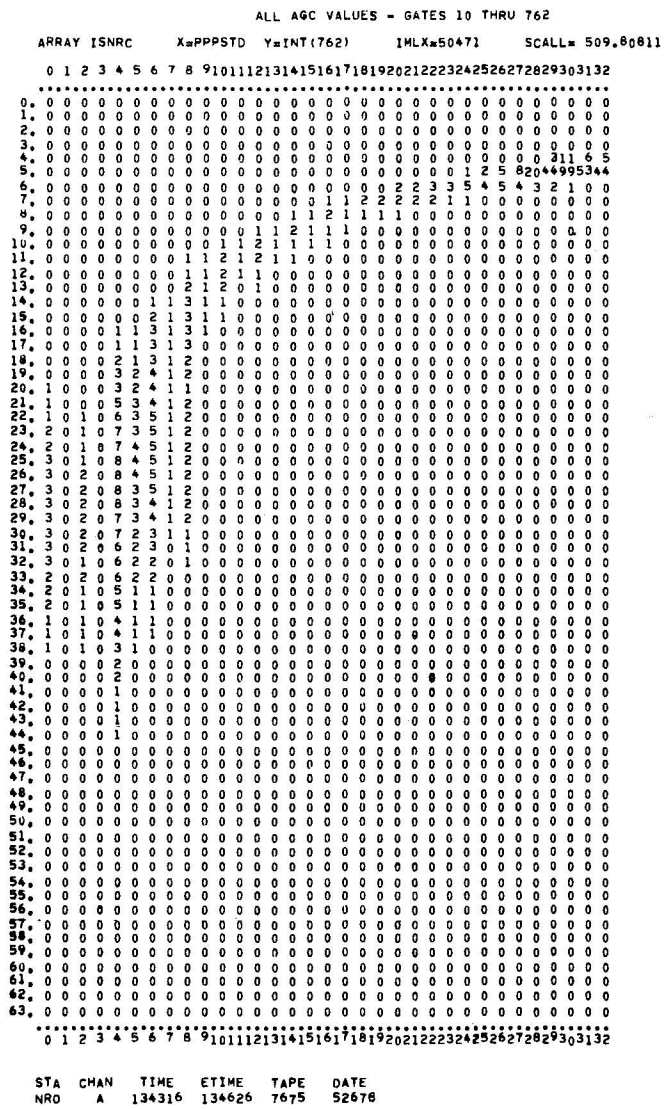

Figure 6.18. Scattergram of hardwired width estimator (W_{PP}) and corresponding integrator value for all signal strengths including noise. Note the absence of width classes 1 and 3 due to hardwired word truncation.

Figure 6.19. Scattergram of hardwired width estimator and corresponding integrator value for signal-to-noise ratio greater than zero dB.

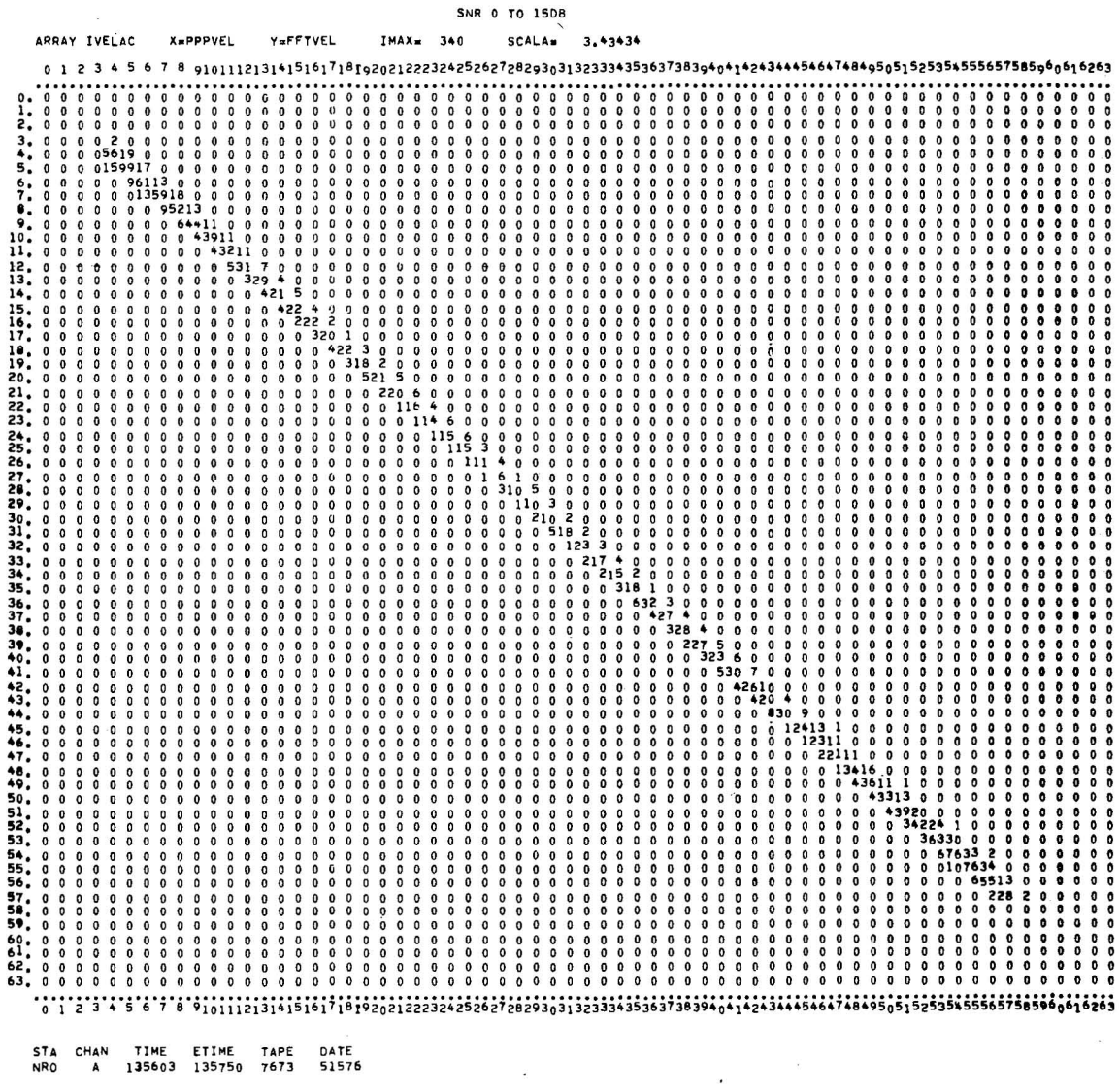

Figure 6.20. Scattergram of hardwired pulse pair velocity and power spectrum derived velocity for the same pulse volume. Only velocities at pulse volumes having a signal-to-noise ratio between zero and 15 dB are included.

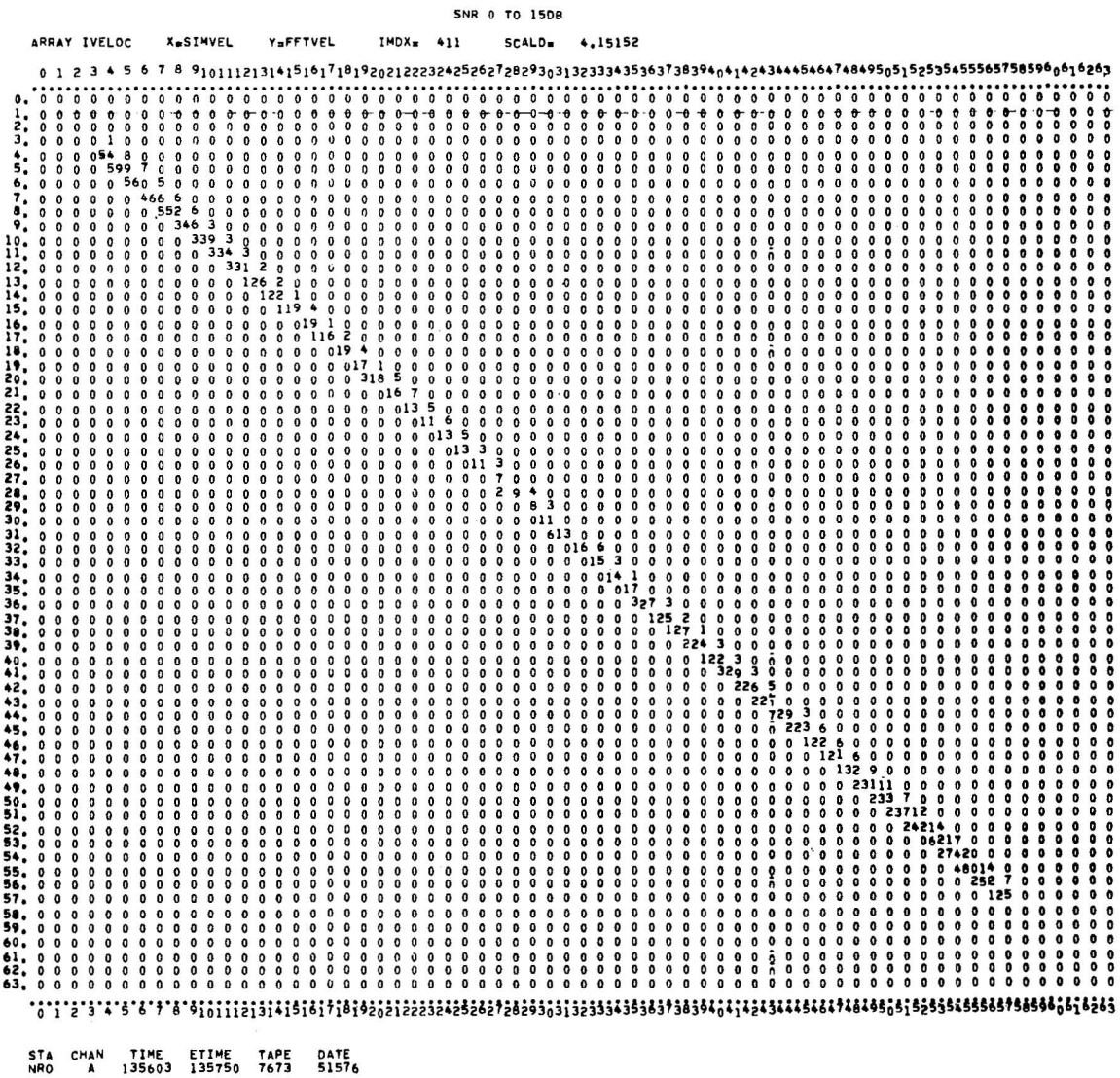

Figure 6.21. Scattergram of simulated pulse pair velocity (pulse pair algorithm applied to time series components) and power spectrum derived velocity. SNR is between zero and 15 dB.

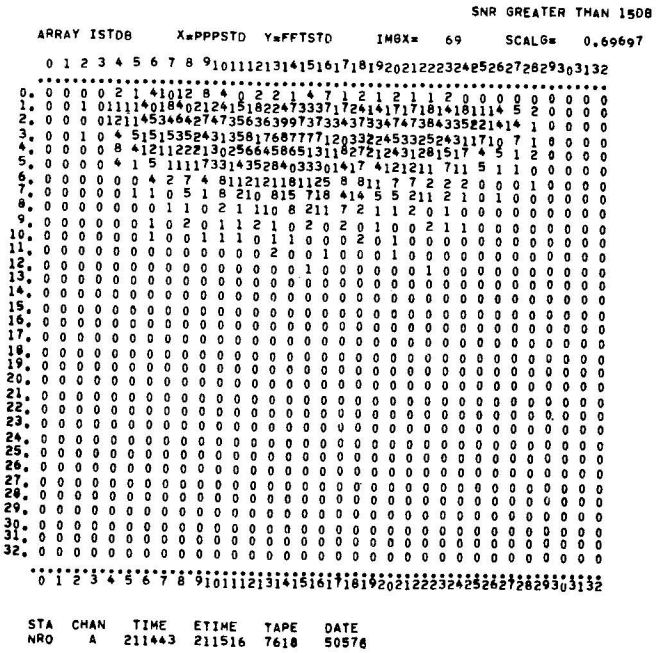

Figure 6.22. Scattergram of hardwired velocity width estimate and corresponding power spectrum width (FFT) for SNR greater than 15 dB.

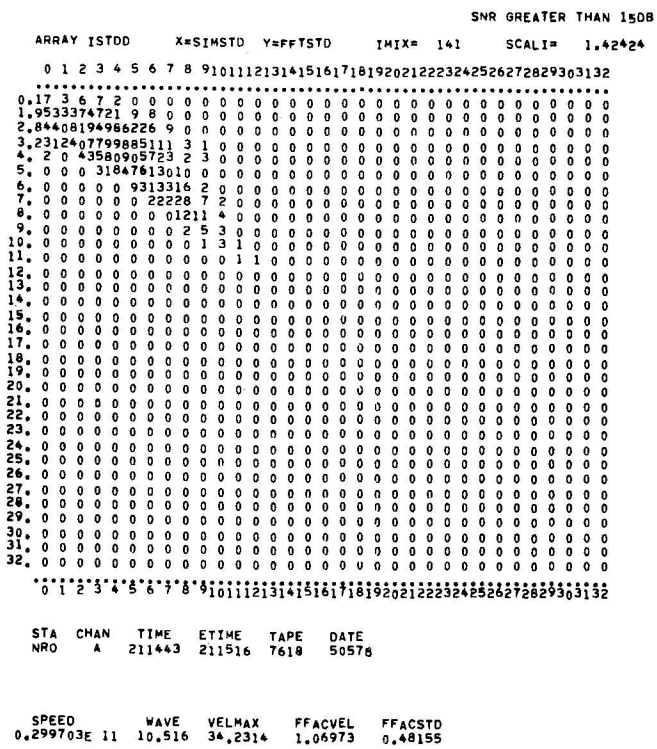

Figure 6.23. Scattergram of simulated pulse pair width estimate and power spectrum derived width estimate for SNR greater than 15 dB.

6.4 Special Purpose Programs

Subtle problems which can arise in a system of this complexity require detail examination of certain parameters. Examples of this type of testing are given in Figs. 6.24 through 6.27. Example parameters are ADC testing, analomas frequencies in the system, ADC malfunction, failure of a single range location, etc.

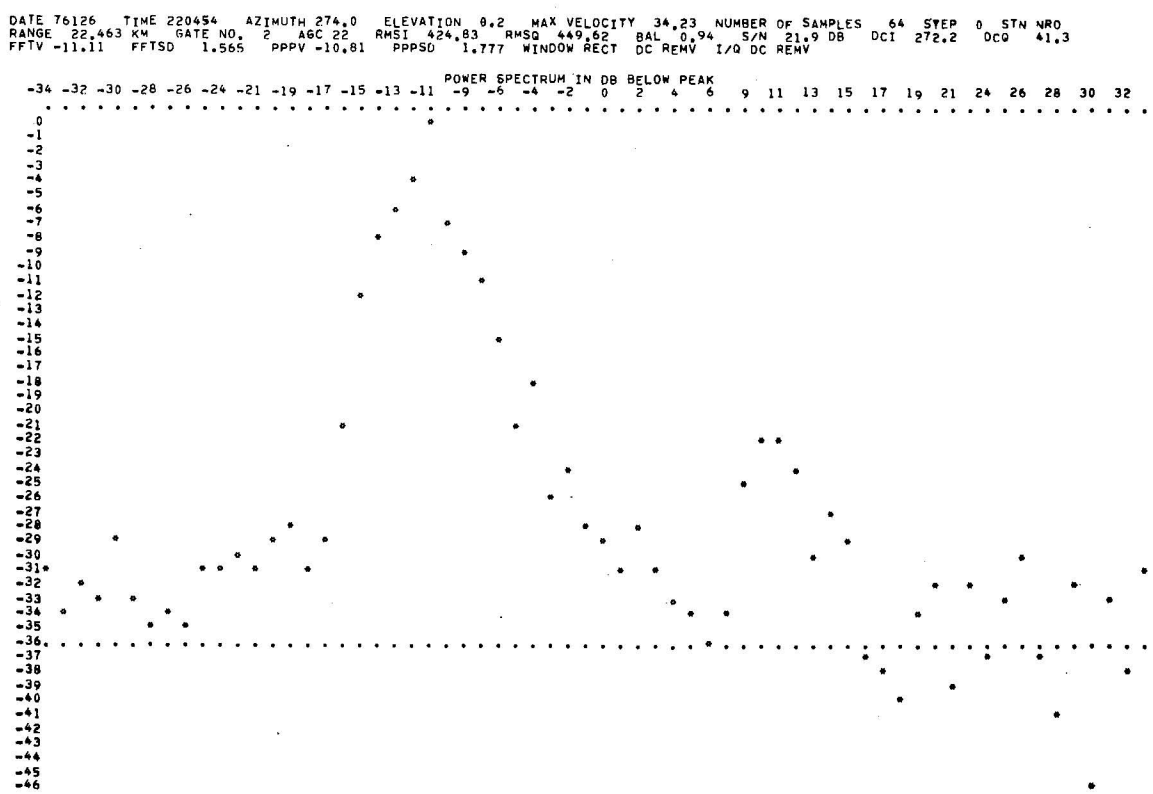

Figure 6.24. Power spectrum plot with power displayed in dB below the peak power versus velocity. For research purposes different "windows" may be applied and D.C. values may be removed from the time series components.

I COMPONENT

-187	-35	397	917	949	239	-507	-593	71	821	1018	645	189	-117	-213	63
341	567	603	426	181	-1	71	277	490	533	363	23	-247	-67	495	970
843	61	-534	-262	587	1059	649	-75	-369	151	623	599	269	59	82	139
151	357	687	715	171	-357	-197	571	1007	645	-181	-393	-133	357	669	789

Q COMPONENT

75	527	631	158	-585	-866	-341	-551	955	583	-130	-658	-546	-146	219	430
375	119	-145	-313	-233	46	251	286	94	-201	-329	-273	119	555	687	174
-625	-781	-105	789	827	39	-745	-529	231	583	283	-226	-297	-73	59	123
254	414	110	-450	-601	-57	638	671	-67	-747	-525	78	587	558	267	-105

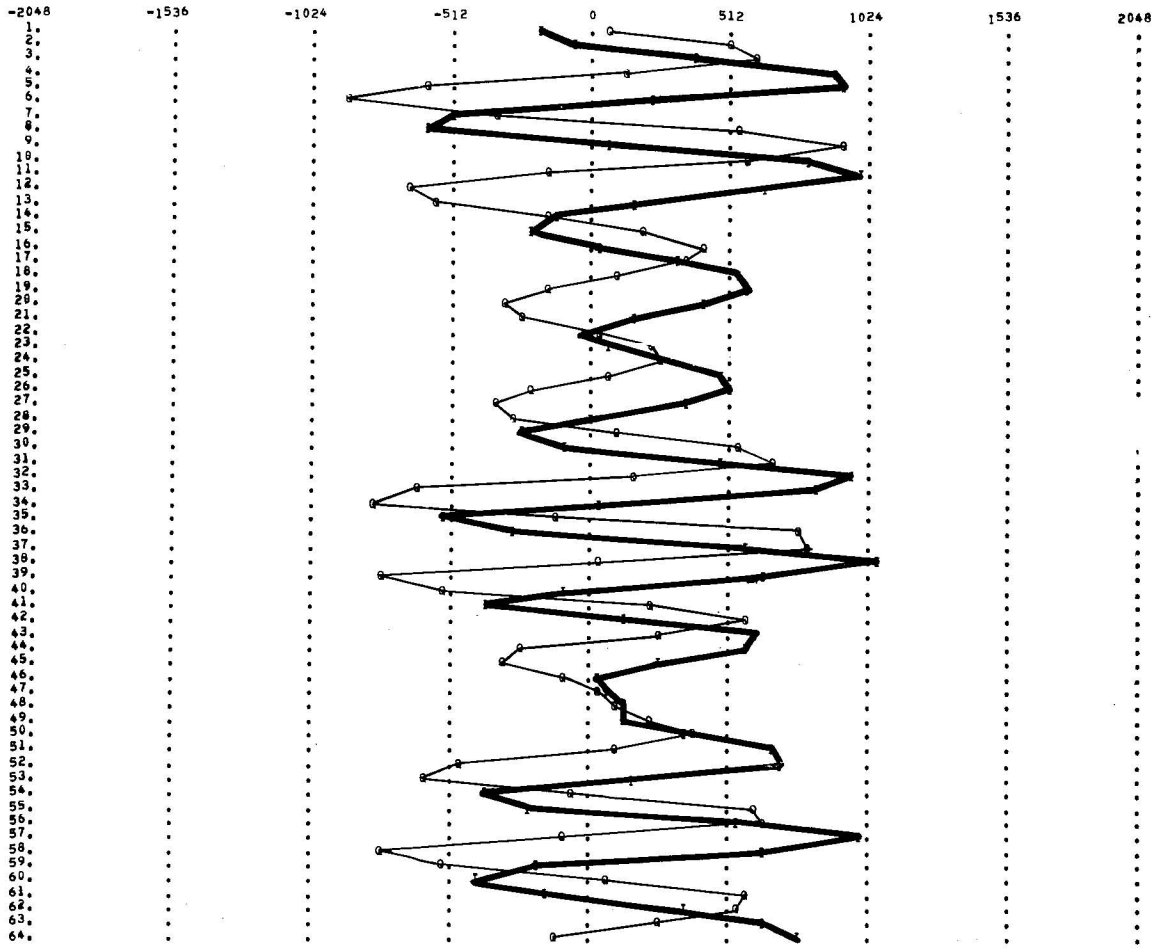

Figure 6.25. Plot of in-phase and quadrature video components (complex video) from which the spectrum in Fig. 6.24 is derived. The I and Q range, -2048 to +2047, correspond to the Norman Doppler 12 bit ADC. The real time spacing between samples (I/Q pairs) is one PRT or 768 μs.

NOR INTEGRATOR RECORD BIT STATISTICS JULIAN DATE 303 TIME 165100 18031R GATES 10 TO 762 RECORDS PROCESSED 1595

GATE	10	11	12	13	14	15	16	17	18	19	20	21	22	23	24	25
6	1577	1577	1577	1577	1576	1576	1574	1548	1507	1461	1457	1548	1558	1531	1523	1551
5	1359	978	834	879	888	528	567	476	482	672	462	372	407	270	348	416
4	660	756	872	796	792	884	889	845	789	756	790	796	887	753	810	851
3	798	820	823	794	798	816	853	804	857	862	837	840	850	834	865	815
2	765	813	784	799	773	773	780	789	780	749	813	797	775	834	784	784
1	774	787	820	818	831	791	798	800	805	789	805	778	800	812	774	767

GATE	26	27	28	29	30	31	32	33	34	35	36	37	38	39	40	41
6	1560	1539	1528	1496	1509	1532	1339	1156	1034	720	724	479	405	229	289	369
5	502	417	517	679	727	472	469	525	618	967	956	1104	1198	1203	1030	998
4	950	844	825	820	840	845	734	739	714	938	803	657	665	618	703	680
3	849	846	842	861	855	844	819	856	825	847	805	833	870	789	831	801
2	809	801	815	786	807	828	796	788	788	798	747	782	800	835	821	858
1	817	786	814	769	768	795	801	822	793	808	793	791	811	789	796	842

GATE	42	43	44	45	46	47	48	49	50	51	52	53	54	55	56	57
6	431	431	249	359	308	310	244	272	148	176	157	158	130	131	118	124
5	1027	966	1050	1086	1102	1173	1153	1197	947	1061	987	888	711	677	699	884
4	637	643	739	608	666	734	714	772	811	743	777	810	896	938	914	794
3	824	798	792	801	824	788	811	813	844	818	752	758	795	756	809	801
2	781	799	797	805	812	861	764	793	821	785	786	734	810	796	788	811
1	768	784	800	802	808	783	822	781	801	813	780	788	790	784	761	758

GATE	58	59	60	61	62	63	64	65	66	67	68	69	70	71	72	73
6	116	147	183	151	180	231	151	127	128	138	151	141	121	218	172	109
5	707	1057	1171	1077	1119	982	851	863	833	765	735	679	584	771	796	822
4	921	795	743	690	771	796	836	879	861	889	918	952	963	874	967	888
3	766	835	791	825	793	771	775	785	781	764	737	741	741	753	782	781
2	773	804	750	747	780	823	761	795	815	761	787	748	807	795	783	777
1	798	799	815	768	816	848	819	800	827	845	787	792	767	786	789	773

GATE	74	75	76	77	78	79	80	81	82	83	84	85	86	87	88	89
6	110	145	163	169	185	198	172	187	149	168	183	190	173	161	207	241
5	677	881	967	938	991	1061	1018	970	1033	969	856	1002	900	863	1035	885
4	952	834	851	835	827	780	810	832	775	804	872	802	827	865	820	910
3	762	809	805	801	807	793	814	774	812	844	777	787	778	801	780	780
2	770	788	760	802	814	762	811	804	803	782	803	806	792	811	745	778
1	778	821	803	805	785	839	837	782	813	813	797	800	764	811	789	825

GATE	90	91	92	93	94	95	96	97	98	99	100	101	102	103	104	105
6	164	194	148	182	234	226	185	132	115	132	121	129	151	120	113	105
5	880	745	766	705	780	806	810	695	673	878	861	921	856	806	648	723
4	873	904	874	913	927	910	852	882	896	830	826	771	865	839	932	882
3	787	746	826	795	766	752	815	753	780	776	797	809	822	778	771	748
2	797	789	818	787	791	797	821	800	769	737	821	755	779	796	776	816
1	803	768	830	825	786	774	792	816	787	765	816	809	853	799	804	815

GATE	106	107	108	109	110	111	112	113	114	115	116	117	118	119	120	121
6	106	106	111	108	98	84	85	82	106	124	83	83	82	82	71	84
5	538	620	657	709	676	576	679	747	852	967	802	619	698	601	534	701
4	931	905	908	886	889	883	874	870	811	775	829	792	839	846	862	827
3	778	784	777	765	810	774	787	764	777	797	777	795	832	831	814	773
2	790	787	812	811	783	776	802	838	792	825	809	821	808	808	821	782
1	815	799	800	787	831	814	777	781	778	818	824	809	803	771	794	797

GATE	122	123	124	125	126	127	128	129	130	131	132	133	134	135	136	137
6	85	69	74	72	57	71	63	55	44	60	56	48	48	31	35	26
5	735	548	632	671	520	683	691	556	482	531	423	385	374	421	383	379
4	791	853	842	865	822	851	865	786	784	789	803	662	568	575	515	508
3	788	789	789	813	850	817	806	867	895	841	907	1032	1111	1061	1132	1137
2	795	821	819	785	844	789	830	836	855	816	820	847	884	878	870	839
1	788	794	772	816	808	816	788	814	815	795	808	780	835	815	804	817

GATE	138	139	140	141	142	143	144	145	146	147	148	149	150	151	152	153
6	23	27	27	25	25	24	20	19	19	24	29	37	45	39	42	79
5	358	359	366	373	368	366	343	351	335	307	299	315	377	370	470	674
4	497	479	468	494	485	475	470	489	466	493	486	600	684	661	728	714
3	1176	1178	1197	1156	1163	1187	1211	1189	1208	1210	1188	1080	1015	1021	952	923
2	870	833	892	871	850	841	872	889	874	874	933	908	825	797	876	812
1	799	825	799	830	836	810	824	797	793	777	759	774	845	831	813	804

GATE	154	155	156	157	158	159	160	161	162	163	164	165	166	167	168	169
6	62	64	48	58	52	58	56	66	63	73	67	62	73	78	77	78
5	668	577	318	316	340	354	366	398	416	420	425	442	530	533	580	565
4	712	689	608	476	498	564	511	544	530	515	507	528	629	637	630	626
3	973	984	1085	1159	1153	1130	1138	1087	1091	1106	1119	1131	988	1022	1032	1037
2	824	831	847	796	766	748	791	800	806	810	784	823	797	808	831	820
1	857	817	820	838	879	873	821	797	816	817	821	826	786	827	771	803

GATE	170	171	172	173	174	175	176	177	178	179	180	181	182	183	184	185
6	78	74	71	68	69	65	63	63	71	73	80	72	68	67	67	73
5	569	636	600	579	566	567	559	568	524	534	524	529	541	550	547	558
4	611	629	631	617	637	645	660	640	648	671	678	651	605	594	609	613
3	1053	1013	1022	1020	1010	989	994	996	1037	966	954	1013	1037	1031	1026	1002
2	788	773	802	801	781	776	807	762	818	848	835	845	834	819	797	821
1	819	858	821	806	813	827	786	852	819	758	803	778	818	819	812	811

GATE	186	187	188	189	190	191	192	193	194	195	196	197	198	199	200	201
6	75	68	66	63	68	80	66	70	67	77	82	80	79	77	80	76
5	548	534	566	577	560	589	567	567	570	553	553	543	539	549	586	563
4	594	587	631	607	604	629	633	650	631	655	653	690	673	661	727	684
3	1017	1058	1016	1019	1039	1048	1045	1005	1030	1016	1029	1006	1014	1029	946	1010
2	859	844	858	873	874	821	839	873	867	870	851	852	850	840	855	862
1	770	818	783	763	791	805	772	762	756	773	792	762	790	777	762	774

GATE	202	203	204	205	206	207	208	209	210	211	212	213	214	215	216	217
6	78	81	75	73	72	66	70	67	69	71	74	73	76	76	75	76
5	570	578	579	570	566	594	622	641	664	671	715	733	763	797	828	839
4	641	614	647	662	671	679	658	675	697	714	678	721	731	702	718	748
3	1008	1033	1046	1018	1037	1020	1043	1042	1010	992	998	956	962	968	942	904
2	886	885	890	887	868	865	902	927	881	867	863	889	843	845	866	867
1	757	770	750	761	748	782	702	722	744	759	754	781	738	780	753	781

GATE	218	219	220	221	222	223	224	225	226	227	228	229	230	231	232	233
6	73	67	68	71	75	76	75	70	67	62	63	62	71	67	69	68
5	866	900	899	893	870	855	840	839	826	807	802	811	792	786	799	817
4	773	788	828	824	813	832	845	867	875	889	912	875	873	883	880	881
3	898	901	899	899	900	894	895	876	864	901	823	875	834	851	853	867
2	863	860	852	845	877	852	838	859	846	868	859	866	844	825	861	880
1	763	782	772	747	794	751	792	778	760	751	790	793	768	787	756	722

GATE	234	235	236	237	238	239	240	241	242	243	244	245	246	247	248	249
6	68	73	72	79	79	84	82	87	88	89	88	86	86	83	84	78
5	833	850	868	879	890	874	877	867	873	874	865	876	888	905	911	925
4	887	911	903	890	899	884	868	884	856	889	912	913	886	897	904	899
3	881	806	841	846	810	818	821	816	850	801	804	804	871	824	830	837
2	852	872	907	836	831	830	864	855	864	865	844	881	878	825	866	875
1	791	784	778	770	754	770	788	783	737	755	769	765	778	811	753	783

GATE	250	251	252	253	254	255	256	257	258	259	260	261	262	263	264	265
6	78	72	72	74	69	67	63	67	59	58	58	54	50	47	46	43
5	942	957	960	955	955	958	970	951	972	955	951	945	964	955	978	978
4	894	882	881	900	909	928	909	896	902	945	935	952	929	941	935	943
3	826	831	835	801	805	812	798	823	786	765	768	774	757	818	770	783
2	838	867	853	843	876	842	872	888	833	826	828	845	871	858	850	855
1	763	772	762	786	769	783	765	790	792	778	781	758	798	801	802	765

Figure 6.26. Frequency distribution of bit classes for integrator values (0-63) for each integrator gate (10-762).

```
DATE 76106   TIME 213841   AZIMUTH 229.4   ELEVATION  6.0   VELOCITY SPREAD -35.67 TO 35.67 M/SEC   AGC OFF
VELOCITY RESOLUTION 1.115 M/SEC   WAVELENGTH 10.96 CM   RANGE FIRST GATE  19.801 KM   GATE SPACING  300. M   PRF TRIP 0  STEP 9
STATION CIM  CUT LEVEL 15.0 DB  WINDOW RECT  DC REMV  I/Q DC REMV  I/Q BAL YES  NO. PULSE PAIRS  63 (1)

                                POWER DENSITY SPECTRUM QUANTIZED IN 1DB STEPS BELOW THE PEAK POWER P
 -36 -33 -31 -29 -27 -25 -22 -20 -18 -16 -13 -11  -9  -7  -4  -2   0   2   4   7   9  11  13  16  18  20  22  25  27  29  31  33
GATE. . . . . .
  1                         C P P D 1 B A D
  2                         A   5 3 7 3 P 6
  3                           A 7   P 3
  4                           4 4 P P
  5                             4 1 4 P
  6                             P 4 5 P
  7                                 P
  8                             5 P 1 6 3 9
  9                             P 6 B A B
 10                             8 7 P 3
 11                       8 5 5 P 3 1 8
 12                   A 4 P 4 7 4
 13                       8 P 7
 14                   D 4 7 1 1 P 3 6   D
 15                       B E P 3 6 4   Q
 16                     E C   7 P 6 4 7 6 7
```

GATE	SLANT RANGE	HORIZ RANGE	ALT	VELOC M/SEC	STD M/SEC	LOGZ	AGC	S	PPS M/SEC	STD M/SEC	RMSI	RMSQ	I/Q	S/N DB	DCI	DCQ
1	19.801	19.686	2.090	-18.42	1.709	0.817	18		-18.47	3.805	120.46	133.51	0.90	22.7	30.8	14.3
2	20.101	19.984	2.123	-16.04	1.959	0.670	17		-16.25	3.487	132.59	142.90	0.93	21.1	30.0	7.6
3	20.401	20.282	2.155	-16.88	1.245	-0.406	10		-16.81	1.763	88.56	97.04	0.91	10.2	39.8	16.7
4	20.700	20.580	2.187	-17.92	1.169	-0.714	8		-18.09	-4.545	87.92	92.78	0.95	7.0	29.9	15.9
5	21.000	20.878	2.220	-17.00	1.274	-0.871	7		-16.88	-6.790	86.49	99.42	0.87	5.3	34.5	13.2
6	21.300	21.176	2.252	-17.30	1.469	-0.858	7		-17.72	5.176	51.17	48.39	1.06	5.3	31.7	14.7
7	21.600	21.474	2.285	-16.72	0.000	-0.846	7		-16.74	-6.155	61.95	72.19	0.86	5.3	30.2	9.0
8	21.899	21.771	2.317	-16.74	1.519	-0.344	10		-16.78	-3.605	138.04	151.19	0.91	10.2	26.9	17.7
9	22.199	22.069	2.349	-18.19	1.274	-0.012	12		-18.41	-1.658	140.97	156.41	0.90	13.4	27.2	13.1
10	22.499	22.367	2.382	-16.75	0.962	-0.480	9		-16.82	2.707	63.14	71.16	0.89	8.6	30.3	11.7
11	22.798	22.665	2.414	-18.55	1.702	-0.468	9		-18.73	-2.412	78.12	87.61	0.89	8.6	28.7	9.4
12	23.098	22.963	2.447	-21.63	1.576	-0.297	10		-21.78	4.812	73.57	81.53	0.90	10.2	38.3	9.1
13	23.398	23.261	2.479	-21.06	0.515	-0.125	11		-20.79	4.774	64.29	75.59	0.85	11.8	33.5	11.2
14	23.697	23.558	2.511	-19.89	1.944	0.506	15		-19.96	3.383	103.86	115.75	0.90	18.0	28.0	7.9
15	23.997	23.856	2.544	-18.93	1.563	1.137	19		-18.81	1.614	221.55	220.10	1.01	24.2	27.4	20.5
16	24.297	24.154	2.576	-17.63	2.230	1.758	23		-17.56	3.099	167.56	173.24	0.97	30.3	35.9	21.0

Figure 6.27. Spectrum dump of one time series record showing abbreviated spectrum plot for each of the 16 gates. Letters sequence in one dB steps below the peak coefficient power in the field.

REFERENCES

Barnes, Stanley L., 1974b: Summary of the 1974 severe thunderstorm observation season and operations. NSSL In-house Report, 144 pp.

Burgess, D. W., L. D. Hennington, R. J. Doviak and P. S. Ray, 1976: Multi-moment Doppler display for severe storm identification. J. Appl. Meteor., 15 (12), 1302-1306.

Wilk, K., K. Gray, C. Clark, D. Sirmans, J. Dooley, J. Carter and W. Bumgarner, 1976: Objectives and accomplishments of the NSSL 1975 spring program. NOAA Tech. Memo. ERL NSSL-78, 107 pp.

NATIONAL SEVERE STORMS LABORATORY

The NSSL Technical Memorandum, beginning with No. 28, continue the sequence established by the U. S. Weather Bureau National Severe Storms Project, Kansas City, Missouri. Numbers 1-22 were designated NSSP Reports. Numbers 23-27 were NSSL Reports, and 24-27 appeared as subseries of Weather Bureau Technical Notes. These reports are available from the National Technical Information Service, Operations Division, Springfield, Virginia 22151, for $3.00 and a microfiche version for $0.95. NTIS numbers are given below in parentheses.

No. 1 National Severe Storms Project Objectives and Basic Design. Staff, NSSP. March 1961. (PB-168207)

No. 2 The Development of Aircraft Investigations of Squall Lines from 1956-1960. B. B. Goddard. (PB-168208)

No. 3 Instability Lines and Their Environments as Shown by Aircraft Soundings and Quasi-Horizontal Traverses. D. T. Williams. February 1962. (PB-168209)

No. 4 On the Mechanics of the Tornado. J. R. Fulks. February 1962. (PB-168210)

No. 5 A Summary of Field Operations and Data Collection by the National Severe Storms Project in Spring 1961. J. T. Lee. March 1962. (PB-165095)

No. 6 Index to the NSSP Surface Network. T. Fujita. April 1962. (PB-168212)

No. 7 The Vertical Structure of Three Dry Lines as Revealed by Aircraft Traverses. E. L. McGuire. April 1962. (PB-168213)

No. 8 Radar Observations of a Tornado Thunderstorm in Vertical Section. Ralph J. Donaldson, Jr. April 1962. (PB-174859)

No. 9 Dynamics of Severe Convective Storms. Chester W. Newton. July 1962. (PB-163319)

No. 10 Some Measured Characteristics of Severe Storms Turbulence. Roy Steiner and Richard H. Rhyne. July 1962. (N62-16401)

No. 11 A Study of the Kinematic Properties of Certain Small-Scale Systems. D. T. Williams. October 1962. (PB-168216)

No. 12 Analysis of the Severe Weather Factor in Automatic Control of Air Route Traffic. W. Boynton Beckwith. December 1962. (PB-168217)

No. 13 500-Kc./Sec. Sferics Studies in Severe Storms. Douglas A. Kohl and John E. Miller. April 1963. (PB-168218)

No. 14 Field Operations of the National Severe Storms Project in Spring 1962. L. D. Sanders. May 1963. (PB-168219)

No. 15 Penetrations of Thunderstorms by an Aircraft Flying at Supersonic Speeds. G. P. Roys. Radar Photographs and Gust Loads in Three Storms of 1961 Rough Rider. Paul W. J. Schumacher. May 1963. (PB-168220)

No. 16 Analysis of Selected Aircraft Data from NSSP Operations, 1962. T. Fujita. May 1963. (PB-168221)

No. 17 Analysis of Methods for Small-Scale Surface Network Data. D. T. Williams. August 1963. (PB-168222)

No. 18 The Thunderstorm Wake of May 4, 1961. D. T. Williams. August 1963. (PB-168223)

No. 19 Measurements by Aircraft of Condensed Water in Great Plains Thunderstorms. George P. Roys and Edwin Kessler. July 1966. (PB-173048)

No. 20 Field Operations of the National Severe Storms Project in Spring 1963. J. T. Lee, L. D. Sanders, and D. T. Williams. January 1964. (PB-168224)

No. 21 On the Motion and Predictability of Convective Systems as Related to the Upper Winds in a Case of Small Turning of Wind with Height. James C. Fankhauser. January 1964. (PB-168225)

No. 22 Movement and Development Patterns of Convective Storms and Forecasting the Probability of Storm Passage at a Given Location. Chester W. Newton and James C. Fankhauser. January 1964. (PB-168226)

No. 23 Purposes and Programs of the National Severe Storms Laboratory, Norman, Oklahoma. Edwin Kessler. December 1964. (PB-166675)

No. 24 Papers on Weather Radar, Atmospheric Turbulence, Sferics, and Data Processing. August 1965. (AD-621586)

No. 25 A Comparison of Kinematically Computed Precipitation with Observed Convective Rainfall. James C. Fankhauser. September 1965. (PB-168445)

No. 26 Probing Air Motion by Doppler Analysis of Radar Clear Air Returns. Roger M. Lhermitte. May 1966. (PB-170636)

No. 27 Statistical Properties of Radar Echo Patterns and the Radar Echo Process. Larry Armijo. May 1966. The Role of the Kutta-Joukowski Force in Cloud Systems with Circulation. J. L. Goldman. May 1966. (PB-170756)

No. 28 Movement and Predictability of Radar Echoes. James Warren Wilson. November 1966. (PB-173972)

No. 29 Notes on Thunderstorm Motions, Heights, and Circulations. T. W. Harrold, W. T. Roach, and Kenneth E. Wilk. November 1966. (AD-644899)

No. 30 Turbulence in Clear Air Near Thunderstorms. Anne Burns, Terence W. Harrold, Jack Burnham, and Clifford S. Spavins. December 1966. (PB-173992)

No. 31 Study of a Left-Moving Thunderstorm of 23 April 1964. George R. Hammond. April 1967. (PB-174681)

No. 32 Thunderstorm Circulations and Turbulence from Aircraft and Radar Data. James C. Fankhauser and J. T. Lee. April 1967. (PB-174860)

No. 33 On the Continuity of Water Substance. Edwin Kessler. April 1967. (PB-175840)

No. 34 Note on the Probing Balloon Motion by Doppler Radar. Roger M. Lhermitte. July 1967. (PB-175930)

No. 35 A Theory for the Determination of Wind and Precipitation Velocities with Doppler Radars. Larry Armijo. August 1967. (PB-176376)

No. 36 A Preliminary Evaluation of the F-100 Rough Rider Turbulence Measurement System. U. O. Lappe. October 1967. (PB-177037)

No. 37 Preliminary Quantitative Analysis of Airborne Weather Radar. Lester P. Merritt. December 1967. (PB-177188)

No. 38 On the Source of Thunderstorm Rotation. Stanley L. Barnes. March 1968. (PB-178990)

No. 39 Thunderstorm - Environment Interactions Revealed by Chaff Trajectories in the Mid-Troposphere. James C. Fankhauser. June 1968. (PB-179659)

No. 40 Objective Detection and Correction of Errors in Radiosonde Data. Rex L. Inman. June 1968. (PB-180284)

No. 41 Structure and Movement of the Severe Thunderstorms of 3 April 1964 as Revealed from Radar and Surface Mesonetwork Data Analysis. Jess Charba and Yoshikazu Sasaki. October 1968. (PB-183310)

No. 42 A Rainfall Rate Sensor. Brian E. Morgan. November 1968. (PB-183979)

No. 43 Detection and Presentation of Severe Thunderstorms by Airborne and Ground-Based Radars: A Comparative Study. Kenneth E. Wilk, John K. Carter, and J. T. Dooley. February 1969. (PB-183572)

No. 44 A Study of a Severe Local Storm of 16 April 1967. George Thomas Haglund. May 1969. (PB-184970)

No. 45 On the Relationship Between Horizontal Moisture Convergence and Convective Cloud Formation. Horace R. Hudson. March 1970. (PB-191720)

No. 46 Severe Thunderstorm Radar Echo Motion and Related Weather Events Hazardous to Aviation Operations. Peter A. Barclay and Kenneth E. Wilk. June 1970. (PB-192498)

No. 47 Evaluation of Roughness Lengths at the NSSL-WKY Meteorological Tower. Leslie D. Sanders and Allen H. Weber. August 1970. (PB-194587)

No. 48 Behavior of Winds in the Lowest 1500 ft in Central Oklahoma: June 1966-May 1967. Kenneth C. Crawford and Horace R. Hudson. August 1970.

No. 49 Tornado Incidence Maps. Arnold Court. August 1970. (COM-71-00019)

No. 50 The Meteorologically Instrumented WKY-TV Tower Facility. John K. Carter. September 1970. (COM-71-00108)

No. 51 Papers on Operational Objective Analysis Schemes at the National Severe Storms Forecast Center. Rex L. Inman. November 1970. (COM-71-00136)

No. 52 The Exploration of Certain Features of Tornado Dynamics Using a Laboratory Model. Neil B. Ward. November 1970. (COM-71-00139)

No. 53 Rawinsonde Observation and Processing Techniques at the National Severe Storms Laboratory. Stanley L. Barnes, James H. Henderson, and Robert J. Ketchum. April 1971. (COM-71-00707)

No. 54 Model of Precipitation and Vertical Air Currents. Edwin Kessler and William C. Bumgarner. June 1971. (COM-71-00911)

No. 55 The NSSL Surface Network and Observations of Hazardous Wind Gusts. Operations Staff. June 1971. (COM-71-00910)

No. 56 Pilot Chaff Project at the National Severe Storms Laboratory. Edward A. Jessup. November 1971. (COM-72-10106)

No. 57 Numerical Simulation of Convective Vortices. Robert P. Davies-Jones and Glenn T. Vickers. November 1971. (COM-72-10269).

No. 58 The Thermal Structure of the Lowest Half Kilometer in Central Oklahoma: December 9, 1966-May 31, 1967. R. Craig Goff and Horace R. Hudson. July 1972. (COM-72-11281)

No. 59 Cloud-to-Ground Lightning Versus Radar Reflectivity in Oklahoma Thunderstorms. Gilbert D. Kinzer. September 1972. (COM-73-10050)

No. 60 Simulated Real Time Displays of Velocity Fields by Doppler Radar. L. D. Hennington and G. B. Walker. November 1972. (COM-73-10515)

No. 61 Gravity Current Model Applied to Analysis of Squall-Line Gust Front. Jess Charba. November 1972. (COM-73-10410)

No. 62 Mesoscale Objective Map Analysis Using Weighted Time-Series Observations. Stanley L. Barnes. March 1973. (COM-73-10781)

No. 63 Observations of Severe Storms on 26 and 28 April 1971. Charles L. Vlcek. April 1973. (COM-73-11200)

No. 64 Meteorological Radar Signal Intensity Estimation. Dale Sirmans and R. J. Doviak. September 1973. (COM-73-11923/2AS)

No. 65 Radiosonde Altitude Measurement Using Double Radiotheodolite Techniques. Stephan P. Nelson. September 1973. (COM-73-11934/9AS)

No. 66 The Motion and Morphology of the Dryline. Joseph T. Schaefer. September 1973. (COM-74-10043)

No. 67 Radar Rainfall Pattern Optimizing Technique. Edward A. Brandes. March 1974. (COM-74-10906/AS)

No. 68 The NSSL/WKY-TV Tower Data Collection Program: April-July 1972. R. Craig Goff and W. David Zittel. May 1974. (COM-74-11334/AS)

No. 69 Papers on Oklahoma Thunderstorms, April 29-30, 1970. Stanley L. Barnes, Editor. May 1974. (COM-74-11474/AS)

No. 70 Life Cycle of Florida Key's Waterspouts. Joseph H. Golden. June 1974. (COM-74-11477/AS)

No. 71 Interaction of Two Convective Scales Within a Severe Thunderstorm: A Case Study and Thunderstorm Wake Vortex Structure and Aerodynamic Origin. Leslie R. Lemon. June 1974. (COM-74-11642/AS)

No. 72 Updraft Properties Deduced from Rawinsoundings. Robert P. Davies-Jones and James H. Henderson. October 1974. (COM-75-10583/AS)

No. 73 Severe Rainstorm at Enid, Oklahoma - October 10, 1973. L. P. Merritt, K. E. Wilk, and M. L. Weible. November 1974. (COM-75-10583/AS)

No. 74 Mesonetwork Array: Its Effect on Thunderstorm Flow Resolution. Stanley L. Barnes. October 1974. (COM-75-10248/AS)

No. 75 Thunderstorm-Outflow Kinematics and Dynamics. R. Craig Goff. December 1975. (PB-250808/AS)

No. 76 An Analysis of Weather Spectra Variance in a Tornadic Storm. Philippe Waldteufel. May 1976. (PB-258456/AS)

No. 77 Normalized Indices of Destruction and Deaths by Tornadoes. Edwin Kessler and J. T. Lee. June 1976. (PB-260923/AS)

No. 78 Objectives and Accomplishments of the NSSL 1975 Spring Program. K. Wilk, K. Gray, C. Clark, D. Sirmans, J. Dooley, J. Carter, and W. Bumgarner. July 1976. (PB-263813/AS)

No. 79 Subsynoptic Scale Dynamics As Revealed By The Use Of Filtered Surface Data. Charles A. Doswell III. December 1976. (PB-265433/AS)

No. 80 The Union City, Oklahoma Tornado of 24 May 1973. Rodger A. Brown, Editor. December 1976. (PB-269443/AS)

No. 81 Mesocyclone Evolution and Tornado Generation Within the Harrah, Oklahoma Storm. Edward A. Brandes. May 1977. (PB-271675/AS)

No. 82 The Tornado: An Engineering-Oriented Prespective. Joseph E. Minor, James R. McDonald, and Kishor C. Mehta. December 1977.

☆ U.S. GOVERNMENT PRINTING OFFICE:1978—777-067 / 1229 REGION NO.8